pH-responsive microencapsulation systems for oral delivery of biopharmaceuticals

by

Bahman Homayun

A thesis submitted in partial fulfillment of the requirements for the degree of

Doctor of Philosophy

in

Materials Engineering

Department of Chemical and Materials Engineering

University of Alberta

Abstract

Oral delivery is the most attractive drug administration route due to many specific advantages. Ease of administration, large and diverse absorption surface area, applicability for solid formulations, patients' compliance, and intensified immune response due to mucosal effects are usually regarded as the main advantages of this route. On the other hand, gastric instability, mucus layer and tight junctions of the small intestine are principal biological barriers against this route. Additionally, technical challenges such as drug denaturation through the microencapsulation process, insufficient loading capacity, unsatisfactory preservation efficiency, and limited fabrication throughput of the systems are considerable challenges against the commercialization of oral delivery systems. Previously in this group, pored microencapsulation was developed to specifically address two principle issues with available oral delivery systems: 1) drug denaturation through the microencapsulation process due to contact with organic solvents, and 2) drug instability in harsh gastric environment. In fact, pored microencapsulation system completely excluded the drug molecules from the fabrication process of the microparticles (MPs). As a consequence, the drugs could be loaded into the MPs through their surface pores in favorable environmental conditions, eliminating any concerns about technical drug denaturation. The surface pores of the MPs were subsequently closed through freeze drying to properly isolate the loaded drugs from the surrounding environment. Accordingly, the drugs were properly protected in stomach, and once the MPs reached the absorption target in small intestine, the surface pores would open due to their pH-responsive nature and release the drug. The remaining activity of vulnerable biomolecules released from pored MPs in simulated digestive conditions was reported to be ~50%.

Although pored microencapsulation systems have successfully resolved the concerns associated with drug denaturation during the fabrication process and preserved the drug to

acceptable levels, they still suffer from the other problems mentioned before, including insufficient loading capacity and low throughput. Additionally, this system could not properly deal with biological barriers such as mucus, which can dramatically reduce the absorption efficiency of the drug at the target. With all these in mind, this project was focused on the development novel architectures of oral pored microparticles, which can address the remaining problems as well. New protocols based on swelling/solvent evaporation and emulsion/solvent evaporation methods were developed for scalable fabrication of the oral microparticles with acceptable narrow polydispersity.

In the first step, a new swelling/solvent evaporation protocol was developed as a facile fabrication process of MPs with pH-responsive surface pores. The MPs fabricated through this process showed up to 65% preservation efficiency of the loaded ingredients against simulated gastric environment and capability for the encapsulation of ingredients with a range of various sizes (100 nm simulating the size of viruses and protein therapeutics, 1 μm representing the size of bacteria, and 4 μm representing the size of cells). Although this part of the project led to improvements in both the fabrication throughput of the system as well as its preservation efficiency, the new MPs were still suffering from insufficient loading efficiency and lack of features for dealing with biological barriers at the absorption site.

In the next step of the project, emulsion solvent evaporation protocol for the fabrication of the MPs, as this method provides a better control over the internal morphology of the MPs for increasing the interior void spaces of the particles. Also, new features were included in the system for co-delivery applications. As a consequence, mucolytic enzymes could be simultaneously delivered to dilute the mucus layer at the absorption site of the drug, make the epithelial layer beneath the mucus easily accessible and consequently improve the absorption efficiency of the drug at the target. The average diameter of the MPs prepared through this process was successfully

increased up to 15x to increase the loading capacity of the system. Indeed, since the main drug in this system is loaded into the interior void space of the MPs, increasing the average diameter of the MPs would be the most effective key to address the issues with loading capacity. As a results, the loading efficiency of the system was improved up to 50x for different sizes of the drug molecules. Additionally, the new fabrication protocol showed promising potentials for scaling up and commercialization. Also, ex-vivo analyses confirmed that the new feature of the system can effectively remove the mucus barrier against the absorption of the drugs. The drug molecules released form the MPs also showed 60% remaining activity, confirming the potentials of the system for further investigations as a new and effective oral delivery architecture.

In the final step, the MPs needed to be coated for further protection in mouth cavity, saliva and esophagus. Indeed, the MPs investigated in this study were all made of anionic hydrogels soluble in neutral and basic environments (pK 5.5); hence, the MPs were coated with cationic copolymers on the outer surface to be stable upper digestive system, before reaching the stomach. The results conformed the success of the coating for protecting the MPs up to the stomach. In summary, the present work presents a new comprehensive oral administration system for preserving vulnerable drug molecules against microencapsulation process and harsh biological media and safely delivering them to the absorption site in the small intestine.

Preface

A more comprehensive version of the first chapter of this thesis was published as “Challenges and Recent Progress in Oral Drug Delivery Systems for Biopharmaceuticals”, B Homayun, X Lin, HJ Choi, Pharmaceutics 11 (3), 129. In that work, I was responsible for the collection of the contents and manuscript composition. A modified version of the 2nd chapter of this thesis was published as “Facile fabrication of microparticles with pH-responsive macropores for small intestine targeted drug formulation”, B Homayun, C Sun, A Kumar, C Montemagno, HJ Choi, European Journal of Pharmaceutics and Biopharmaceutics 128, 316-326. My contribution in that work entailed data collection and analysis as well as the manuscript composition. A modified version of the 3rd chapter of this thesis is under preparation for publication in Biomaterials as “A novel microencapsulation design and formulation for successful oral drug delivery”, B Homayun, HJ Choi, Biomaterials. I have been responsible for the development of the experimental design, data collection and analysis as well as the manuscript composition. A modified version of the 4th chapter of this thesis was also published as “Macropored microparticles with a core–shell architecture for oral delivery of biopharmaceuticals”, B Homayun, A Kumar, PTH Nascimento, HJ Choi, Archives of pharmacal research 41 (8), 848-860. In that work also, I was responsible for data production and analyses as well as manuscript composition. Chapter 5 of this thesis concerns the new steps of the project, which are still under progress. The new steps involve two mainstreams: 1) long-term stability of the formulations developed in this study and 2) the application of this microencapsulation system for other delivery routes, including intranasal delivery. These parts need further investigations, which will be continued in future by other colleagues.

Acknowledgment

I would like to express my gratitude to my supervisor Dr. Hyo-Jick Choi, who valued my ideas and supported me for continuing this long and fruitful journey. I would strongly like to thank Dr. Vinay Prasad, who always supported me, patiently listened to my concerns and problems and kindly gave me the most effective solutions and advice. Dr. Ravin Narain and Dr. Philip Choi for all their helps, which made the completion of this work possible. My many thanks to my family and colleagues, especially Chengmeng Sun and Surjith Kumaran. I am also very grateful to national research council (NRC) and national institute for nanotechnology (NINT) for providing resources and equipment needed for the completion of this project.

Table of Contents

Table of Figures

Table of Tables

The List of Abbreviations

BET: Brunner-Emmett-Teller theory

DCM: dichloromethane

DI: Deionized Water

Eth: Ethanol

FHNT: Functionalized Halloysite Nanotube

FNP: Fluorescence Nanoparticle

FTIR: Fourier-transform infrared spectroscopy

GI: Gastrointestinal

HNT: Halloysite Nanotube

HPLC: High Performance Liquid Chromatography

IPA: Isopropanol

M Cells: Microfold Cells

MP: Microparticle

PVA: Poly-vinyl Alcohol

SEM: Scanning Electron Microscopy

SGF: Simulated Gastric Fluid

SIF: Simulated Intestinal Fluid

SRB: sulforhodamine b

T20: Tween 20

TEM: Transmission Electron Microscopy

Preface

Oral administration is always introduced as the best drug delivery route due to its specific advantages, although there are several principal biological and technical barriers against this approach. Chapter 1 in this thesis provide a detailed understanding of the main biological and technical challenges against oral delivery systems, which is adopted from the review paper published in Pharmaceutics entitled as "Challenges and Recent Progress in Oral Drug Delivery Systems for Biopharmaceuticals" [1]. Microencapsulation systems have been investigated for several decades to address most of the biological barriers; especially to deal with gastric instability of the drug, delivering it to the target, long-term stability, and improving oral bioavailability. Although these systems have achieved relative success in affording a number of these requirements, such technical issues as drug denaturation during the encapsulation process and insufficient throughput are considerably impeding the wide-spread commercialization of these systems. This project was aimed at developing a new oral microencapsulation scheme addressing a number of these challenges. In order to make sure of the applicability of the system for biopharmaceuticals, this project was designed based on pored microencapsulation systems with pH-responsive macropores previously developed in this group to separate the fabrication step of the microparticles (MPs) from the encapsulation process of the drug. This would in turn resolve the concerns associated with drug denaturation during the microencapsulation process [1]

Since the pored MPs had shown insufficient fabrication throughput, the first priority of this project was dedicated to the development of a new facile and scalable fabrication protocol to improve the payload of the system. At the same time, it was aimed to increase the average diameter and the surface pore size of the MPs to improve their loading capacity, especially for large size

biomolecules. The results of this phase of the project were summarized in chapter 3, which has also been published in the European Journal of Pharmaceutics and Biopharmaceutics entitled as "Facile fabrication of microparticles with pH-responsive macropores for small intestine targeted drug formulation".

Although the swelling/solvent evaporation protocol developed in chapter 3 had successfully addressed the problem with fabrication output, it did not yield satisfactory loading capacity for ingredients. Hence, a modified emulsion/solvent evaporation process was developed for the next step of the project to have a better control over the interior/exterior morphology of the MPs, chapter 4. At the same time, new morphological features were added to the new MPs to improve the mucus-permeation of the system and increase the drug uptake efficiency. The system also showed meaningful fabrication throughput and narrow polydispersity of the final product. This part of the project has been submitted to Biomaterials under the title "A novel microencapsulation design and formulation for successful oral drug delivery".

Since all the MPs investigated in this project were made of anionic copolymers for oral enteric formulations, there was a need for additional cationic coating on the surface to protect the particles against neutral conditions in mouth cavity and subsequently in esophagus. The extra coating would also improve the preservation efficiency of the system against gastric conditions, especially for MPs with non-closed surface pores. This part of the project was published in Archives of Pharmacal Research, "Macropored microparticles with a core–shell architecture for oral delivery of biopharmaceuticals".

Finally, as a main advantage of the oral solid formulation, the system developed in this project was analyzed for long-term environmental stability. The samples were tested under different protections (microencapsulation/formulation, gelatin capsules casing, and blister packaging) and

were tested under various environmental conditions. The activity of the samples were tested after each incubation window to confirm the environmental stability of the samples. Also, the application of the microencapsulation system developed in this project does not really limit to oral administration, but can be extended to other administration routes. To investigate this possibility, the samples were tested for intranasal delivery as well. These two new steps of the project have been just started and will be under progress for a while.

1. Chapter 1

Oral delivery systems: Advantages, Disadvantages and considerations

1.1. Oral route

Among the various drug delivery routes, the oral pathway has attracted the most attention due to its unique advantages, including sustained and controllable delivery, ease of administration, feasibility for solid formulations, patient compliance and an intensified immune response in the case of vaccines [2–6]. In addition, a large surface area (>300 m^2) lined with a viscous mucosal layer paves the way for drug attachment and subsequent absorption [7,8]. Furthermore, drug molecules trapped within mucus are protected against the shear stresses caused by flowing gastric juices [9]. The epithelium of the human intestine is very absorptive due to the abundance of enterocytes in different parts of the intestine, especially microfold cells (M cells) covering the Peyer's patches, the lymphoid segment of the small intestine [10–14]. However, in comparison with other routes, the absorption mechanism of oral drugs is more complex. Oral drugs need to be soluble in gastric fluid so they can be absorbed in the stomach, the small intestine or the colon. Orally administered drugs can be absorbed in four types of pathways: Transcellular, paracellular, carrier-mediated transcellular and facilitated transport. Among these pathways, the transcellular pathway is the main mechanism. The challenges of drug absorption/efficacy do not limit the barriers met in the gut, but they include the hepatic barriers after they enter the vessels under the intestinal epithelium as well. In summary, oral drugs are not applicable for emergencies due to their slow absorption as well as the multiple levels of barriers they need to deal with.

Although the oral route is the most desirable administration method for small therapeutic molecules, there are not so many oral vaccines on the market due to the harsh conditions along the GI tract, which can degrade/denature active antigens. However, the attraction of the mucosal immunity, which appears to be induced by oral and nasal routes, promotes the study of oral vaccines [15]. Besides, the convenience and other advantages of oral delivery make it a very

promising strategy for mass vaccination programs. The inductive sites in the GI tract consist of Peyer's patches, lymphoid follicles in lymph nodes and antigen presenting cells (APCs). Intestine mucosal immunity is similar to that of nasal mucosal immunity. The main barrier for vaccine delivery is the change of pH in different sites in the GI tract and various enzymes, making it hard to permeate the mucus and reach the inductive site in gut-associated lymphoid tissue (GALT) [16]. Additionally, the mucosa may lead to the structural change of proteins and peptides due to various possible interactions [8]. Hence, delivery vehicles and formulations should be developed to gain a stronger immunogenicity to meet the required therapeutic efficacy. Currently, seven live oral vaccines have already been approved by FDA.

To meet the increasing demand for biopharmaceutical oral products, research has been focused on developing devices for oral delivery. While still at an early stage, recent devices include intestinal patch systems, microneedle capsules and particulate systems [17]. The intestinal patch systems are based on a unidirectional drug release depot, which is similar to a microdevice adhered to the intestinal wall [18]. The microneedle capsule increases the penetration rate of drug molecules by piercing the mucosa directly with microneedles. A recent study developed a method to inflate a microneedle into the mucosa by responding to the change in pH [19]. Particulate devices are the most common oral vehicles, which have been investigated for the encapsulation and targeting of a vast variety of therapeutics. In general, the current technologies are still at the preclinical stage. Therefore, more research efforts should be directed to solve the existing technical challenges of oral drug delivery systems and prove the feasibility in clinical use.

1.2. Challenges Associated with Oral Delivery

Oral drugs are transported and absorbed in the GI tract, which is in the shape of a conduit. Some drugs have local effects in the gut, while most of them are sent to the bloodstream in the systemic circulation to act in other parts of the body. The GI tract can be divided into upper and lower parts. The upper GI tract includes the oral cavity, pharynx, esophagus, stomach and the initial part of the small intestine, known as the duodenum. The lower GI tract includes the rest of the small intestine (jejunum and ileum), as well as the large intestine segments: The cecum, colon and rectum [20,21]. The structure of the GI tract is similar in all segments. The lumen is enveloped by smooth muscle cells, covered by mucus, submucosa and several muscle layers [22]. The mucosal layer which lines the inner part of the GI tract consists of a layer of epithelial cells, lamina propria and muscularis mucosae, which play significant roles in food/drug molecule transport and gastrointestinal immunity [20,21]. A large absorption area and long residence time provides greater opportunities for drug absorption, which is one of the reasons why drug absorption mostly occurs in the small intestine. Further, between the three main parts of the small intestine (duodenum, jejunum and ileum), the jejunum and ileum have a higher absorption capability compared to the duodenum [23,24].

The environmental factors that influence drug integrity and absorption include the average length of the segment, pH, thickness of the mucus, residence time of the drug and the bacterial diversity/population in different segments [8,25,26]. The obstacles against oral administration may be broadly classified into biological barriers and technical challenges. Biological barriers include any biological factors that denature the orally administered drugs or prevent their successful absorption in the target. On the other hand, technical challenges relate to any difficulty in the fabrication process of the oral delivery devices. The technical challenges may either be issues with

creating specific properties for addressing the biological barriers or complications with scaling up and commercializing a system. The details of each category will be discussed in the following sections.

1.2.1. Biological Barriers

Any digested ingredient will be dealing with three main biological environments along the gastrointestinal (GI) tract, regardless of its absorption mechanism or target. These environments are the lumen (i.e., the interior space), mucus and tissue. Each of these three environments may have interactions with the drug molecules.

Lumen

The first biological barrier against any orally administered drug is the harsh acidic conditions inside the stomach (pH 1–2.5), denaturing/depurinating most of the administered molecules, drastically lowering their effectivity [27–30]. In addition to stomach acid, gastric enzymes such as pepsin and gelatinase can degrade biopharmaceuticals. pH-responsive hydrogels can encapsulate the drugs and protect them not only against the harsh acidic environment, but against gastric enzymes as well. These materials can remain intact in unfavorable surrounding conditions to protect the loaded drug (promptly reacting to environmental stimuli such as the pH in the target) and release the cargo. For instance, Yamagata et al. confirmed that pH-sensitive hydrogel microparticles (MPs) can efficiently preserve sensitive drugs such as insulin against gastric/intestinal enzyme fluids [31]. In another study, Cerchiara et al. also developed an oral pH-responsive microencapsulation system and demonstrated its capability for protection against both gastric acidic and gastric enzymatic environments [32].

Notably, in addition to the gastric enzymes, there are also pancreatic enzymes synthesized inside the pancreas and secreted into the intestinal lumen. These enzymes include lipase (degrading fats), trypsin (decomposing proteins), amylase (degrading starch) and peptidases (disintegrating peptides), and are especially abundant at the main entrance of the small intestine (duodenum). They can readily decompose nucleic acids and reduce the gastric residential stability of biomolecules [33,34]. Although pancreatic enzymes are also introduced as biological barriers against oral delivery, they are not considered as a major challenge due to three principal reasons. First, these enzymes are mainly abundant in the duodenum, and their concentrations considerably decrease in the jejunum and later parts [35]. In addition, Layer et al. attempted to deliberately deliver pancreatic enzymes to the intestine and noticed that even the concentration of the delivered enzymes substantially decreases in the midjejunum compared to that in the duodenum (they reported up to a 90% drop in enzymatic activities) [36]. The second aspect is the short transit time of the digested food inside the duodenum (Table 1), which is not enough for the enzymes to degrade the drugs. Fallingborg et al. reported that duodenal residence comprises only 10% of the whole small intestine average residence time [37]. Lastly, the pH of the duodenum is lower than that of the later parts of the lower small intestine (Table 1), meaning that unwanted release of the drugs inside the duodenum can be successfully avoided by controlling (increasing) the pKa of the delivery carriers. For example, Lozoya-Agullo et al. employed poly(lactic-co-glycolic)acid (PLGA) nanoparticles for colon delivery and confirmed that duodenal release may be significantly avoided due to the insufficient environmental pH [38].

Table 1. Characteristics of different segments of the human gastrointestinal (GI) tract.

Segment	pH	Length (cm)	Mean Diameter (cm)	Mucus Average Thickness (μm)	Mucus Turnover (hour)
Stomach	**0.8–5 [39]**	**20 [39]**	**NA**	**245 ± 200 [8]**	**24–48 [40]**
Duodenum	**~7 [8]**	**17–56 [41]**	**4 [42]**	**15.5 [39]**	
Jejunum	**≥7 [8]**	**280–1000 [41]**	**2–2.5 [42]**	**15.5 [39]**	**24–48 [40]**
Ileum	**≥7 [8]**		**3 [42]**	**15.5 [39]**	
Colon	**7–8 [8]**	**80–313 [41]**	**4–4.8 [42]**	**135 ± 25 [8]**	**24–48 [40]**

In addition to the acidic and enzymatic degradation, the lumen can cause other damages to drug molecules. Osmotic stresses along the GI tract, peristalsis of the GI muscles, as well as the shear stresses by the flow rate of the gastric juice inside the lumen are other factors that decrease drug efficiency due to mechanical degradation inside the lumen [2,8]. Flowing gastric juice may also decrease the contact time between the drug molecules and the epithelial layer, thus impeding their absorption [33]. Enveloped biologics such as viruses, vaccines and cells are usually the main components sensitive to mechanical destruction. Valon et al. studied the possible effects of mechanical stresses on various types of cells, and reported that shear stresses and compaction may lead to apoptosis and cell death [43]. Choi et al. also found that hyperosmotic pressure can destroy virus integrity in an acidic environment [2]. Although mechanical stresses by the lumen can destroy biological agents, microencapsulation can properly address these problems as well. Indeed,

MPs are hardly studied for mechanical testing, and mechanical strength is usually discussed in regard to hydrogel properties, which in turn is a function of the molecular weight of the monomers as well as the degree of crosslinking of the matrix. Nanoparticles may also be added to hydrogels as reinforcing components. For instance, France et al. recently employed cellulose nanocrystals (CNCs) to create physical crosslinking in a hydrogel matrix, proving their significant impact on mechanical behavior (up to a 35-fold increase in the shear storage modulus of the final composite) [44]. Yang et al. also reported up to a 3.5-fold improvement in the Young's modulus of poly(ethylene glycol) (PEG) hydrogels through the addition of 1.2 vol % CNCs [45]. As an instance of ceramic-polymer composite systems, Gaharwar et al. used hydroxyapatite as the reinforcing agent in a ceramic-polymer composite and reported up to a 1.7-fold improvement in the compressive strength of the matrix. It should be noted that the addition of secondary components to form a composite will not only affect the mechanical properties, but may also affect the swelling behavior, gelation rate and degradation rate of the hydrogels as well [44,45]. Furthermore, the distribution mechanisms of CNCs throughout the polymer matrix are poorly understood, and there are underwhelming (sometimes contradictory) reports about the improvements in mechanical properties of composites. However, the greatest and most effective improvement reported by the formation of a hydrogel composite to date concerns the addition of CNCs to hydrogels, without the need for any surface or other secondary modification of the particles.

Mucus

Mucus is the second compartment of the GI tract, which any digested moiety interacts with. The entire GI tract is lined by mucus (a sticky, elastic and viscous layer), responsible for the

capture of foreign moieties, especially hydrophobic molecules, impeding their contact with the underlying epithelial layer. The mucus then discards such foreign moieties, acting as one of the main compartments of the immune system, known as mucosal immunity [46–49]. The mucus itself is mainly composed of water and mucin protein molecules coated with proteoglycans, giving the mucus a negative charge [50]. Carbohydrates, salts, bacteria, antibodies and cellular remnants are the other compounds found in mucus [51]. The thickness of this layer is reported to vary along the GI tract, as summarized in Table 1 [8].

Mucins are large macromolecules (0.5–40 MDa) made of monomers connected through disulfide bonding, and these macromolecules are subsequently crosslinked to build up the mucosal layer [52,53]. The mucosal layer itself is usually composed of two separate overlaying layers: An outer loosely adherent layer and an inner firmly adherent layer (Figure 1) [54]. The inner layer is composed of glycoproteins, glycolipids and cell-bound mucin [55,56]. It has been claimed that the thicker outer mucus acts as a barrier against the transition of released drugs to the submucosal tissue. For instance, Marie Boegh and Hanne Mørck Nielsen studied the diffusion of peptides and proteins through mucus and found that mucus is the main obstacle against the bioavailability of oral drugs [57]. On the other hand, the narrower inner mucus is known to help the absorption/enhance the uptake efficiency of drugs, justifying the dual role of mucus in the absorption/desorption of orally delivered drugs (Figure 1) [58,59]. There is an equilibrium between mucin secretion, degradation and clearance in each segment of the GI tract to protect the epithelium and control the nutrition absorption rate, which in turn defines the final thickness of the regional mucosal layer (Table 1) [8,60].

The approaches taken regarding mucus in the field of oral delivery can be generally classified into two opposite mainstreams: Mucopenetration and mucoadhesion. Mucopenetrating oral

vehicles may be made through controlling the hydrophobicity/hydrophilicity nature of the carriers' matrix. In other words, due to the hydrophobic nature of the outer mucus, it tends to have significantly less interactions with hydrophilic materials. Additionally, regulating the electrostatic interactions between the carriers and the mucus can dramatically facilitate the transition of particles through mucus. Li et al. incorporated Pluronic F127 (PF127) into the matrix of liposomes to induce hydrophilicity and nullify the electrostatic charge of the particles, demonstrating considerable improvements in the mucopenetration and uptake efficiency of the liposomes [61]. Cu et al. reported similar improvements in terms of the mucopenetration of poly(lactic-co-glycolic)acid (PLGA) nanoparticles by coating them using PEG, which neutralized the surface charge of the nanoparticles [62].

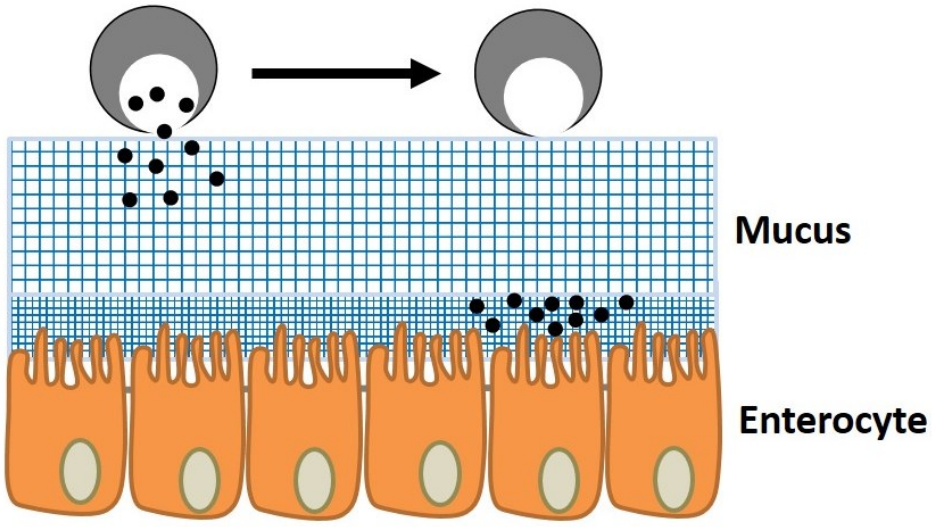

Figure 1. The structure and function of the mucus. The schematic shows the gastric mucus layer, the attachment of particles to the outer and inner mucus, and the drug delivery vehicle on the outer mucus.

The other platform employed for penetrating through mucus is the application of mucolytic enzymes. Muller et al. fabricated nanoparticles made of complexes of poly(acrylic acid) (PAA)

and papain (a mucolytic enzyme) through physical adsorption [63]. They showed that the enzyme-conjugated particles can reduce the viscosity of fresh mucus by up to 5 times, reflecting the potential of the system for improved oral bioavailability. Pereira de Sousa implemented a similar study comparing bromelain (another mucolytic enzyme) with papain for the same purpose [64]. They showed that the bromelain-modified particles exhibited a significantly enhanced mucopenetration behavior compared to the papain-conjugated particles (up to a 4-fold increase in mucopenetration compared to the papain-conjugated particles, and up to a 10-fold increase compared to the blank samples).

On the other hand, the protective and sticky properties of mucus can be exploited to protect the digested ingredients and extend their transition time along the GI tract. As a result, mucoadhesive drug carriers have attracted significant attention [65,66]. For this purpose, cationic hydrogels such as chitosan have been extensively investigated [67–69]. Recently, Kim et al. derived catechols from mussels and conjugated it with chitosan to develop a new complex with significantly better mucoadhesive properties and negligible cytotoxicity compared to chitosan alone [70]. Lectin functionalization has been another strategy employed for the same purpose. The study implemented by Ertl et al. is one of the first works with this approach, in which they conjugated wheat germ agglutinin with PLGA MPs and increased their mucoadhesion [71]. The advantage of this new system is that lectin-conjugated MPs exhibited improved adhesion not only to the mucus but also to the enterocyte (cell) surfaces, minimizing the problems associated with the short turnover period of mucus. Additionally, in specific parts of the GI tract where the mucus is not thick enough, this system can still show improved absorption efficiency.

In the case of anionic MPs, their surfaces have been functionalized with thiol functional groups to exhibit mucoadhesive properties by forming disulfide bonds with thiol groups existing in mucins

[72–77]. Several studies have confirmed that such chemically-modified MPs show a significantly longer residence time in the target, acting as potential candidates for the sustained oral delivery of specific drugs, such as insulin and losartan [66,78]. For instance, Zhang et al. functionalized Eudragit L100 with thiol groups and confirmed improvement in the absorption and bioavailability of orally administered insulin compared to the unmodified polymer by monitoring the blood glucose concentration [78]. However, it should be noted that mucus is constantly secreted by goblet cells along the GI tract and is subsequently shed and cleared from tissues due to the rapid turnover of cells. This leads to a very short residence time for the attached agents to reach the epithelium for absorption (50–270 min) [79,80]. Mucus, with around a two day turnover period, plays the most significant role as a barrier [81,82]. Hence, sustained delivery using mucoadhesive particles may not represent the ideal strategy in this regard. In addition to this, it is difficult to model the real effects of mucus on delivery carriers in vitro due to its changing thickness along the GI tract and the constant effects of flowing gastric juice [8,33,82]. Since sustained oral delivery itself is a major challenge, it will be discussed under a separate subsection later in this review.

Tissue (Extracellular Barriers)

The characteristics of the drug molecule will determine its absorption sites and its pathway to cross through the intestinal epithelial cells in the GI tract. There are two main pathways for the absorption of oral MPs or drugs: Transcytosis by cells (transcellular route) and diffusion through the spaces between epithelial cells (paracellular route). Figure 2 schematically represents all the possible absorption scenarios that a digested molecule may encounter in the intestinal lumen. In the transcellular pathway, the drug molecules enter the enterocytes by crossing the membrane of the epithelial cells. The paracellular pathway permits only small hydrophilic molecules to be

absorbed, playing a minor role in drug absorption as it is narrow and only occupies a small area fraction of the whole epithelium [87]. The principal extracellular biological barrier against oral delivery is known as tight junctions, which concern the paracellular absorption route for orally administered agents [83,84].

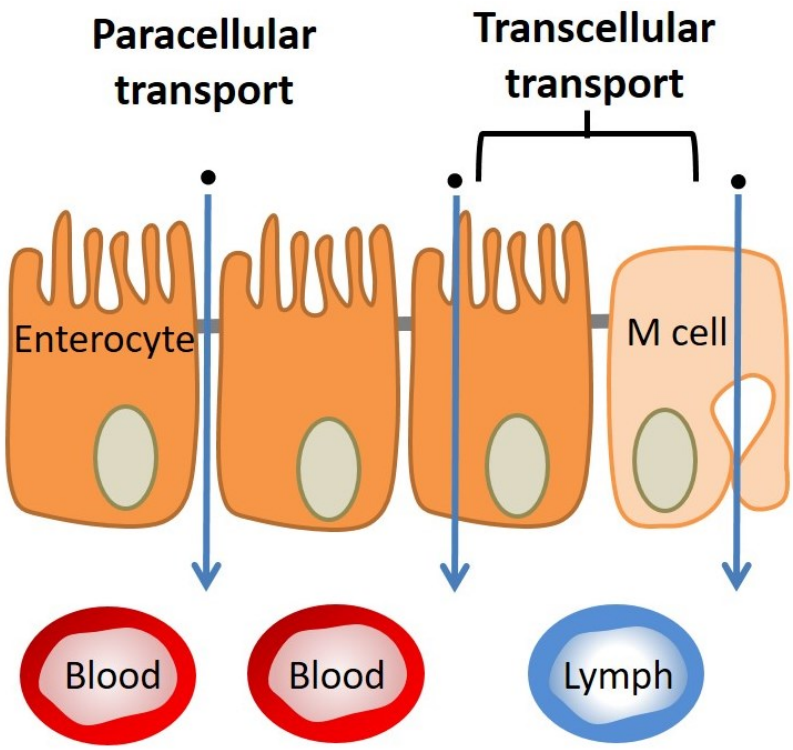

Figure 2. Absorption mechanisms through the mucosal layer. Paracellular route to lamina propia and transcellular route (enterocytes, M-cells, transfection of the epithelial cells, direct absorption through dendritic cells and active transport).

The transport of MPs or drug molecules through tissue depends on both their chemistry and their size. Generally, hydrophobic drug molecules, nanoparticles, vesicles and micelles prefer to be absorbed through transcellular routes due to their large size and chemistry, while hydrophilic small drug molecules prefer paracellular routes [33,85]. There are also barriers due to the structure of the cells. At the outer regions of the membrane bilayers, the high molecular density of the polar

head groups of the lipid membranes makes it difficult for the drug molecules to pass through the cell membranes. Furthermore, after entering the cell membrane, cellular components such as enzymes may degrade/decompose the drug molecules in the cytosol, decreasing the therapeutic efficiency [89].

Passive diffusion of MPs through intercellular routes is only possible for agents with sizes of up to a few nanometers (0.5–3 nm), which is too small for the delivery of most drug molecules [86,87]. A notable example of this problem is the poor bioavailability of doxorubicin (DOX), which is attributed to its limited paracellular absorption in the intestine. Kim et al. developed a medium-sized chain glyceride-based water-in-oil (W/O) microemulsion system to overcome the paracellular barrier against DOX intestinal absorption [88]. The improvements in the absorption level of the drug were ascribed to the lipidic components of the carriers, inducing the paracellular enhancing effects. In addition to the chemistry of the carriers, there are few absorption enhancing agents that have been used in oral delivery systems. Sodium *N*-[8 (2-hydroxylbenzoyl) amino] caprylate (SNAC) is a paracellular permeability enhancer which has been recently used for clinical trials by Davies et al. [35]. The problem with this agent is that there is no distinct mechanism identified for its function. Recently, Taverner et al. identified other peptides (PIP peptides: 250 and 640), which could enhance the paracellular permeability of insulin through intestinal tissue [89]. They claimed that these peptides can dynamically adjust endogenous mechanisms, inducing myosin light chains (MLCs), opening the tight junctions and facilitating paracellular transition, especially for peptide therapeutics. Almansour et al. (in the same group) studied PIP 640 further and confirmed its stability in the intestinal lumen environment and explained its functioning mechanism: PIP 640 selectively enhances the MLC-pS^{19} levels of the cytoplasm of enterocytes in the epithelial layer [90]. Apart from the recent studies and the progress made, tight junctions are

still one of the main challenges against the absorption of biopharmaceuticals. The lack of a fundamental understanding of the mechanisms controlling tissue permeability and the effects of various agents may be one of the principal reasons for this problem.

1.3.Technical Challenges

In addition to biological barriers, oral delivery systems face technical difficulties as well, in terms of deciding whether to induce new properties addressing biological barriers or to scale up existing systems for commercial purposes. In this section, most common oral delivery devices, sustained delivery strategies, solvent-free microencapsulation techniques, co-delivery systems and the challenges associated with the scaling-up of systems are analyzed.

1.4.Oral Delivery Devices and Materials

The devices developed for oral drug administration may be classified as intestinal patches, gastrointestinal microneedles and particulate carriers (including micro/nanoparticles, micelles and liposomes), as illustrated in Figure 3. Intestinal patches are millimeter-sized mucoadhesive blankets that attach to the inner walls of the GI tract, providing a drug reservoir at the target. These patches can protect the drug against the harsh environment and luminal loss, improving the bioavailability of the drug by providing a unidirectional diffusion regime towards the intestinal tissue. They have been especially attractive for improving the oral bioavailability of drugs and sustained delivery. Insulin, interferon-α and calcitonin are examples of drugs investigated for delivery using such devices [91]. As far as intestinal patches are concerned, the mucosal adhesion

properties, loading capacity, release rate and release direction are the main factors to be considered. Mitragotri et al. have used mucoadhesive polymers, such as Eudragit copolymers or pectin, to prolong the gastric residence time of devices [92]. They also used impermeable ethyl cellulose sheets to create a unidirectional release pattern and seal the opposite side of the patches. Shen et al. also showed that incorporation of drug-loaded microspheres into the patches, instead of direct loading of the drugs, can provide significantly enhanced control over the release behavior of the drug [93]. Toorisaka et al. developed a lipophilic formulation (drug-in-oil formulation) to improve the compatibility of the system with intestinal cell lines and enhance the absorption of insulin [94]. However, their formulation lacked enough retention time at the target. They later solved this issue by designing a bilayer patch consisting of a drug-impermeable layer to guarantee a unidirectional drug release regime and a mucoadhesive layer to prolong the gastro-residence time [95]. The drug-in-oil formulation was also impregnated into the porous mucoadhesive layer. Although it has been more than two decades since the development of these oral devices, they have not attracted as much research attention as other designs, such as MPs. Oral patches are mainly applicable in the initial segments of the duodenum, since solid boluses of digested food can detach the patch from the lumen wall in later parts of the GI tract, significantly decreasing the transient time. Even in the duodenal part, the device needs strong bonding/binding with the mucus to avoid being washed away by gastric juice. Furthermore, the mucus turnover cycle limits the real application of these devices for sustained delivery.

Intestinal microneedles are the newest design developed as an oral delivery device. Microneedles were first developed for transdermal delivery (transdermal patches), and their application was subsequently extended to other administration routes including the vagina, anus and scalp [96]. In 2014, Ma et al. employed microneedles for oral vaccine delivery to the mouth

cavity, which was the first time microneedles were used for oral administration [97]. They investigated the system for the delivery of two HIV antigens (DNA vaccines and virus-like particles), comparing the induced immune response with the response generated by the intramuscular injection of the drugs. They reported that only orally administered agents showed a stimulated antigen-specific IgA response in saliva. The limitation of this design is that it could only be employed for delivery to the oral cavity rather than the GI tract. Traverso et al. in 2015 tried to overcome the biological barriers of the GI tract using orally ingested microneedles and improved drug bioavailability [98]. They claimed that their device can be safely excreted from the GI tract. This design is especially promising for the delivery and successful absorption of large-size biomolecules. Their system demonstrated significant improvements in insulin bioavailability compared to the subcutaneous administration route. As a newly developed system, oral microneedles need to be studied considerably more, especially through clinical trials. There are currently not many investigations on this system.

Spherical carrier designs, including micelles, liposomes and MPs, are the most commonly studied oral delivery vehicles. Micelles are colloidal carriers (5–100 nm) developed to improve the aqueous solubility of hydrophobic pharmaceuticals and facilitate their oral delivery. They are made of amphiphilic molecules, enfolding the hydrophilic ingredients inside their hydrophobic core, with hydrophilic segments oriented on the outer walls. For instance, Dabholkar et al. developed a polymeric composition (polyethylene glycol-phosphatidylethanolamine conjugate) and increased the water solubility of paclitaxel (an anticancer drug) up to 5000 times [99]. Due to their very small average size (20–80 nm), micelles show spontaneous penetration through the interstitium of various tissues, improving their permeation efficiency and retention time.

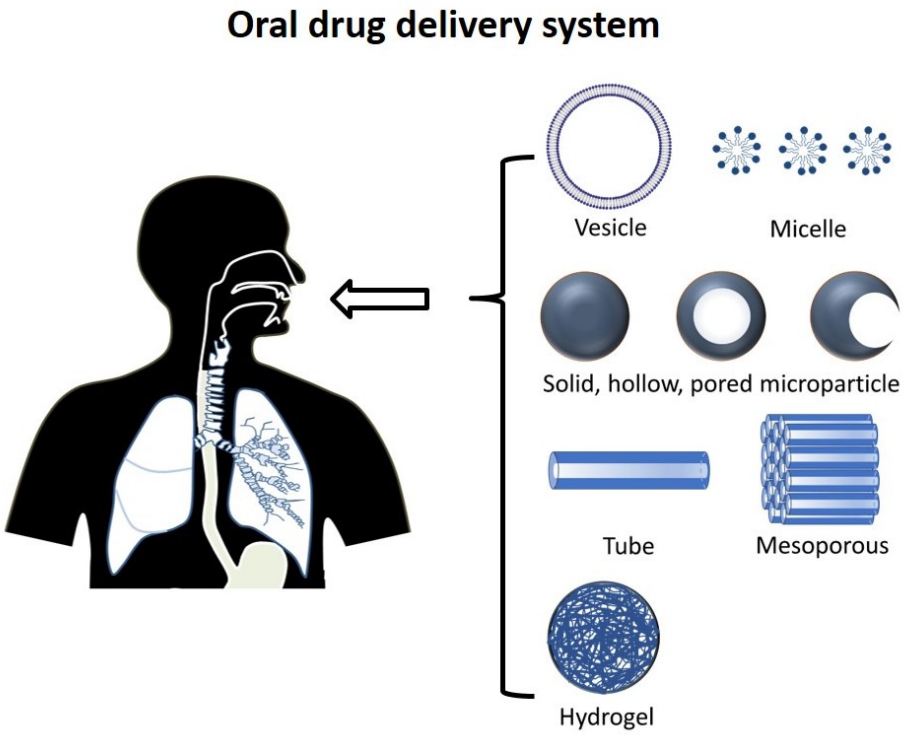

Figure 3. Schematic illustration of the principle oral vehicles

Yu et al. developed dual-responsive (pH and light) micelles to improve the passive tumor targeting of doxorubicin and address tumor resistance against the drug [100]. The micelles could trigger both deep tumor penetration and cytoplasm drug release, which in turn considerably improved treatment efficiency. Additionally, they found that the micelles could prolong the blood circulation cycle of the drug.

In addition to passive penetration, micelles can also help the active penetration of drugs. Suzuki et al. used cationic micelles (PLGA-b-bPEI-b-PLGA; Mw(PLGA): 36 kDa, Mw(bPEI): 25 kDa) for the encapsulation of doxorubicin and confirmed up to a 40-fold increase for in vitro drug penetration into multilayer cell cultures [101]. They claimed that iterative transcytosis via macropinocytosis and exocytosis are the main mechanisms for the penetration of the cationic micelles into cells. Although micelles are constantly proving their potential for improving

therapeutic efficacy in bench-scale studies, they have hardly been commercialized. The clinical trials for these delivery devices are limited to a few cases for parenteral cancer therapies: Doxorubicin and its derivatives. A possible reason for this may be the safety of the materials, in terms of the physicochemical interactions between the carriers and mucus in real conditions [102]. On the other hand, liposomes are phospholipid vesicles (>200 nm) which can encapsulate both hydrophobic drugs in their hydrophobic compartment and hydrophilic drugs in their inner hydrophilic core. These carriers can be chemically modified through the immobilization of antibodies on their surfaces for improved target specificity. It should be noted that antibody-decorated liposomes may suffer from a short life cycle in blood circulation due to their accumulation in the liver, especially in the absence of sufficient target antigens [103].

MPs are the other common oral delivery architecture. The materials used in oral microencapsulation systems can be broadly classified into polymers and ceramics. Ceramics are usually safe materials for delivery applications due to their bio-inert nature. There are various ceramic materials used for delivery applications, including silica, alumina and calcium phosphate. For instance, cisplatin, methotrexate and hydrocortisone acetate have been successfully delivered using calcium phosphate carriers, and silica nanoparticles are dominantly used for chemotherapy [104]. Regarding the polymers employed for oral delivery, hydrogels are the most attractive structural materials, mainly due to their controllable chemical composition, tunable mechanical properties, water absorption, ability for internal material flow, and, above all, their capacity for stimuli-responsivity [105–109]. One of the primary features to control in hydrogels is porosity, since pore size can significantly affect the mechanical properties, uptake efficiency of extrinsic occupants, water/material flow through the polymer matrix and swelling ratio of the gel. The larger the mesh size, the easier the transport of materials through the structure is, and the higher the

swelling ratio. For instance, Torres-Lugo et al. could regulate the release rate of salmon calcitonin from poly-(methacrylic acid) (PMAA) acid MPs by up to 50% by controlling the swelling ratio and mesh size of the hydrogel [110].

There are other strategies to increase the porosity of the hydrogel structure to a larger scale (micron scale) [111–113]. For instance, leaching out the template materials from the structure network is a common method for making porous materials [114]. Also, the number of crosslinking sites can be decreased through selective removal of one phase from the gel. Similarly, the aqueous/organic liquid absorbed inside the gel may be lyophilized, and the volume increase through the freezing process can create pores inside the polymer matrix [115–117]. The size of the pores created through this process depends upon the size of the ice crystals formed in the solid state and may range from nanoscale, by freezing the remaining molecular water contents inside the structure, to microscale macropores by concentrating the liquid at specific spots [118]. It should be noted that although removing crosslinking sites considerably affects the mechanical properties and the swelling ratio of the polymer, the porosity created by the frozen liquid does not change the hydrogel mesh size and consequently its properties/behavior [113].

In addition to achieving the optimum porosity for delivering small drug molecules, another major challenge is obtaining macropores for loading large biomolecules and cells into hydrogels [119,120]. If the pores are aligned in well-oriented geometries, the hydrogels can be used for directional cell growth and the creation of arrays [121]. Also, pore size and geometry define the nutrition transfer rate and cell migration pattern [122–124]. With all these aspects taken into account, developing methods for accurate control over the porosity of the hydrogel and size and morphology of pores in polymers has always been regarded as a main research topic for a range

of various applications. France et al. recently reviewed the major methods developed for creating macroporous hydrogels [113].

1.5. Solvent-Free Microencapsulation

1.5.1. Multiemulsion Systems

MPs have been the main candidates for oral microencapsulation systems [66,125–127]. MPs can be classified into two main categories: (1) Solid MPs, which are solid polymeric MPs with drug molecules dispersed in their matrix, and (2) hollow MPs, which are polymeric shells with hollow interior spaces that accommodate the delivered drug molecules [128,129]. In most of the protocols developed for the fabrication of MPs, drug molecules are directly involved in the fabrication process of the carrier, leading to direct contact between the drug molecules and the harsh organic solvents, raising concerns over drug denaturation, especially for biopharmaceuticals [130]. As such, the development of solvent-free microencapsulation technologies is of primary importance in drug delivery applications.

Multiemulsion systems (W/O/W and O/W/O) were originally developed to minimize contact between the drug and solvents, however, the traditional versions of these systems were difficult to make, control and stabilize, additionally being inefficient in terms of throughput [131–137]. While these systems minimized the contact between the drug molecules and organic solvents, they were not able to completely eliminate it due to partial contact at the O/W phase interface. For a wide range of applications of the emulsion technology, it is important to fully characterize and address the issues of drug denaturation along the fabrication process of the carriers, such as shear stresses caused by mechanical agitation or sonication and local temperature increases due to sonication.

Microfluidic devices were successful in addressing a number of fundamental problems associated with the emulsion technique: highly uniform MPs with very small polydispersity index and considerable stability in liquid state emulsion [138,139]. Also, making multi-channel devices with various geometries is more straightforward and significantly more efficient in terms of minimizing O/W phase contact. Furthermore, there is no need for sonication or mechanical agitation to stabilize the emulsion made by microfluidic devices, resolving various problems associated with traditional emulsification techniques [140]. Due to these advantages, this new approach has attracted considerable attention for cell encapsulation/delivery. For example, pancreatic islet cells, as one of the most significant treatments for type 1 diabetes, can be successfully encapsulated and delivered using microfluidic devices [141]. The size, morphology and loads of the carriers can be controlled by regulating the flow rate of the phases (flow rate of the continuous phase and infusion rate of the dispersed phase), the geometry of the channels and nozzles and the concentrations of the emulsifiers [142]. Although microfluidic devices contributed to advance the emulsion technology, there are still problems with these systems, including the clogging of channels, attachment of oil phase/polymer fragments to the channel walls and also O/W contact at the interface [143,144]. As the main challenge against the widespread application of these systems is their low throughput, this prevents them from being scaled up to commercial extents and entering the pharmaceutical industry for mass production.

1.5.2. Pored and Hollow Microencapsulation Systems

Another strategy for solvent-free microencapsulation is to employ separate processes for MP fabrication and drug encapsulation. That is, the drug can be loaded into the MPs in their favorable

environmental conditions after the MP fabrication is complete, minimizing the possibility of drug denaturation due to the formation of MPs in the presence of the drug [145]. For this aim, several fabrication methods were previously developed, almost all of which were based on the same idea: coating solid spheres as templates with the desirable polymer material [146–148]. The templates (solid cores) were subsequently removed from the inside through either calcination or etching, leaving hollow polymeric spheres behind as the final product. These methods could hardly be successful due to the complications associated with diffusional material flow through the solid state polymeric shells. Since the drug can be loaded only by soaking the particles in a concentrated solution of drug, this method does not yield satisfactory levels of loading efficiency, limiting its general application [146,149,150].

Hyuk Im et al. proposed an idea to fabricate hollow polymeric microspheres with single surface pores using a solvent evaporation method [118]. Swollen solid polystyrene particles in organic solvents were plunged in liquid nitrogen, followed by slow evaporation of the solvent. The solvent would diffuse into the particles throughout the incubation step and would expand due to freezing, creating a hollow interior space inside the particles. The evaporation step would also generate surface pores, allowing for encapsulation of the cargo. It was demonstrated that the surface pores could then be closed through the thermal treatment of the particles above their glass transition temperature.

More recently, a simplified method of making single pored-MPs was reported by Kumar et al. based on ultrasonic O/W emulsification [145]. The obtained macropores could be used for the direct loading of the drugs in their favorable conditions by applying vacuum cycles, and then closed to protect the drug during transition inside the stomach (Figure 4) [145]. In this method, the surface pores were sealed through freeze drying, thus eliminating the concern over the possible

thermal denaturation of the biopharmaceuticals during the heat treatment of the MPs. It has been proposed that the pore closure mechanism is due to polymer-polymer interactions, followed by the removal of water. This new design was later modified to make larger MPs with larger surface pores, suitable for the delivery of large biomolecules and cells.

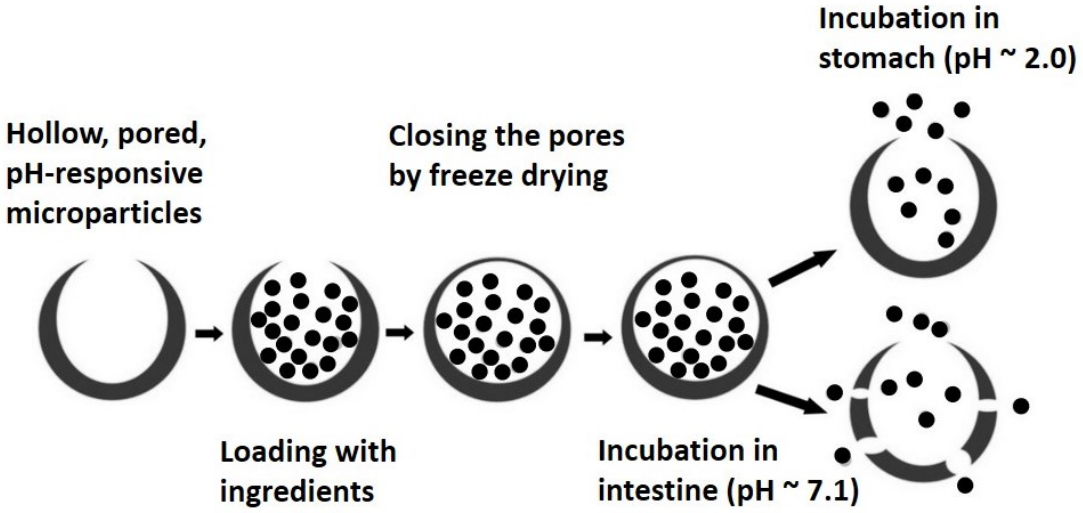

Figure 4. The schematic sequence of polymeric pored microencapsulation/release behavior

1.6. Milestone of the present work

Considering the biological and technical challenges against current microencapsulation systems, we decided to develop new schemes addressing the issues in hand. In the first step, we decided to continue with pored microencapsulation systems previously developed in this group to prevent drug denaturation during the fabrication process of the carriers. In order to increase the throughput of the system, we decided to develop a new facile fabrication process for the particles

with higher fabrication payload in shorter time window. Chapter 2 explains the details of that step of the project.

2. Chapter 2

Facile Fabrication of Microparticles with pH-responsive Macropores for Small Intestine Targeted Drug Formulation

2.1. Preface

Oral drugs present the most convenient, economical, and painless route for self-administration. Despite commercialization of multiple technologies relying on micro- and nanocrystalline drugs, research on microparticles (MPs) based oral biopharmaceuticals delivery systems has still not culminated well enough in commercial products. This is largely due to the drugs being exposed to the destabilizing environment during MP synthesis process, and partly because of complicated process conditions. Hence, we developed a solvent swelling-evaporation method of producing pH-responsive MPs with micron-sized macropores using poly(methacrylic acid-co-methyl methacrylate) in 1:1 ratio (commercial name: Eudragit® L100-55 polymer). We investigated the effects of temperature and evaporation time on pore formation, freeze-drying induced pore closure, and the release profile of model drugs (fluorescent beads, lactase, and pravastatin sodium) encapsulated MPs in simulated gastrointestinal tract conditions. Encapsulated lactase/pravastatin maintained > 60% of their activity due to the preservation of pore closure, which proved the potential of this proof-of-concept microencapsulation system. Importantly, the presence of macropores on MPs can be beneficial for easy drug loading, and solve the problem of bioactivity loss during the conventional MP fabrication-drug encapsulation steps. Therefore, pH-sensing MPs with macropores can contribute to the development of oral drug formulations for a wide variety of drugs and bio-macromolecules, having a various size ranging from genes to micron-sized ingredients with high therapeutic efficacy.

2.2. Methods

2.2.1. Materials

Poly(methacrylic acid-co-methyl methacrylate) in 1:1 ratio, commercially known as Eudragit® L100-55 (hereafter referred to as L100), was obtained from Evonik Canada Inc. (Burlington, Ontario, Canada). 2-Nitrophenyl β-D-galactopyranoside, β-galactosidase from Aspergillus Oryzae, galactose and lactose assay kit, sodium dodecyl sulfate, acetonitrile, and disodium hydrogen phosphate were acquired from Sigma-Aldrich (St Louis, Missouri, USA). Yellow-green fluorescent beads with different sizes (100 nm, 1 μm, and 4 μm) were purchased from Life Technologies (Carlsbad, CA, USA).

2.2.2. Fabrication of pored MPs and pore closure by freeze-drying

To investigate the effect of incubation time of L100 polymer-DCM mixture on the morphology of MPs, the suspension in the sealed container was further stir-incubated at 39 °C (50-60 rpm) in a water bath. This is based on the prediction that the temperature just below the boiling point of the DCM would maximize the diffusion of the organic phase into the polymer matrix. Aliquots (10 mL) were taken over the course of several incubation time intervals (0, 30, and 120 min; abbreviated as MP0 min, MP30 min, and MP120 min, respectively). These samples were dried in a glass petri-dish in an incubator (Isotemp Incubator, Thermo Fisher Scientific). After the initial drying at 65 °C for 30 min, the temperature was brought down to 37 °C for overnight incubation. Subsequently, MPs were collected for further analysis.

Pores on MPs were closed by utilizing a freeze-drying method, following the protocol developed by Kumar et al [145]. Briefly, 20 mg of each sample was suspended in 1 mL DI water, which was then frozen in the liquid nitrogen and freeze-dried using the protocol reported in the above-mentioned study. (AdVantage Pro Freeze Dryer, SP Scientific; Warminster, PA). The presence of residual DCM of MPs was investigated using Fourier transform infrared (FTIR) spectroscopy (Thermo Nicolet NEXUS 870 FTIR ESP, Thermo Fisher Scientific).

2.2.3. Preparation and pH-dependent release behavior of fluorescent bead-encapsulated MPs

Encapsulation ability of MPs based on the size of the ingredients was tested using three different types of fluorescent beads: 100 nm, 1 μm, and 4 μm. In a typical procedure, 50 mg of MP sample from each condition, i.e. MPOriginal, MP0 min, MP30 min, and MP120 min, was added to 1 mL carboxylate-modified yellow-green fluorescent bead solution. The bead solution had been 10-fold diluted in DI water from the original product. Vacuum on/off cycle was applied four to five times to lower the surrounding pressure, replace the air pockets inside the MPs with the ingredients solution and fluorescent beads through the surface pore [145]. Fluorescent bead-encapsulated MPs were subsequently centrifuged at 500 RCF for 2 min (Eppendorf Model 5810; Hamburg, Germany) and collected. Then, the pellets were resuspended in DI water, rapidly frozen in liquid nitrogen, and freeze-dried. Fluorescence microscopy was employed to observe and analyze fluorescent bead-encapsulated MPs.

Freeze-dried samples were washed with a potassium chloride (KCl, 0.2 M)/hydrochloric acid (HCl, 0.2 M) buffer at pH 2.0 (simulated gastric fluid, abbreviate as SGF) twice. Washed MPs

were suspended in the same buffer at 37 °C for 2 hrs to simulate the digestion process of the stomach. The samples were subsequently incubated in a solution composed of KCl (0.05 M), HCl (0.05 M), and Na2HPO4 (0.1 wt%, pH 7.1) at 37 °C for 4 hrs (simulated intestine fluid, abbreviated as SIF). Throughout the whole simulated GI tract digestion process, fluorescence emission was measured every 10 min to monitor the time-dependent release behavior of the fluorescent bead-encapsulated MPs. The excitation wavelength was kept at 490 nm and the emission wavelength was between 500 and 530 nm, with a step size of 1 nm.

2.2.4. Preparation and release/stability tests of lactase-encapsulated MPs

For the encapsulation and stability tests using lactase enzyme, MPs prepared after the incubation for 120 min (MP120 min) were used. This was due to their highest pore/particles size ratio as well as the highest loading ability for larger ingredients. Similar to the encapsulation process for the fluorescent beads, 1 g of MP120 min sample was suspended in the lactase enzyme-containing formulation (20 mg/mL lactase enzyme, 15 wt% trehalose, 5 wt% carboxymethyl cellulose), followed by vacuum cycles for the encapsulation and freeze-drying for the pore closure [145].

After the washing step in SGF solution, the lactase-encapsulated sample was incubated in the simulated GI tract conditions, as described in section 2.3. The concentration of the released enzyme was measured using micro BCA assay kit, and the activity of the released enzyme was assayed using a 2-nitrophenyl β-D-galactopyranoside (ONPG), following the previously reported protocol [145]. Based on the concentration acquired from the BCA assay, three different controls were employed for this part of the experiments: 1) the same concentration of intact enzyme (same as the

concentration measured using micro BCA assay) in SGF as the negative control, 2) the same concentration of the intact enzyme (same as the concentration measured using micro BCA assay) in SIF as the positive control, and 3) the same concentration of the intact enzyme incubated in SGF for 2 hrs and subsequently transferred to SIF.

2.2.5. Characterization methods

Scanning Electron Microscopy (SEM)

The morphology of the MPs was characterized using the scanning electron microscope (SEM; S4800 Electron Microscope; Hitachi, Japan). The pore-particle size ratio of the MPs (acquired from 300 measurements) was measured from the image analysis using Adobe Photoshop CS3. The image analysis was performed to study the effects of the fabrication protocol on the samples, the effects of solvent evaporation on the pore formation or pore extension in MPs, and to evaluate the pore closure efficiency of the freeze-drying process. The SEM images were also used for measuring the number ratio of the number of pored particles divided by the total number of particles to monitor the effect of the solvent evaporation process on the extension or formation of the surface pores on MPs. In a typical procedure, MPs in the powder form were placed uniformly on a double-sided carbon tape. The sample was coated with a 7-nm gold layer to minimize the charging effect and observed at 15 kV (20 μA). To observe the pH-dependent change in morphology of MPs, 40 μL of the sample solution obtained at each time interval. This solution was carefully dropped on a glass coverslip and the major portion of the water was quickly removed

by a filter paper using the blotting technique, and the sample was further dried in a fume hood at RT.

Fluorescence Microscope

An Olympus IX81 inverted microscope (Olympus, Germany), coupled with a DP 80 digital camera and dual CCD sensor, was used for the fluorescence microscopy analysis. The images were recorded at the 40X objective (Olympus LCPlanFl, 1 μm depth of field, NA 0.6) using CellSens software (Olympus, Germany). Sample solutions obtained from the release test at different time intervals were placed on a glass slide, covered with a glass coverslip, and imaged using FITC filter sets.

2.2.6. Statistics

Student's t-test and One-way ANOVA in Minitab software (State College, PA, USA) were utilized for analyzing the data. A *P*-value of less than 0.05 implied a significant difference.

2.3. Results

Previous work reported a technique to produce MPs with a pH-responsive single pore on their surfaces by controlling the evaporation rate of the organic solvent in the emulsion [145,151]. The protocol was effective in fabricating hundreds of nanometer-sized macropore on MPs of a few micrometers in size. However, it was not successful in producing MPs with micron-sized macropores. In this study, swelling of original L100 particles with dichloromethane (Tb: 39.6 °C, abbreviated as DCM), followed by the solvent evaporation was used to form new pores and/or

increase the size of the existing pores. The effects of process parameters on forming MPs with micron-sized macropores and their potential as a small intestine-targeted drug delivery system has been evaluated below.

2.3.1. Fabrication of MPs with macropores

Effects of preincubation in solvent on pore formation

To further evaluate the effects on the pore size by swelling in DCM solvent, L100 powders were preincubated at 39 °C for three different time intervals (0 min, 30 min, and 120 min) prior to solvent removal by incubation at 65 °C (30 min)/37 °C (overnight). Their pore-to-MP size ratio was characterized by SEM analysis. The as-prepared samples were abbreviated as MP0 min, MP30 min, and MP120 min, respectively. As shown in Figure 5, pores in MPs were greatly expanded with the longer incubation time in the solvent. As shown in the histograms for the pore-to-MP size of Figure 5, the population peak shifted to the right with the increase of preincubation time, indicating the increase of pore size with incubation (One-way ANOVA, $P < 0.001$).

The average diameters of the pores were measured to be 1.8 ± 1.6 μm (MP0 min), 2.2 ± 1.6 μm (MP30 min), and 3.1 ± 2.8 μm (MP120 min) from samples at three different incubation time in DCM before solvent evaporation (see Fig. 6). As a result, 120 min incubation in DCM, followed by evaporation at 65 °C for 30 min and at 37 °C overnight, generated the most pored MPs with the largest pore size among all the conditions tested in this study. These results suggest that the size of MP surface pores strongly depends on the incubation time in the solvent. Furthermore, a higher degree of swelling of L100 polymer in DCM, followed by evaporation, plays an important role in

producing MPs with larger pores. This can be further supported by comparing SEM images of fractured MPOriginal and MP120min samples (see Fig. 5 e and f for representative SEM images). Freeze-drying of the MP samples resulted in two types of MPs: MPs with closed pores and few MPs with unsealed pores (see Fig. 6c for SEM images of freeze-dried MPs and 3d for the size distribution of remaining pores). Similar to the observation in Fig. 6 c and d, while the majority of freeze-dried MPs exhibited closure of their pore-mouth, MPs with incomplete pore closure also showed a significant decrease in their pore size due to freeze-drying (compare Figs. 5 c and a for morphological evolution of pored MPs, and Figs. 5 b and d for pore-to-MP size distribution).

As shown in Fig. 6, the average diameter of unsealed pores was analyzed to be 1.5 ± 1.2 μm (MP0min), 1.8 ± 1.2 μm (MP30min), and 2.0 ± 1.5 μm (MP120min). These analyses clearly demonstrate the effectiveness of the freeze-drying process in sealing the pores of MPs.

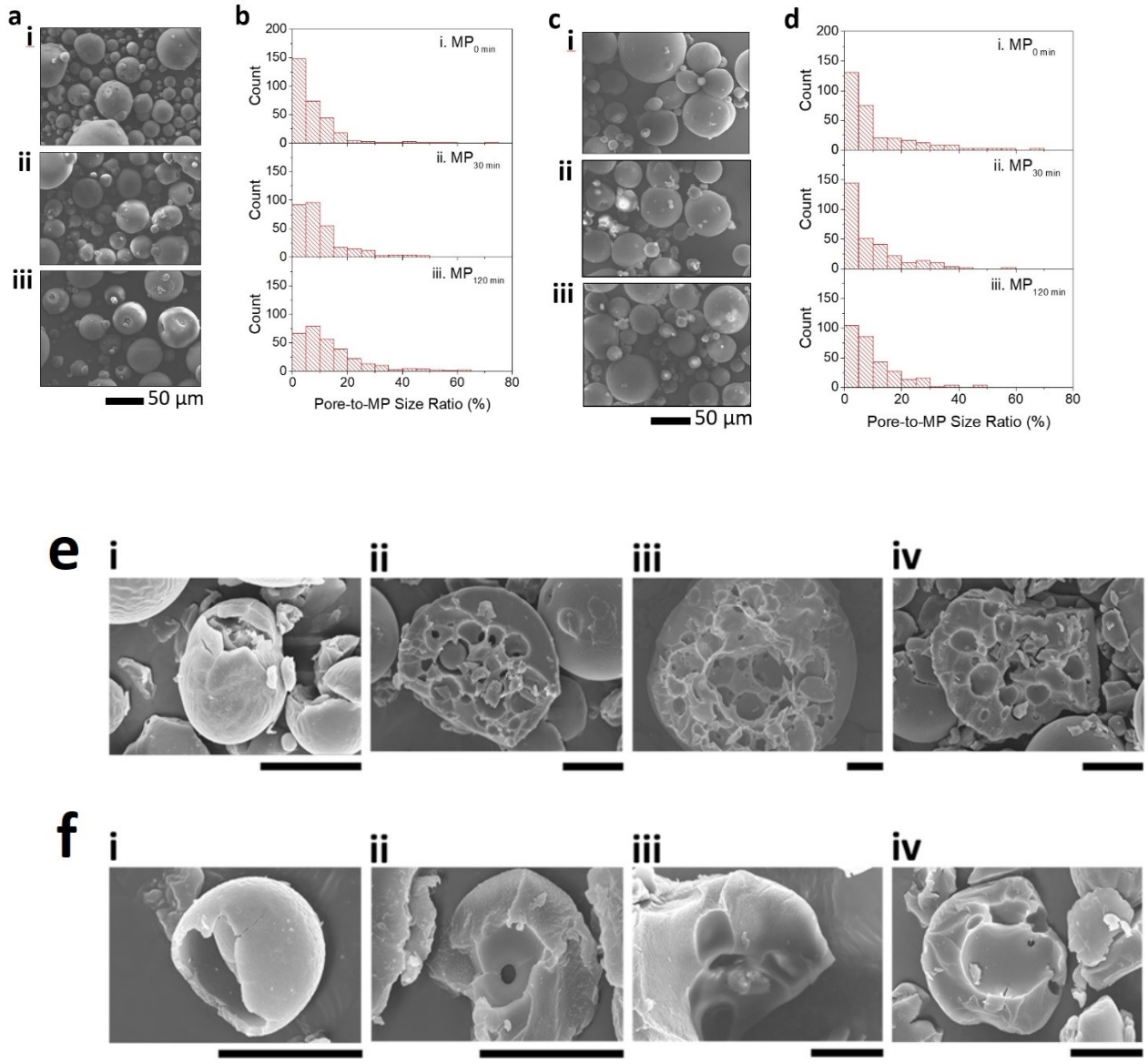

Figure 5. Effects of preincubation in DCM on pore formation. a) Histogram of pore-to-MP size ratio and b) its corresponding SEM images: i) MP0 min, ii) MP30 min, and iii) MP120 min (n = 300). c) Histogram of pore-to-MP size ratio measured from MPs with unsealed, d) its corresponding SEM images: i) MP0 min, ii) MP30 min, and iii) MP120 min (n = 300). e and f) SEM images of cross-sectional view of e(i-iv) MPOriginal and f(i-iv) MP120min. Scale bar in e and f represents 20 µm and 10 µm, respectively (prepared by Bahman Homayun and Chengmeng Sun collaboratively).

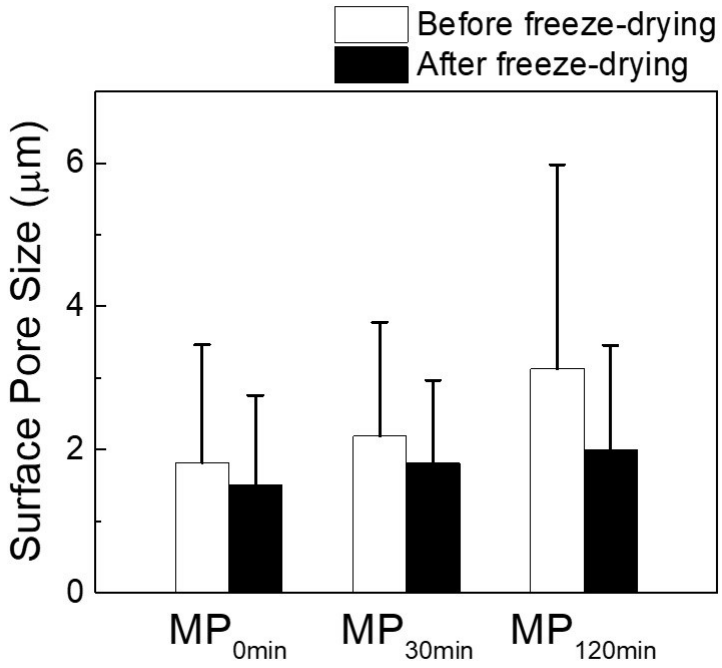

Figure 6. Effect of freeze-drying on the average surface pore sizes of MP0 min, MP30 min, and MP120 min. Since freeze-drying induces closure of pores, the pore sizes after freeze-drying in the plot represent those measured from MPs with unsealed pores. (n = 300; prepared by Bahman Homayun and Chengmeng Sun collaboratively).

2.3.2. Encapsulation and release test of MPs with macropores

Fluorescent beads-encapsulated MPs

Three different sizes of fluorescent beads (i.e. 100 nm, 1 μm, and 4 μm) have been incorporated into MPs through their surface pores by applying vacuum/release cycles, in order to evaluate their encapsulation/release characteristics. Subsequently, MPs were exposed to the simulated GI tract pH conditions for monitoring time-dependent release behavior.

Fig. 7 represents release profiles measured from fluorescent beads-encapsulated MPs by monitoring fluorescence intensity changes (Fig. 7a: 100 nm, Fig. 7b: 1 μm, and Fig. 7c: 4 μm). As shown in Fig. 7a, all MP samples could successfully encapsulate 100 nm-sized fluorescent nanobeads and remain intact in SGF. On the other hand, micron-sized beads could be only encapsulated into MP30min and MP120min, which can be explained by the presence of larger pores (> 2 μm) as shown in Fig. 7 a and b (see Fig. 7 b and c for time-dependent release profile).

The examination of the release profile also shows that within 20 min, MPs exhibit initial release of fluorescent beads upon exposure to SGF, followed by a slow rise or saturation in the release profile of up to 5–34% over the course of 2 hr-incubation. Transferring the bead-loaded MPs to SIF, however, led to a faster release of beads (~ 90–100%) within 10 min. The initial release profile during 2-hr incubation in SGF can be explained mainly by the release of fluorescent beads from MPs with partially sealed pores. At the same time, the observed plateau during incubation in SGF prior to a fast release in SIF indicates the maintenance of the intact MP structure with closed pores in the simulated gastric environment. The secondary rapid change in the release profile upon exposure to SIF after 2 hrs of incubation in SGF can be associated with the release of fluorescent beads from i) opening of the pH-responsive macropores or ii) dissolution of MP polymer matrix. This step-wise release profile in response to GI tract pH conditions was similarly observed for pored MPs fabricated using o/w emulsion technique [145]. Furthermore, these studies proved the efficiency of this new fabrication protocol for developing the pored microencapsulation system.

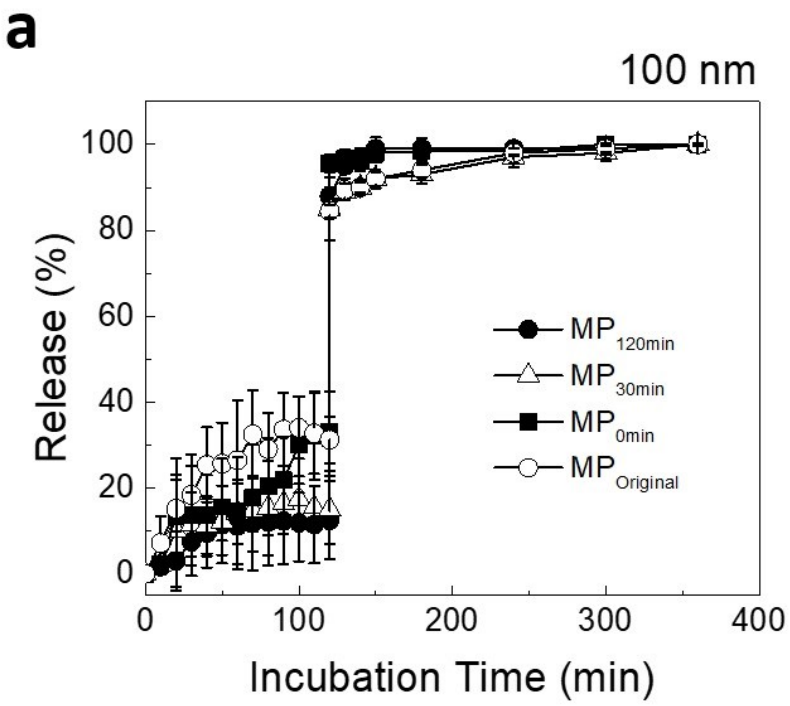
a
100 nm
Release (%)
Incubation Time (min)
MP120min
MP30min
MP0min
MPOriginal

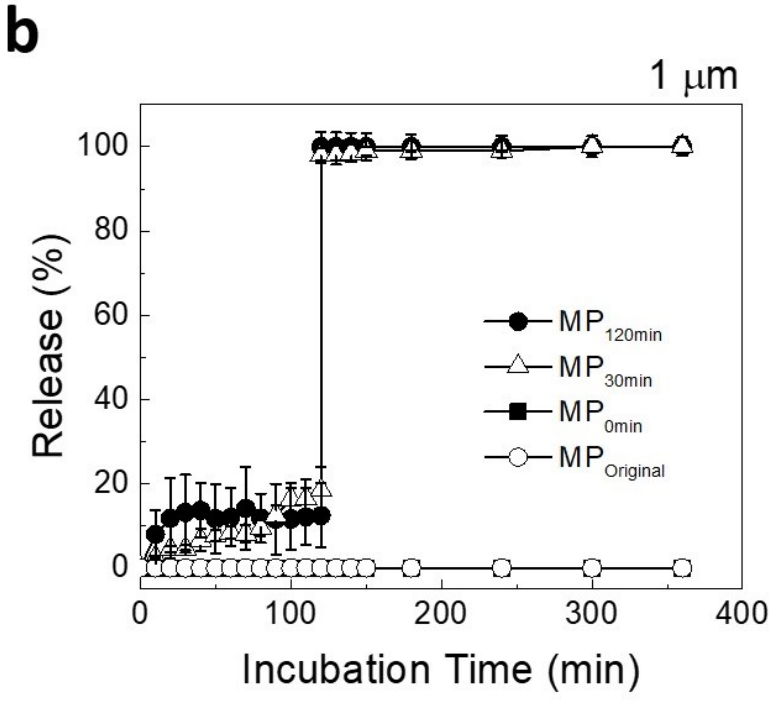
b
1 μm
Release (%)
Incubation Time (min)
MP120min
MP30min
MP0min
MPOriginal

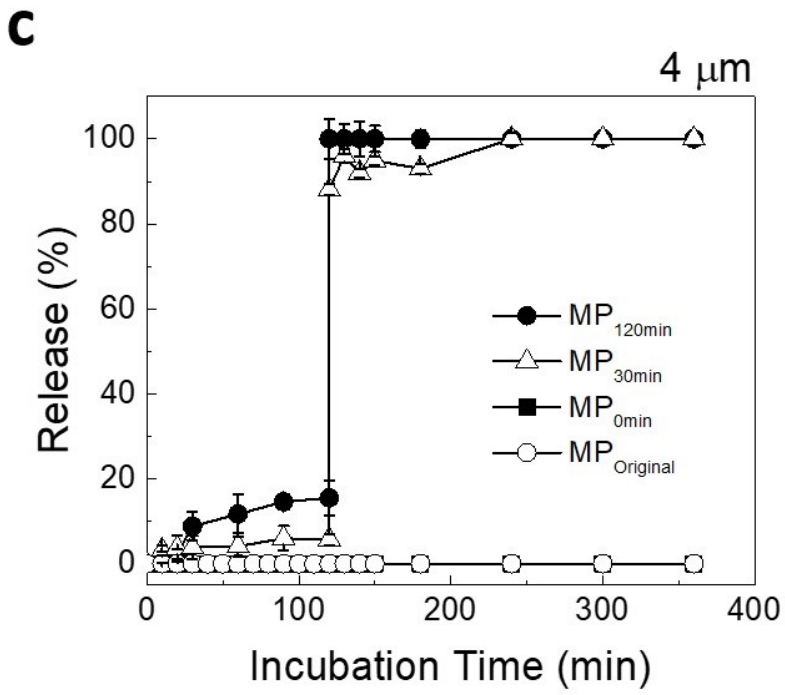

Figure 7. Release of fluorescent beads from MPs in simulated GI conditions. Time-dependent release profile of encapsulated (a) 100 nm fluorescent nanobeads, (b) 1μm microbeads, and (c) 4 μm microbeads from MPs (MPOriginal, MP0 min, MP30 min, and MP120 min) subjected to simulated GI tract environment (SGF: 2-hr incubation at pH 2.0 and 37 °C, and SIF: 4-hr incubation at pH 7.1 and 37 °C). Release rate of fluorescent beads was calculated by measuring the relative fluorescent intensity of a sample (i.e. fluorescent intensity of a sample relative to that of a control with a complete release at pH 7.1) To achieve a complete release, fluorescent bead-encapsulated MPs were vortexed for 5 min after 4-hr incubation at pH 7.1. (n=5, mean SD)

Fluorescence microscopy analysis was performed to monitor pH-dependent release behavior of MPs over the course of incubation in the simulated GI digestive conditions. As shown in Fig. 8a, fluorescent nanobead-encapsulated MPs upheld their intact spherical morphology during the 2 hrs of incubation in SGF. However, when the MPs were subjected to SIF, the majority of encapsulated fluorescent beads were released from the MPs within 10 min (see Fig. 8a), which is in agreement with our observation in Fig. 8.

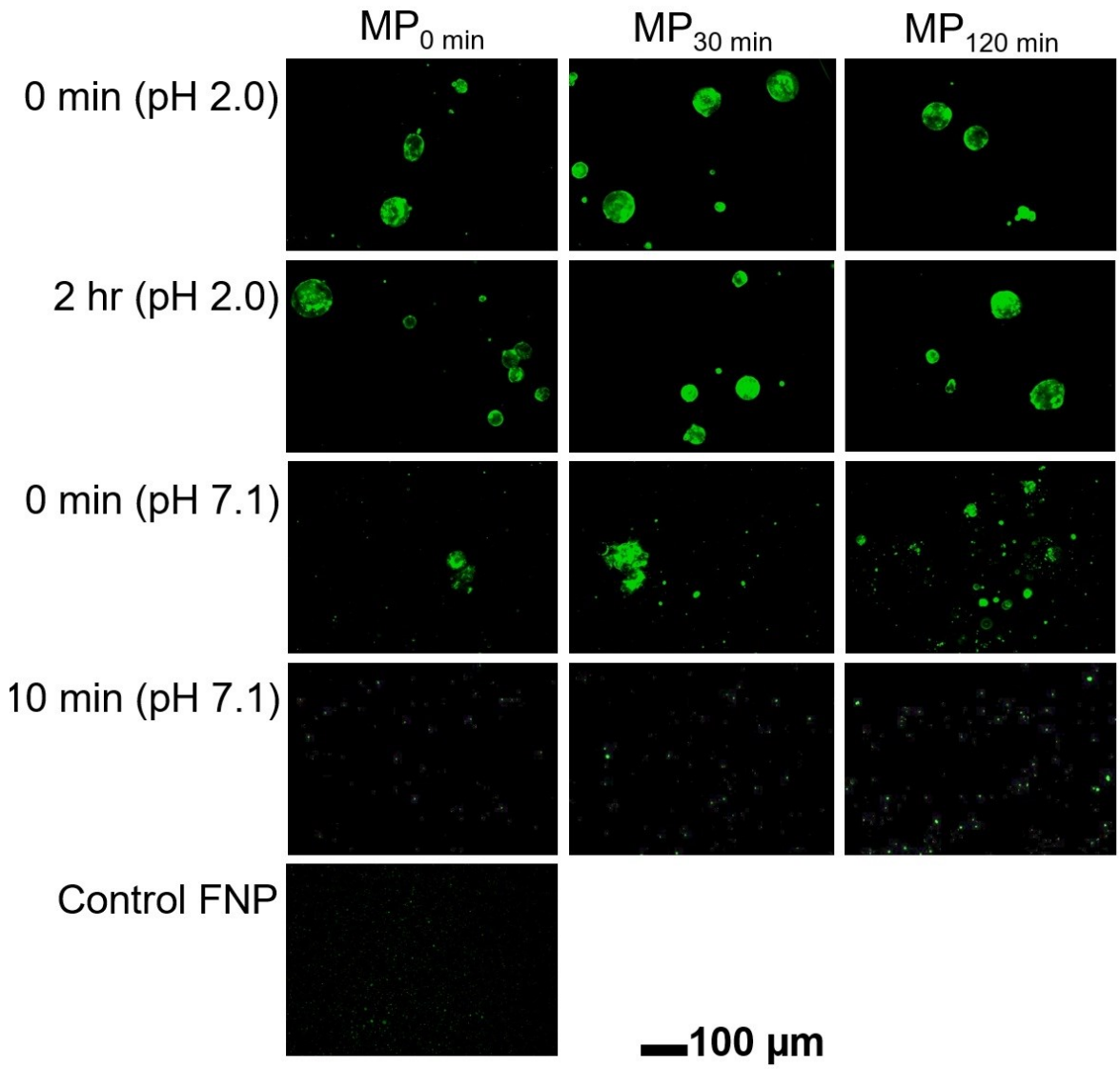
MP0 min
MP30 min
MP120 min
0 min (pH 2.0)
2 hr (pH 2.0)
0 min (pH 7.1)
10 min (pH 7.1)
Control FNP
100 µm

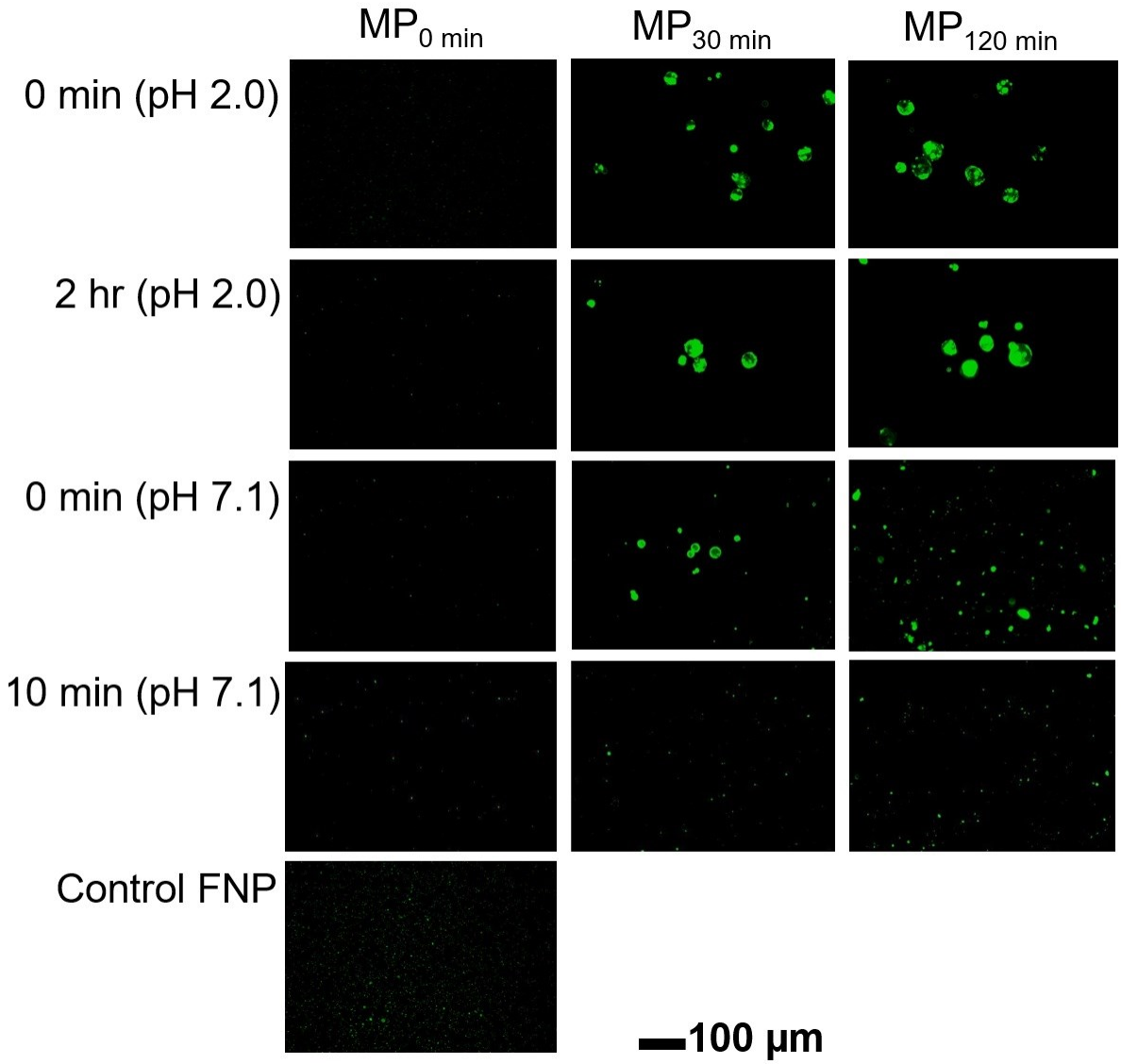
MP0 min
MP30 min
MP120 min
0 min (pH 2.0)
2 hr (pH 2.0)
0 min (pH 7.1)
10 min (pH 7.1)
Control FNP
100 µm

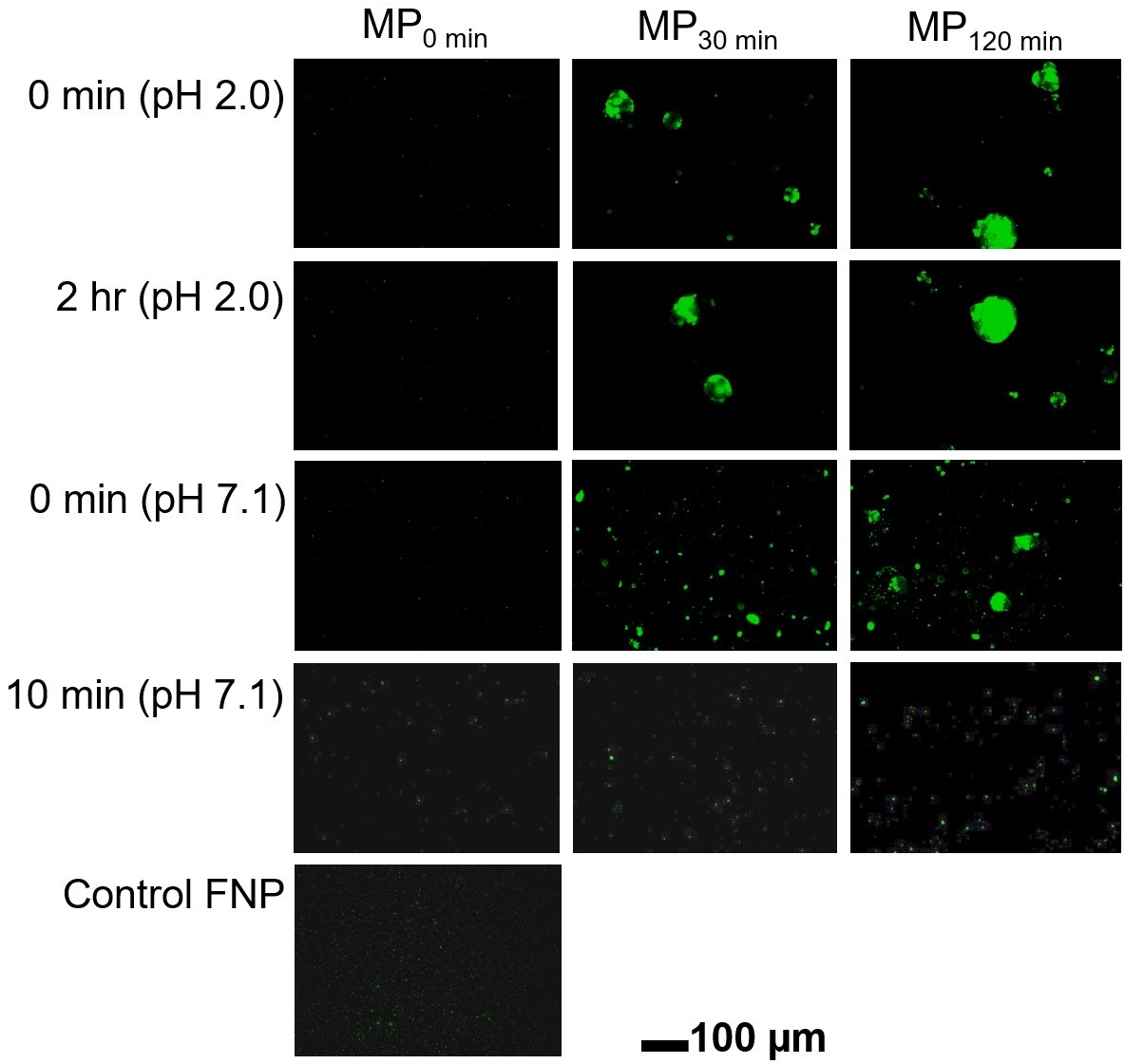

Figure 8. Fluorescence microscopy of fluorescent beads-encapsulated MPs. Representative fluorescence micrographs of (a) 100 nm fluorescent nanobead-, (b) 1 µm microbead-, and (c) 4 µm microbead-encapsulated MPs subjected to simulated GI tract environment (SGF: 2-hr incubation at pH 2.0 and 37 °C, and SIF: 4-hr incubation at pH 7.1 and 37 °C). As a control, fluorescent micrographs of fluorescent microbeads without MPs are shown for comparison.

Also, in the case of 1 μm and 4 μm beads-encapsulated MPs, majority of fluorescent beads leaked out of MPs after 10 min of incubation in SIF, as can be clearly seen by comparing the fluorescent microscope images at different time intervals to the control group (fluorescent beads only) (Fig. 8 b and c). An important aspect of this observation is that the release of ingredients is not dependent on their sizes, as opposed to previous observation for emulsion-based S100 MPs [145]. Similar to the results presented in Fig. 8, this can be explained by the rapid pore opening/dissolution behavior in the neutral pH environment. Therefore, this study qualitatively illustrates that this pored MP system can encapsulate a variety of drugs (e.g., from tiny molecules to micron-sized ingredients), and shield them from gastric fluids, and then rapidly discharge them in the intestinal environment.

β-galactosidase-encapsulated MPs

The encapsulation of fluorescent beads provided helpful information about their loading capacities, their persistent behavior in SGF environment, and their release performance in SIF environment. The results, however, do not provide information about the preservation efficiency of the MPs encapsulating biopharmaceuticals. To this end, pH-vulnerable enzyme-- β-galactosidase from Aspergillus Oryzae, was encapsulated into MP120min, and its remaining activity was measured using ONPG assay in the simulated GI digestive conditions. Fig. 9 represents the activity of the released enzyme in comparison with the intact enzyme. It is noted that unprotected enzyme lost almost all its activity in the simulated gastric environment (Lactase (pH 2.0) in Fig. 9; t-test, $P < 0.001$) and does not recover when transferred to the simulated intestinal medium (Lactase (pH 2.0>7.1) in Fig. 9; t-test, $P < 0.001$). On the other hand, the enzyme

released from the MP120min (Lactase-MPs (pH 2.0>7.1)) exhibited about 63.7 ± 5.8% of the activity of the intact enzyme with the same concentration, incubated only in intestinal conditions (i.e. positive control, Lactase (pH 7.1) in Fig. 9).

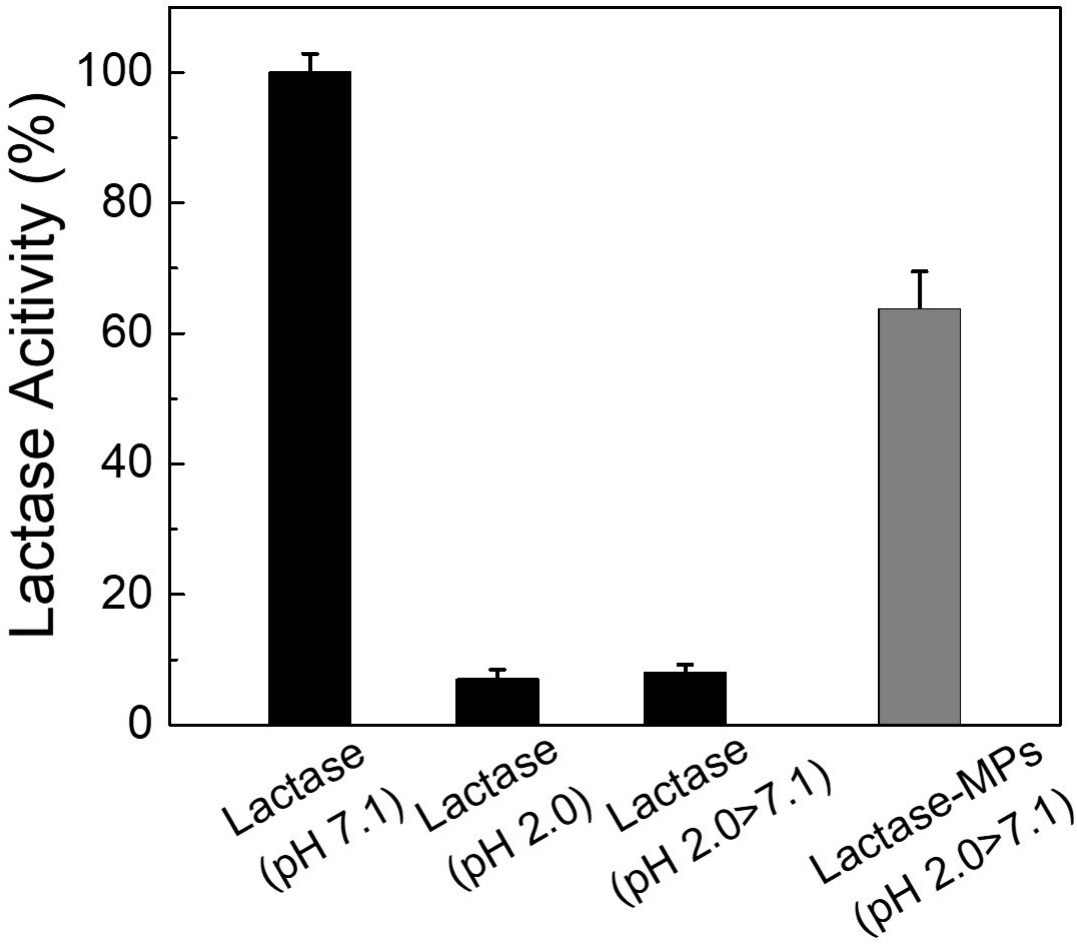

Figure 9. Protective effect of the MPs on lactase functional activity. The remaining activities of lactase after 4-hr incubation at pH 7.1 (Lactase (pH 7.1)), lactase after 2-hr incubation at pH 2.0 (Lactase (pH 2.0)), lactase after incubation in simulated GI conditions (i.e. 2-hr incubation in SGF, followed by 4-hr incubation in SIF; Lactase (pH 2.0>7.1)), and MP-encapsulated lactase after incubation in simulated GI conditions (Lactase-MPs (pH 2.0>7.1)). (n = 5, mean ± SD)

This notable improvement in the protection efficiency of the MPs can be attributed to the maintenance of pore-closure state at acidic pH, consistent with the previous data from fluorescent beads in Figs. 7 and 8. Therefore, our results further indicate that i) pore-closure efficiency by the freeze-drying process and ii) maintenance of closed pores in the gastric environment are critical factors in preserving a higher level of stability and therapeutic efficacy of MP-based drug formulations.

2.4. Discussion

An emulsion-free microencapsulation system was designed to overcome the technical challenges of the current MP-based drug delivery systems, including the exposure of drugs to organic solvents during the particle fabrication stage, loss of bioactivity in the GI tract, and low production yield. The novelty of this approach was developing a facile protocol for fabricating large-size pored MPs and using their surface pore of MPs for the encapsulation and release of drug/vaccine due to pH-dependent pore closing/opening behavior. Microemulsion method was previously applied to make a few micron-sized MPs with hundreds of nanometer-sized pores for their application in the delivery of small-molecule of drugs, having size of a virus. However, it was difficult to employ the same process to make tens of micron-sized MPs with a few micrometer-sized pores that would have the capability of encapsulating and delivering a wide range of macromolecular drugs.

To solve aforementioned technical problems, L100 MPs that have pH-responsive pores were produced by a newly modified solvent evaporation method, based on the observation that the L100 polymer powder consists of MPs with surface pores. The initial research efforts were focused to

evaluate the solvent evaporation conditions for maximum pore formation and to verify the pore closure by the freeze-drying process. Under the test conditions, it was found that a longer incubation in the solvent and evaporation at a higher temperature resulted in the most promising pored MPs (i.e. MP120 min). The increase in the size of the surface pores can be attributed to the diffusion of a higher quantity of the organic phase into the particles during the incubation period, whose subsequent evaporation generated strong vapor flux to expand the pores [118]. Specifically, the solvent evaporation rate and degree of solvent swelling of polymers are critical factors in forming new pores and/or widening existing pores. This was confirmed through image analysis of MPs by measuring the pore/particle size ratio and the pored particles/total particles number ratio.

The controllable stimuli-sensitive surface pores can be used for direct solvent-free encapsulation of ingredients as well as their fast release at the target [145]. The extent of pore closure is critical to ensure the efficacy of drugs against the harsh acidic environment of the stomach. As shown in Figs. 5c and 5c, freeze-drying process induced an effective closure of a few micron-sized pores on MP surface. It is important to observe that unlike the previous findings from the emulsion-based MPs, these MPs did not exhibit ingredient size-dependent release behavior. Faster release by the L100 MPs in comparison with MPs made of S100 can be attributed to their different release mechanisms. Compared with S100 with a pKa of 6.8, L100 with a lower pKa (~ 5.5) will induce instantaneous deprotonation of carboxylic groups, leading to a rapid disentanglement/dissolution of MPs in the intestinal pH. In the case of S100 MPs, ingredient release is triggered by the opening of the surface pores due to a slow dissolution of MP matrix. However, the release mechanism of L100 MPs, having easily ionizable moieties, may depend on both the dissolution of MP matrix and the pore opening. This hypothesis is supported by comparing different release patterns from S100 and L100 MPs. In the case of S100 MPs prepared by emulsion,

a rapid pore opening upon exposure to SIF resulted in the release of ingredients. This explains why release rate depended on the size of ingredients (i.e. slower release for larger ingredients), as proven in the previous report [145]. On the other hand, L100 MPs with pH-responsive pores formed by solvent evaporation exhibited the burst-release mechanism. MP matrix dissolved rapidly in addition to the pore opening in SIF. Interestingly, regardless of the size of the ingredients loaded, L100 MPs displayed similar release patterns, i.e. in a size-independent manner, supporting our hypothesis (see Fig. 7). The lower pKa of the polymer will also ensure the release of the drug in the intestine since some animal studies have shown that intact S100 MPs may leave the body without releasing the drug [152,153]. Considering that the drug release depends between the competitive mechanisms of matrix dissolution and pore opening, our observation implies that the swelling/dissolution behavior of anionic polymers through the deprotonation of the carboxylic acid groups exerts a significant impact on the release behavior of ingredients-encapsulated MPs with macropores.

The practicality of the pored MPs was evaluated by quantifying the release behavior and the remaining activity of lactase and pravastatin in the simulated GI environment. The reasons for selecting these drugs were: 1) they are completely denatured once placed in the gastric conditions ($pH \leq 2.0$), 2) once denatured in the acidic conditions, they do not recover their intact structure when transferred to a neutral environment, 3) they maintain the highest level of activities in the intestinal environmental conditions. In the test conditions, about one milligram of lactase was encapsulated into one gram of MPs. The loading efficiency of the pored MP system will substantially be a function of the drug solution concentration and the amount of the added MPs. Importantly, since the encapsulation step is merely a physical process and does not induce any concern about the drug denaturation/instability, the non-encapsulated drug solution can be

recovered by centrifugation process and reused by new MP powders, minimizing the loss of drugs. Therefore, it is believed that not only small drugs such as lactase and pravastatin but also many large molecule drugs that have complicated structures (e.g., vaccines) can also be encapsulated into our MPs.

All these analyses confirm the efficiency of our fabrication protocol for fulfilling the requirements of an innovative pored microencapsulation system: open pore for direct encapsulation, followed by an efficient pore closure state to preserve the loaded ingredients, and finally provide a complete release at the target sites. According to ICH guideline, dichloromethane used in MP fabrication is classified into the second group (class 2) with 6.0 mg/day of permissible daily exposure limit (PDE; concentration limit: 600 ppm) [154]. Despite the need of the systematic investigation on the residual solvent and its toxicity effects, in this work, FTIR analysis showed no evidence of residual solvent for the MP120min by comparison with spectra of MPOriginal and DCM (Fig. 10). This supports the possibility of eliminating concern over residual organic solvent by controlling oven incubation time and temperature for MP fabrication, and freeze-drying recipe. In future, the efficiency of solvent evaporation process in pore formation and the polydispersity of the MPs fabricated using this protocol will be investigated for more favorable intestinal absorption. Also, in vivo demonstration will be carried to prove the efficacy of our MP system.

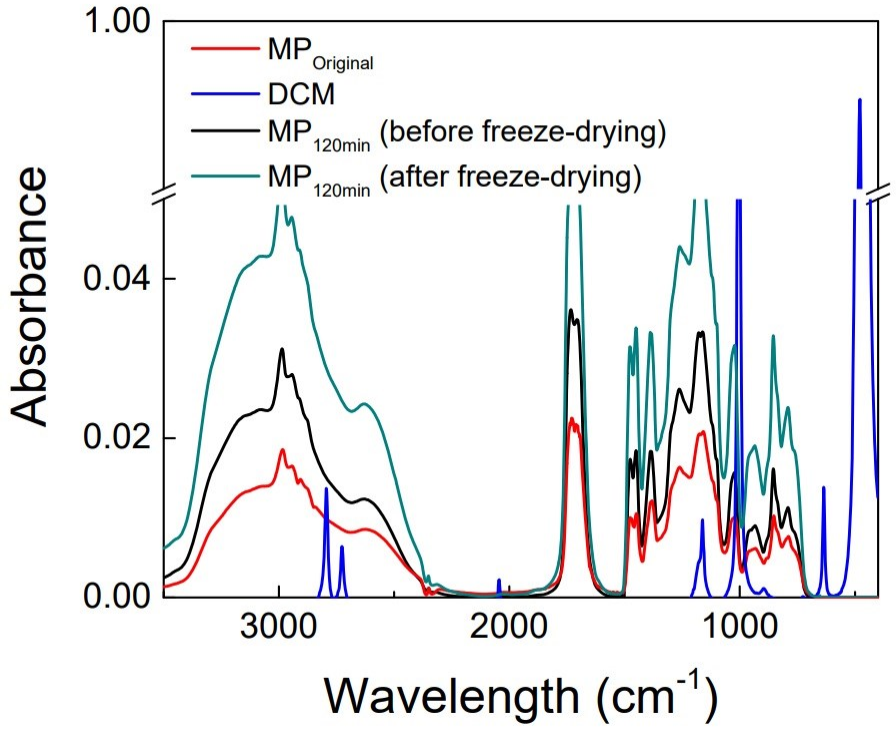

Figure 10. FTIR spectra of MPOriginal, DCM, MP120min (before freeze-drying), and MP120min (after freeze-drying).

2.5. Conclusion

This research strives to develop a universally applicable and highly efficient oral drug delivery system, targeting small intestine. Here we report a new fabrication protocol for pored MPs that have surface pores wide enough for easily encapsulating ingredients as large as 4 μm. Also, our MP system would rapidly respond to the desired environmental pH and completely release the encapsulated drugs. The presence of the surface pore allows for the direct encapsulation of drugs and distinctively separates the MPs' fabrication process from the drug loading step. This, in turn,

resolves concerns regarding the denaturation of the drug due to its direct contact with harsh organic solvents or because of high shear stresses during emulsification process in microemulsion delivery systems. The observation of a higher level of remaining activity (> 60%) of encapsulated drugs demonstrates the applicability of our pored MPs. Therefore, the system has the potential to be further investigated for the encapsulation/delivery of biomolecules and other large size ingredients.

3. Chapter 3

A novel microencapsulation design and formulation for successful oral drug delivery

3.1. Preface

Microparticles (MPs) with pH-responding macropores have recently proved their significance for the delivery of vulnerable biomolecules for oral drug administration. The previous MP systems were proven to provide enhanced protection against the gastric environment, however, were suffering from insufficient loading efficiencies and deficient penetration capability of encapsulated drugs across the mucus barrier. The present work introduces a new co-delivery approach based on amine-functionalized halloysite nanotube (HNT)-embedded MPs (amine-HNT-MPs) with pH-responding macropores specifically designed for dealing with the mucus barrier in the absorption site. The results implied significant improvements in the drug loading capacity of the system compared to the previously developed pored MPs. This is due to the improvements in the size of the surface pores and interior void spaces of the particles. Also, efficient pore sealing of the new MP system after the encapsulation of the drug showed a considerable improvement in the preservation of the therapeutics against gastric conditions. The amine-HNTs on the surface of the MPs modified the surface charge of the MPs for better interactions with the mucosal layer. Furthermore, a mucolytic enzyme (i.e. bromelain)-loaded HNTs played a significant role in facilitating the diffusion of drugs through the mucus barrier. Apart from the quality of the MPs, the new fabrication protocol offered promising payload in a reasonable time, which can be easily scaled up to an industrial application. The new microencapsulation design proposed in this study provides a promising solution to the major issues hampering the wide-spread application of MPs to the development of oral drug formulations for biopharmaceuticals and vaccines.

3.2.Materials and Method

3.2.1. Materials and Chemicals

Poly(methacrylic acid-co-methyl methacrylate) in 2:1 ratio, known as Eudragit® S100, and Poly(methacrylic acid-co-methyl methacrylate) in 1:1 ratio, known as Eudragit® L100-55 (hereafter referred to as S100 and L100, respectively), were received from Evonik Canada Inc. (Burlington, Ontario, Canada). Halloysite nanoclay, 2Nitrophenyl β-D-galactopyranoside; poly (vinyl alcohol) (PVA) Mw: 9,000–10,000; D-(+)-Trehalose dehydrate; Carboxymethylcellulose (CMC) sodium salt (low viscosity); and β-galactosidase from Aspergillus oryzae were purchased from Sigma Aldrich (St Louis, Missouri, USA). Yellow-green fluorescent nanoparticles (FNPs) with different sizes (100 nm and 1 μm) were purchased from Life Technologies (Carlsbad, CA, USA). And detergent Tween 20, Fisher BioReagents, was purchased from Fisher Scientific (Mississauga, ON, USA).

3.2.2. Fabrication of MPs

Small and Large S100 MPs

Small S100 MPs with pH-responsive macropores (MPs with an average diameter of 1-2 μm) were fabricated following the procedure reported previously [46]. Briefly, 10 ml of organic phase (5 wt% S100 dissolved in the cosolvent system (dichloromethane:ethanol:isopropanol = 2: 1:1)) was added to 200 ml of the aqueous phase (0.5 wt% PVA and 5% Tween 20), stirred at 600 rpm and sonicated at 50 W for 5 min using a GE-130 ultrasonic processor (Sonics & Materials, Inc.; Newtown, CT). The emulsion was stirred at 125 rpm at room temperature for 1 hour to allow

the formation of MPs through solvent extraction/evaporation. The emulsion was filtered using a sieve (Fisherbrand™ U.S. Standard Brass Test Sieves, 45 μm mesh size; Ottawa, ON, CA), centrifuge-washed at 15000 g in DI water 4 times (Eppendorf Model 5810; Hamburg, Germany), and finally filtered through Whatman filter papers (grade 5) to collect small MPs (≤ 2.5 μm).

In the next step, the emulsion formulation and the fabrication conditions were slightly modified to increase the average diameter of the MPs, their interior space and their surface pore size. To this aim, 10 ml of the organic phase was added to 200 ml of the aqueous phase, stirred at 325 rpm and sonicated at 15 W for 5 min. The emulsion was stirred at 125 rpm at room temperature for 1 hour to allow the formation of MPs through solvent extraction/evaporation. The suspension was then filtered using the same sieve, and the filtered particles were centrifuge-washed in DI water 4 times at 10,000 g for 10 min. In order to control the polydispersity of the sample, the final suspension was intensely vortexed, followed by centrifugation at 100 g for 1 min, and the MPs suspended in the supernatant were collected (hereafter referred as the large S100 MPs).

The MPs were subsequently divided into aliquots of 1 ml, transferred into 2 ml Eppendorf tubes, plunged into liquid nitrogen and finally freeze dried (AdVantage Pro Freeze Dryer, SP Scientific; Warminster, PA) according to the lyophilization cycle already published elsewhere [16,17,46]. The freeze dried powder was divided into aliquots of 30 mg for further analyses. In the first step, the samples were analyzed before and after freeze-drying to investigate the effects of lyophilization on the pore closure of the MPs.

Amine functionalization of HNTs (Amine-HNTs)

HNTs were amine-functionalized through the method previously reported [47]. Briefly, 3 g of HNTs were suspended in 120 ml of toluene through 5 min sonication at 20 W. 10 ml of (3-aminopropyl)triethoxysilane was added to the mixture, sonicated for another 5 min, heated at 120 °C and stirred under the protection of N_2 for 20 hours. The HNTs were centrifuged at 5,000 g for 20 min, washed five times in fresh toluene and twice in ethanol. The remaining solvents were dried out through vacuum rotary evaporator under 15 kPa at 95 °C for 3 hours and 37 °C overnight.

Fabrication of HNT-embedded S100 MPs (HNT-MPs)

HNT-S100 MPs were also fabricated using emulsion-solvent evaporation technique. 500 mg HNTs were added to 200 ml of aqueous phase, stirred at 325 rpm and sonicated at 15 W for 5 min. Subsequently, 10 ml of the organic phase was added to the mixture, and HNT-S100 MPs were fabricated following exactly the same fabrication steps as described for large S100 MPs in section 2.2.1.

3.2.3. Encapsulation of drugs into HNTs and MPs

Loading into HNTs

To prove the concept of amine-HNT-MP system for co-delivery applications, amine-HNTs were loaded with a model drug, sulforhodamine B (SRB), inside the vacuum oven for pH-dependent loading/release behavior. Briefly, amine-HNTs in the aliquots of 200 mg were suspended in 10 ml SRB-containing formulation (1 mM SRB, 15 wt% trehalose, 0.5 wt% CMC),

followed by applying vacuum on/off cycles. The amine-HNTs loaded with SRB (SRB/HNT) were then collected from the bottom of the tubes and freeze dried. The lyophilized HNTs were coated with L100: they first were suspended in 50 mg/ml L100 in ethanol solution, then gently stirred (~ 300 rpm using magnetic stir bar) for 1 min and finally dried under fume hood for about 2 to 3 hours. The same process was used for loading amine-HNTs with bromelain (bromelain/HNT), a mucolytic enzyme: 200 mg amine-HNTs were suspended in bromelain-containing formulation (20 mg/ml bromelain, 15 wt% trehalose, 0.5 wt% CMC) encapsulated in a vacuum oven, freeze-dried, and coated with L100.

Loading into MPs

HNT-MPs were fabricated according to the protocol explained in section 2.2 using drug-loaded amine-HNTs. The lyophilized amine-HNT-MPs were divided into aliquots of 30 mg in 2 ml Eppendorf tubes, and 1 ml of the model drug solution (100 nm FNPs, 10-fold diluted in DI water) was added to each tube. The MPs were encapsulated under vacuum on/off cycles. Loaded HNT-MPs were resuspended in DI water, frozen in liquid nitrogen, and finally freeze dried under the same protocol. A similar encapsulation method was used for the real drug. Briefly, amine-HNT-MPs were suspended in drug formulation (20 mg/ml lactase, 15wt% trehalose, 0.5wt% CMC), encapsulated using vacuum on/off cycles, resuspended in DI water, and frozen in liquid nitrogen, followed by freeze-drying.

3.2.4. pH-dependent release behavior

Stability/release of model drugs (SRB and FNPs) loaded into MPs

Lyophilized, encapsulated amine-HNT-MPs were first washed in potassium chloride (KCl, 0.2 M)/hydrochloric acid (HCl, 0.2 M) buffer at pH 2.0 as the simulated gastric fluid (SGF). Washed MPs were resuspended in the same buffer (SGF) and incubated at 37 °C for 2 hours to simulate the stomach environment. The MPs were subsequently transferred to another solution composed of KCl (0.05 M), HCl (0.05 M), and Na_2HPO_4 (0.1 wt%, pH 7.1) as the simulated intestinal fluid (SIF) and incubated at 37 °C for 4 hours. The encapsulation/release behavior of the MPs during the course of 6 hours of simulated digestion process was monitored through an Olympus IX81 inverted fluorescence microscope (Olympus, Germany) and a Flexstation 3 benchtop multi-mode microplate reader (Molecular Devices; Sunnyvale, California, USA). Noteworthy, for fluorescence microscopy analysis, amine-HNT-MPs were loaded with both SRB (into a hollow interior of HNTs), abbreviated as amine-SRB/HNT-MPs, and FNPs (into a hollow interior of MPs), abbreviated as amine-HNT-FNPs/MPs, to evaluate the encapsulation/release behavior of the system for co-delivery applications. However, for fluorescence spectroscopy analyses, SRB-loaded MPs (i.e. SRB/HNT-MPs) and FNP-loaded MPs (i.e. HNT-FNPs/MPs) were prepared and tested separately to eliminate any possible synchronized emission effects on the values obtained at each time interval.

Stability/release of lactase loaded into MPs

Lyophilized, encapsulated amine-HNT-MPs were washed in SGF once and incubated in the same simulated digestion process as described in section 2.4.1. The concentration of the released

enzyme was measured through a micro-BCA assay (Micro BCA™ Protein Assay Kit, ThermoFisher Scientific; Ottawa, ON, CA) based on which two controls were prepared: the same concentration of the enzyme in SIF (positive control) and the same concentration of the enzyme in SGF for two hours and subsequently transferred to SIF (negative control). The remaining activity of the released enzyme as well as the controls was measured using ONPG assay, according to the protocol described in our previous publications [16,17,46].

Stability/release of bromelain loaded into HNTs

Bromelain-loaded amine-HNT-MPs (i.e. bromelain/amine-HNT-MPs) were fabricated according to the protocols discussed above. In order to prevent the possible concurrent/counter effects of other drugs (lactase) on the measurements, the MPs were not loaded with any other drugs. After lyophilization, the bromelain-loaded samples were incubated in SGF for 2 hours and subsequently in PBS 50 mM pH 8, containing 2 mM EDTA and 5 mM L-cystein for 4 hours to completely release the enzyme. The concentration of the released enzyme was measured using micro-BCA assay kit. The remaining activity of the released enzyme was measured through casein assay published elsewhere [32,33,48]. Briefly, 500 µl of the supernatants as well as the control samples in PBS 50 mM pH 8, containing 2 mM EDTA, 5 mM L-cystein and 30 mg/ml polymer background, were mixed with 500 µl of 2 wt% casein solution. After incubation at 37 °C for 30 min, 200 µl of 100 wt% TCA was added to each tube, vortexed well, and centrifuged at 14,000 rpm for 15 min. The absorbance of the supernatants was measured at 280 nm, reflecting the concentration of the tyrosine formed. The results were confirmed using Lowry assay as well. Two controls were prepared at the same concentration as the released sample: bromelain in SGF and

bromelain in PBS 50 mM pH 8, both containing 2 mM EDTA and 5 mM L-cystein (the positive control also contained the polymer background).

3.2.5. Characterization of the MPs

Morphology of the MPs

The morphology of the MPs before and after freeze-drying (pore-closure treatment) were investigated through field-emission scanning electron microscopy (SEM, S4800 Electron Microscope; Hitachi, Japan). MPs from each condition were uniformly spread on double-sided carbon tape on aluminum stubs, coated with 15 nm Au/Pd layer, and analyzed at 10 kV and 20 μA. $R_{Pore}/R_{Particle}$ size ratios of the MPs were acquired from 300 direct measurements on SEM images from each sample condition using Adobe Photoshop CS3. The other measurement on the images involved the ratio between the number of pored MPs to the total number of the particles in each image.

Porosity measurements

The porosity of the samples was measured through Brunauer–Emmett–Teller (BET) method using an Autosorb IQ and ASiQwin (Quantachrome Instruments**;** Boynton Beach, FL, USA). The MPs before and after freeze-drying as well as the HNTs before and after surface functionalization were analyzed. The samples from each conditions were balanced, transferred to the chamber, and degassed at 60 °C under vacuum for overnight. The N_2 adsorption/desorption isotherm was carried

out at the final outgas temperature of 60 °C. The total pore volume was obtained from the saturation pressure point ($P/P_0 = 0.99$), and the average surface area was calculated based on BET theory.

Particle size measurements

The average diameter of the small S100 MPs was measured by dynamic light scattering (DLS) using zeta sizer (Nano ZS, Malvern, UK), and the average size of the large S100 MPs as well as the amine-HNT-S100 MPs were measured using a Mastersizer 3000 laser particle size analyzer (Malvern Panalytical, Worcestershire, UK).

Surface charge of the MPs

Zeta potential of bare HNTs, S100 MPs, HNT-S100 MPs and amine-HNT-S100 MPs were measured following the protocol previously published. Briefly, the samples were suspended in 1 mM KCl solutions (0.1 mg/ml), sonicated for 5 min, and tested using zeta sizer (Nano ZS, Malvern, UK).

3.2.6. Histology studies

Fresh porcine gut was purchased from a local slaughter house. The small intestine tissue was taken apart from the rest of the organs, cut into smaller pieces of 1 cm × 1 cm, frozen in liquid nitrogen, and stored in -80 °C freezer for future use. Amine-HNT-MPs with bromelain loaded into

HNTs and 100 nm FNPs loaded into the hollow space inside the MPs were prepared according to the protocols discussed above. Bromelain-free large S100 MPs and bromelain-free amine-HNT-MPs both loaded with 100 nm FNPs were also prepared as the controls for this part of the experiments. 50 mg of each sample was suspended in 1 ml of SGF in 2 ml Eppendorf tubes at 37 °C for 2 hours to simulate the stomach environment. The medium was then replaced with 1 ml of SIF, and the samples were incubated under the same conditions for 1 hour to simulate the duodenum and jejunum. The caps of the tubes were subsequently removed, the inner side of the tissue pieces (thawed at room temperature conditions) were placed as the cap of the tubes and sealed using parafilm (Fig. 11). The tubes were then rotated for 60 min using a rotary machine (Tube revolver/rotator, ThermoFisher Scientific; Ottawa, ON, CA) at 24 rpm and 37 °C to simulate the environment, the residence time, and the peristalsis of the human intestine. The tissues were subsequently collected, embedded in cryo-paraffin wax (Fisher HealthCare, Tissue Plus®, O.C.T. Compound), and frozen at -20 °C freezer. The molded tissues were cut into 10 µm sections. The sections were stained using trypan blue and analyzed through fluorescence microscopy analysis.

3.2.7. Packaging

The bromelain/amine-HNT-lactase/MPs were transferred to gelatin capsules, placed in blister packs and sealed using Blister Sealing Machine (ABM-I; CapsulCN International Co., Ltd, China).

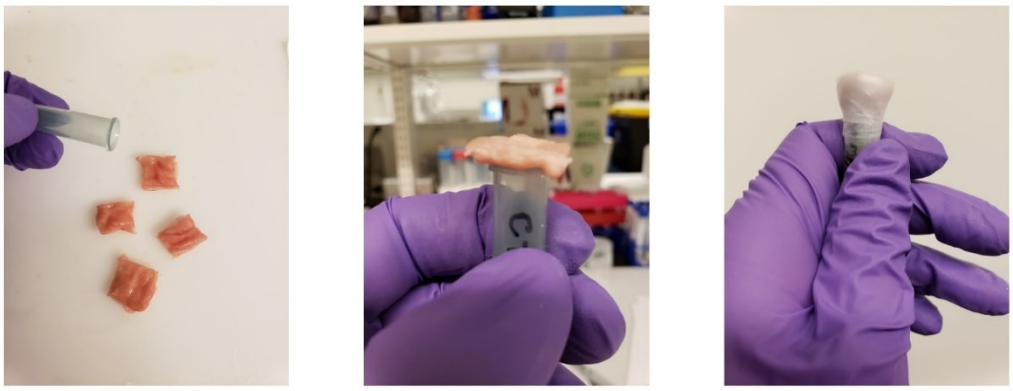

Figure 11. Preparation of tissue samples for histology test

3.3. Results

3.3.1. Fabrication of S100 MPs with pH-responsive macropores in two different size regimes

S100 MPs in a few micron size range (hereafter called small MPs) were prepared following our previously reported method [46]. To fabricate S100 MPs with sizes of a few tens of microns (hereafter called large MPs), a modified particle formation process was employed as explained in section 2.2.1. The morphology of the MPs before and after freeze-drying was characterized by SEM analysis (Fig. 12(a): small MPs, Fig. 12(b): large MPs; i: before freeze-drying, ii: after freeze-drying). As shown in SEM images of Fig. 12 a(i) and b(i), two different methods generated spherical MPs of different sizes (i.e. smaller MPs with a previous method and larger MPs with a new method from the comparison of Fig. 12(a) and (b)). This suggests that the new process has been successful in making large MPs while maintaining their spherical morphology and forming the surface pores (Fig 12(b)). Importantly, freeze-drying induced pore closure of the MPs regardless of their original size regimes (Fig. 12a(ii) and 1b(ii)), indicating the effectiveness of

freeze-drying process in sealing the surface pores of MPs regardless of their size, which is critical for the preservation of the loaded ingredients in harsh gastric environment [16,17,46]. Particle size analysis revealed that the average diameters of the freeze-dried MPs were measured to be 0.94 ± 0.32 μm (PDI: 1.11, Fig. 12c(i)) and 22.47 ± 10.22 μm (PDI: 1.21, Fig. 12c(ii)) for small and large MPs, respectively. This result is consistent with the SEM images shown in Fig. 12 (a) and (b). The narrow polydispersity of the large MPs along with other structural features (spherical morphology and surface pores) promise a new fabrication method with a good quality control over the size of the MPs with macropores.

To determine pore closure behavior of MPs, the size changes of MPs and their pores upon freeze-drying were investigated by measuring pore-to-MP size ratio (RPore/RMP) (Fig. 13(a)) and pored MP-to-total MP number ratio (Fig. 13(b)) for small (i) and large (ii) MPs using SEM images. As shown in Fig. 13a (i) and (ii), freeze-dried MPs exhibited significantly lower RPore/RMP size ratios compared to the samples before freeze-drying, implying the decrease in the population of MPs with large pores. Similar to this observation, freeze-drying was also found to induce the pored MP-to-total MP number ratio to shift toward the smaller population, indicating the closure of pores due to freeze-drying for both small and large MPs (Fig. 13b). This observation is consistent with SEM analysis shown in Fig. 13 (a) and (b). Freeze-drying induced pore-closure may be attributed to the depletion of the water from the MPs matrix, which in turn intensifies polymer-polymer attractions and facilitates solid state materials flow to close the pores and form a homogenous surface [49]. It is also interesting to note that the comparison of the number ratios of pored MPs between small and large MPs reveals a significant increase in the population of pored particles in the case of large MPs (Fig. 13(b)). In other words, the formation of surface pores is more dominant in larger MPs, which will in turn significantly increases the loading efficiency of the system. In

pored MP systems, ingredients are loaded into the interior hollow of the MPs directly through the surface pores; accordingly, the greater the number of pored particles, the higher the loading capacity. Facile surface pore formation in large S100 MPs can be explained by the higher amounts of organic solvents contained in large emulsion droplets, whose subsequent evaporation would generate stronger vapor flux to form the surface pores [50].

BET results in Fig. 13(c) also show considerable differences between the volume of the gas infused to/desorbed from the MPs before and after freeze-drying at a similar relative pressure value. This is in complete agreement with observations in Fig. 13(a) and (b), i.e. decrease in the size of surface pores of MPs and population of pored MPs. The average surface area of the samples as well as their total volume obtained from BET plots are summarized in Table 1. The values reflect much smaller surface areas and volumes after freeze-drying, which may be attributed mainly to the sealing of the surface pores.

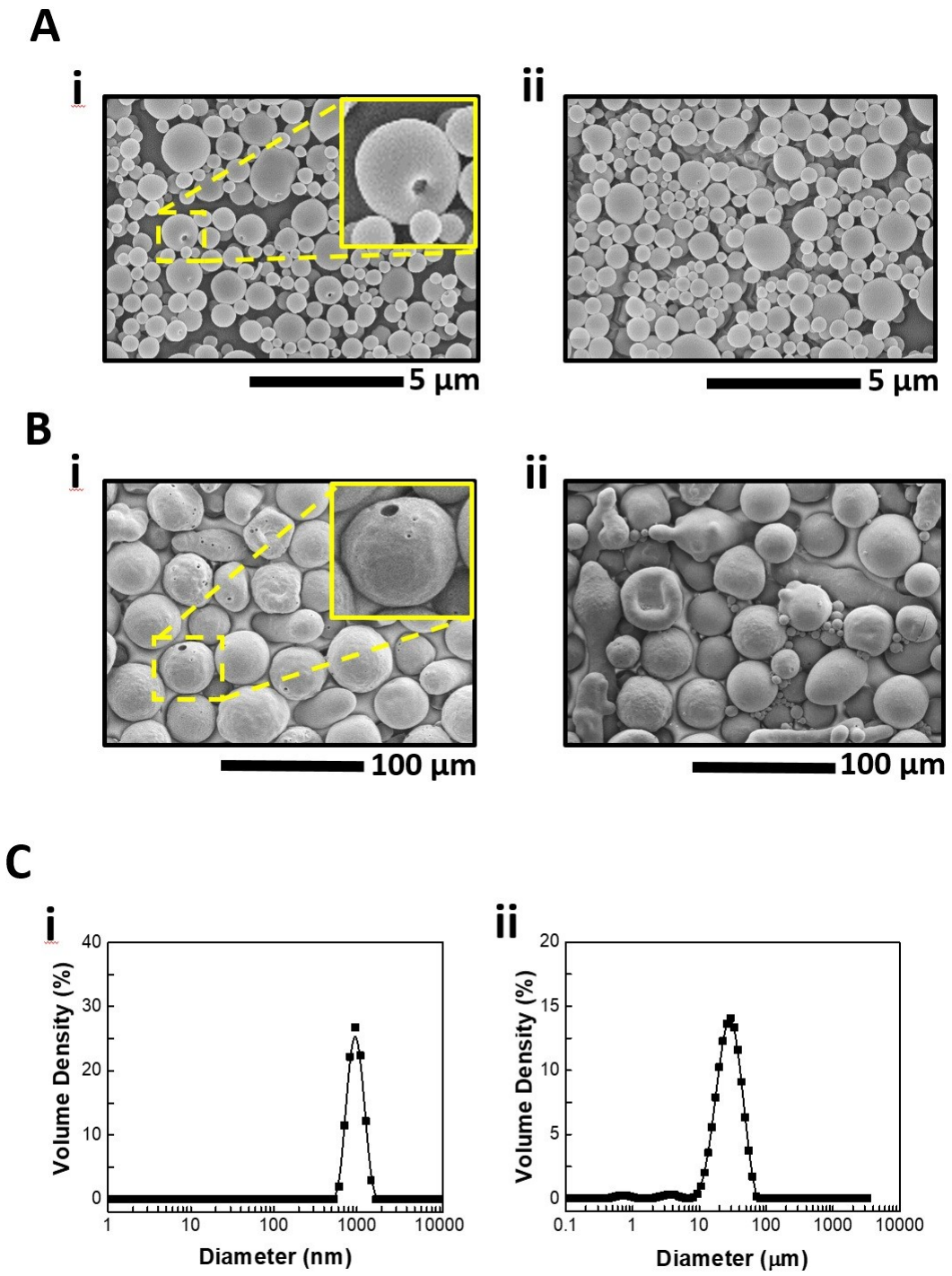

Figure 12. Fabrication of macropored MPs of two different sizes. SEM images for **a**) small and **b**) large S100 MP (**i**: before freeze-drying, **ii**: after freeze-drying), and **c**) their corresponding particle size distribution (**i**: small MPs, **ii**: large MPs).

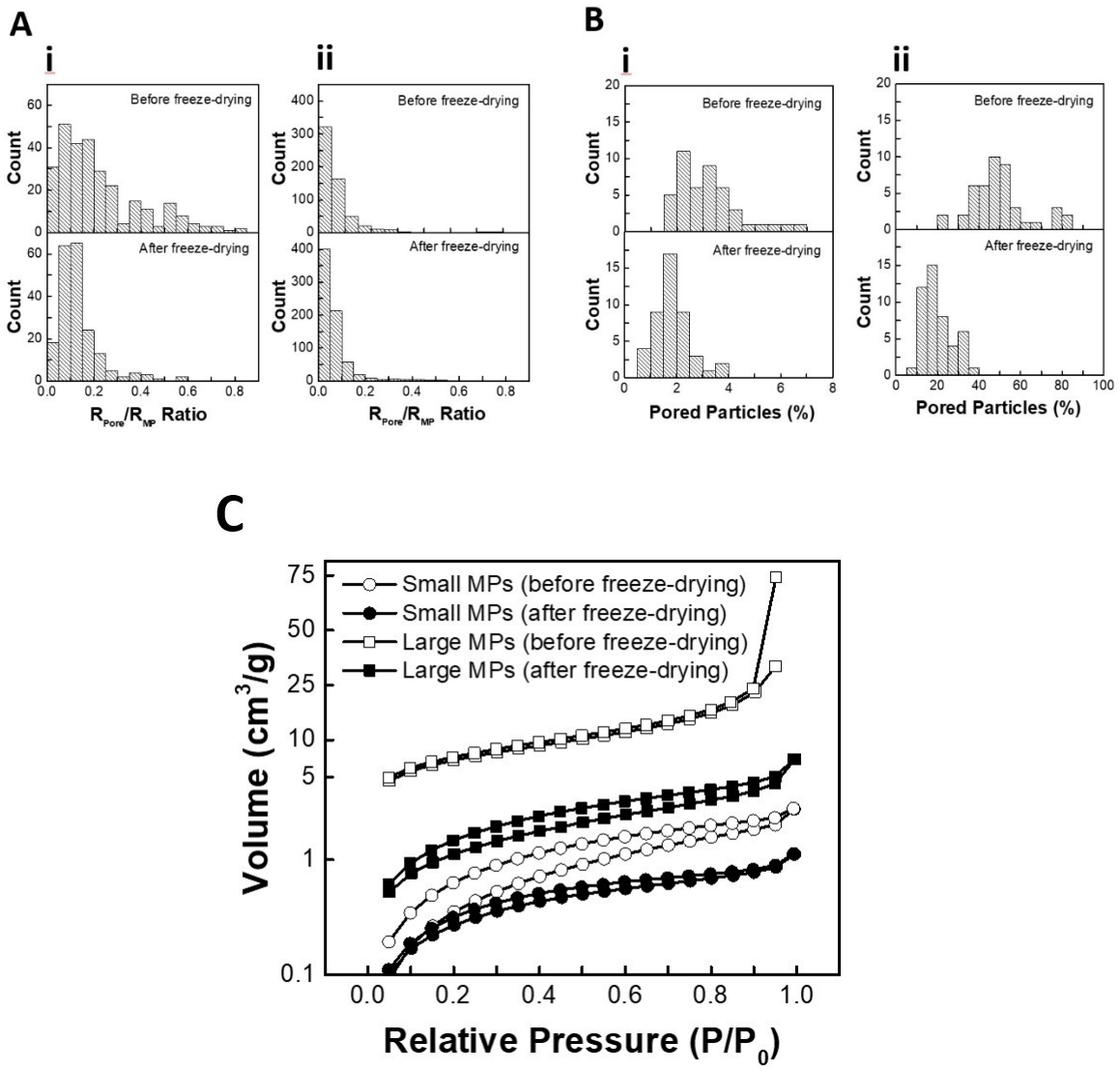

Figure 13. Effect of freeze-drying on the pore-closing behavior of MPs. a) Histogram of pore-to-MP size ratio (R_{Pore}/R_{MP}) (based on SEM image analysis), b) histogram of pored MP-to-total MP population ratio (based on SEM image analysis), and c) nitrogen adsorption isotherm measured from MPs before and after freeze-drying (i: small and ii: large MPs). n = 201-287 for a(i), n = 582-724 for a(ii), n = 45 for b(i), and n = 45 for b(ii).

3.3.2. Preservation/release behavior of S100 MPs

Following the successful fabrication of large MPs with macropores, their loading capacity was investigated by using lactase and model drugs, i.e. two different types of FNPs (100 nm and 1 μm FNPs), to test potential applicability of the macropored MPs for oral drug delivery. As shown in Fig. 14(a), large S100 MPs exhibited significantly higher level of encapsulation efficiency for all types of the ingredients used than that of the small MPs with macropores: lactase (102 ± 1.8 μg/mg of MPs); 100 nm FNPs (11.96 ± 0.27 μg/mg of MPs); 1 μm FNPs (3.14 ± 0.07 μg/mg of MPs). That is, the effective dose of the large MPs has been measured to be approximately 50 times, 40 times, and 20 times higher than that of the small MPs for lactase, 100 nm FNPs, and 1 μm FNPs, respectively. Such an increase in loading capacity of the MP system is in good agreement with size ratio results shown in Fig. 12: larger MPs can load more drugs. In addition, the higher level of porosity of large MPs compared to that of small MPs in Fig. 13(b) is believed to yield superior drug loading capacity.

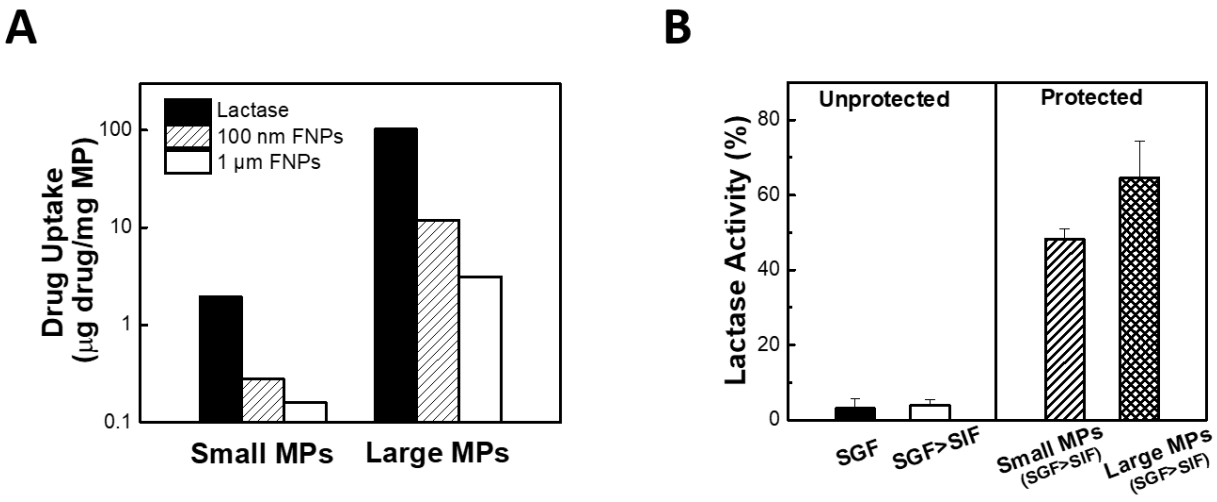

Figure 14. Encapsulation, preservation efficiency, and glass transition temperature of the MP systems. a) Encapsulation efficiency of the MP system for various ingredients (lactase, 100 nm FNPs, and 1 μm FNPs; n = 14), b) remaining activity of the drug (i.e. lactase) released from the protected formulation (i.e. small and large S100 MPs) compared to the unprotected formulation (n = 14)

The main principal characteristic of the MPs with macropores includes the protection of encapsulated pharmaceuticals against harsh GI tract conditions such as acidic pH of the stomach, which is associated with pH-responsive closing of surface pores. Thus, to further test the protective efficacy of large MPs, lactase from Aspergillus oryzae was selected as an indicator in investigating the preservation efficiency of the MP system due to its vulnerability to acidic pH: it completely denatures at gastric pH and does not recover its native conformation through transfer to intestinal pH (neutral/basic pH) [16,46]. To this end, lactase has been encapsulated into small and large MPs, followed by freeze-drying to seal surface pores. Then lactase-encapsulated MPs (lactase/MPs) were exposed to simulated GI digestive conditions, i.e. incubation in SGF for 2 hours to simulate the gastric environment and subsequently in SIF for 4 hours to release the loaded drugs, for the

comparative estimation of the protective efficacy (1: w/ vs. w/o MP formulation, 2: small vs. large MPs). As shown in Fig. 14 (b), the unprotected lactase w/o MP formulation lost almost all its activity in simulated gastric environment (2 hour incubation at pH = 2.0; remaining activity: 3.8 ± 2.5%) or in simulated GI tract conditions (2 hour incubation at pH = 2.0, followed by 4 hour incubation at pH 7.1; remaining activity: 3.8 ± 1.8%). On the other hand, the lactase released from macropored MP formulations exhibited 64.6 ± 9.7% and 48.2 ± 2.8% of remaining activity from large and small MPs, respectively, indicating a significant improvement in protection efficacy. Comparison of remaining activities further confirms that large MPs provide a higher protection compared to smaller MPs. In this MP architecture with pH-responsive macropores, preservation would be mainly attributed to the pore-closure efficiency, isolating the loaded ingredients from the environmental conditions surrounding the MPs. As a consequence, although mechanism for size-dependent pore-closure of MPs was not investigated in this work, higher preservation efficiency of the large S100 MPs can be accounted for by more facile materials flow within the polymer matrix in that sample.

Table 2. Values acquired from BET results

Sample	Total volume @ saturated point (cc/g)	Surface area (m^2/g)
Small S100 MPs (before freeze-drying)	2.73	2.975
Small S100 MPs (after freeze-drying)	1.11	1.402
Large S100 MPs (before freeze-drying)	220.57	25.281
Large S100 MPs (after freeze-drying)	7.05	5.117
HNTs (HNTs before treatment)	192.13	51.832
Amine-HNTs (HNTs after treatment)	197.72	53.714
Amine-HNT-S100 MPs (before freeze-drying)	7.03	6.814
Amine-HNT-S100 MPs (after freeze-drying)	5.06	2.685

3.3.3. Fabrication of amine-HNT-S100 MPs

HNTs are indeed aluminosilicate kaolin sheets, with alumina covering the interior and silica covering the exterior walls of the spiral tubes [42]. As a consequence, HNTs are negatively charged on the outer surface, which in turn induces electrostatic repulsive forces between the mucus layer and the MPs. Amine-functionalization of HNTs, on the other hand, can neutralize the negative zeta potential on the outer surface of HNTs and promises a better interaction between the amine-HNT-

S100 MPs and the tissue surface at the absorption site [47]. Fig. 15a (i) and (ii) show the SEM images of amine-HNT-S100 MPs fabricated through the method explained in section 2.2.3 before and after freeze drying, respectively. As shown in Fig. 15a(i) and its inset image, the amine-HNTs have been successfully incorporated onto S100 MPs surface without hampering their spherical morphology (compare Fig. 15(a) with Fig. 12(b)). In addition, the presence of HNTs did not affect the pore closing behavior by freeze-drying (Fig. 15a(ii)). The particle sizer analysis (Fig. 15a(iii)) confirmed the formation of uniform amine-HNT-S100 MPs with a narrow size distribution (particle sizer analysis: 37.6 ± 1.3 µm, SEM image analysis: 26.5 ± 5.2 µm, PDI: 1.15).

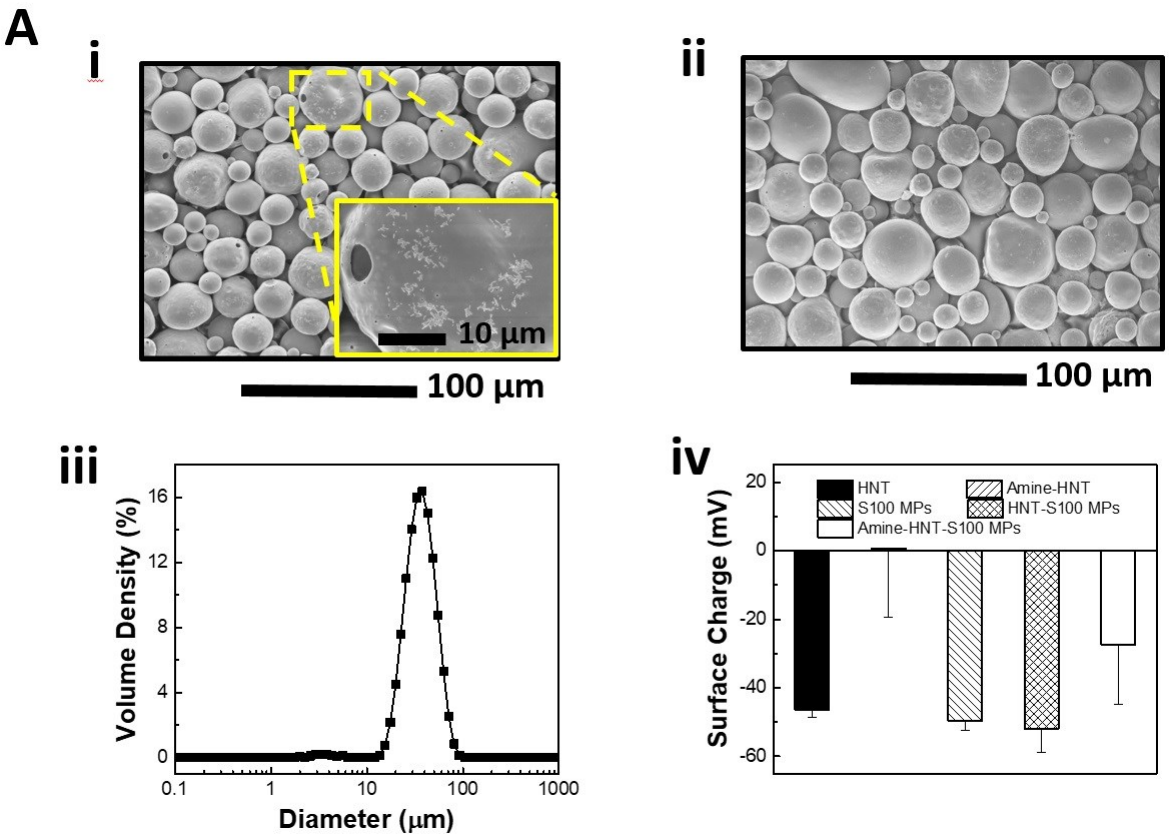

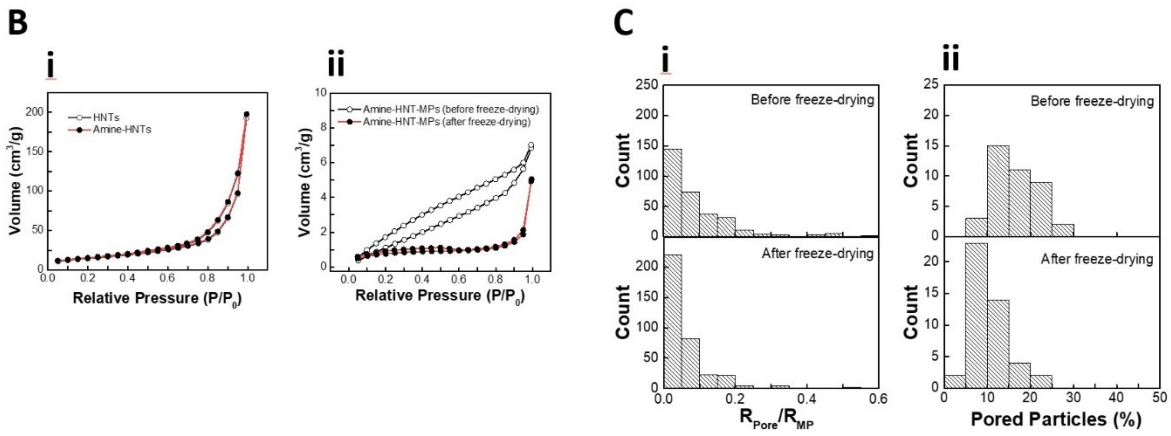

Figure 15. Fabrication and characterization of amine-HNT-S100 MPs. **a**) SEM images of amine-HNT-S100 MPs (**i**) before and (**ii**) after freeze-drying, (**iii**) particle size distribution, and (**iv**) zeta potential measurement (n = 13). **b**) BET analysis on (**i**) HNTs with and without amine functionalization and (**ii**) amine-HNT-S100 MPs before and after freeze-drying. **c**) (**i**) R_{Pore}/R_{MP} size ratio (n = 317) and (**ii**) MP-to-total MP number ratio analysis (n = 41) before and after freeze-drying for amine-HNT-S100 MPs (based on SEM image analysis).

Fig. 15a(iv) shows the surface charge of both the amine-HNT-S100 MPs and the control samples (i.e. S100 MPs, HNTs, amine-HNTs, and HNT-S100 MPs). As shown in the plot, zeta potential of S100 MPs and HNTs was measured to be negative, and thus making the zeta-potential of the HNT-S100 MPs even more negative compared to S100 MPs [42,44,45,53]. Mucin as the principal building ingredient of the mucus conveys significant negative charge, inducing the same surface charge on the whole inner wall of the GI tract [19,54–56]. This will in turn cause significant repulsive forces between the MPs and the absorption site at the target, and reduce the drug uptake efficiency [57]. From another point of view, MPs with positive surface charge will not be suitable for delivering drugs to the ending parts of the small intestine (such as ileum), since they may easily attach to the mucus in upper parts of the GI system (stomach, duodenum, or jejunum) before they reach the target [58]. Based on this reason, it was necessary to slightly shield the negative surface charge of the HNT-MPs. For this purpose, the surface of HNTs were functionalized with amine

groups, making amine-HNT-S100 MPs. As shown in Fig. 15a(iv), a significantly lower level of surface charge was monitored from amine-HNT-S100 MPs, which can considerably improve mucoadhesion at the absorption site.

Considering the application of amine-HNTs in the delivery of mucolytic enzyme, the porosity of the HNTs was examined by BET analysis before and after amine-functionalization. As shown in Fig. 15(b), there is no considerable change in the porosity of the HNTs due to the chemical modification of their surface. This resolves a concern raised about the possible clogging of the hollow tubular interior of HNTs. BET results were also used for further evaluation of the amine-HNT-encapsulated S100 MPs (amine-HNT-MPs). As can be seen in Fig. 15b(ii), amine-HNTs-S100 MPs exhibited significant drops in the volume of the N_2 infused into the system after freeze-drying. This is consistent with the previous observation confirming successful pore-closure of the MPs. In fact, the order of the samples based on the relative decreases of the volume of the gas infused into the system at the saturation point ($P/P_0 = 0.99$) before and after freeze-drying would be: large S100 MPs (~ 90%), amine-HNT-S100 MPs (~ 70%), and small S100 MPs (~ 43%).

Pore-closure behavior of the amine-HNT-S100 MPs was also characterized by analyzing SEM images of the MPs taken before and after freeze-drying (see Fig. 15c (i) and (ii) for R_{Pore}/R_{MP} size ratios and pored particle number ratio, respectively). As shown in Fig. 15c(i), freeze-drying induced a shift of R_{Pore}/R_{MP} size ratio toward lower values, supporting successful pore-closure. As was explained before, the surface pores are used for direct loading of the ingredients into the MPs. Thus, the subsequent sealing of the surface pores is essential for the protection of the loaded materials from environmental harsh conditions surrounding the MPs (especially in the stomach) [16,17,50]. Pored particle counting (Fig. 15c(ii)) confirms decreases in the quantitative fraction of amine-HNT-S100 MPs with surface pores after lyophilization. Surface pore-closure can be

attributed to the replacement of water-polymer interactions for polymer-polymer attractions, facilitating the migration of polymer chains for creating a homogenous surface.

3.3.4. Encapsulation/release behavior of amine-HNT-S100 MPs

Encapsulation/release of the model drugs

Amine-HNT-S100 MPs were loaded with two different model drugs to demonstrate the capability of the system for co-delivery of pharmaceuticals. SRB (red) and 100 nm sized FNPs (green) were encapsulated inside the interior hollow of amine-HNTs and MPs, respectively. The time- and pH-dependent release behavior of the freeze-dried MPs were analyzed using fluorescence microscopy throughout the incubation in simulated digestion process (2 hour incubation in SGF, followed by 4 hour incubation in SIF). Fig. 16a shows the fluorescence microscopy images of the MPs at different stages of the digestion process. The images acquired through TRITC filter were used to track SRB, and those captured through FITC filter were employed for tracking FNPs (see combined images for a mixture of images separately taken using TRITC and FITC filters). From the image at 0 min in SGF, it was clear that SRB and FNPs have been successfully loaded into interior hollow space of amine-HNTs and S100 MPs, respectively, and SRB-encapsulated amine-HNTs (i.e. SRB/amine-HNTs) infused onto the surface of the FNP-encapsulated MPs. Importantly, as shown in other images captured throughout the incubation window in SGF, no noticeable leakage of SRB and FNPs was observed from SRB/amine-HNT-FNPs/S100 MPs. This confirms a successful pore closure of the S100 MPs as well as the proper sealing of the amine-HNTs openings with an anionic copolymer, L100. Furthermore, MPs with

closed pores maintained their intact structure in SGF to prevent unpunctual release of the drugs and thus to protect loaded pharmaceuticals against gastric acids.

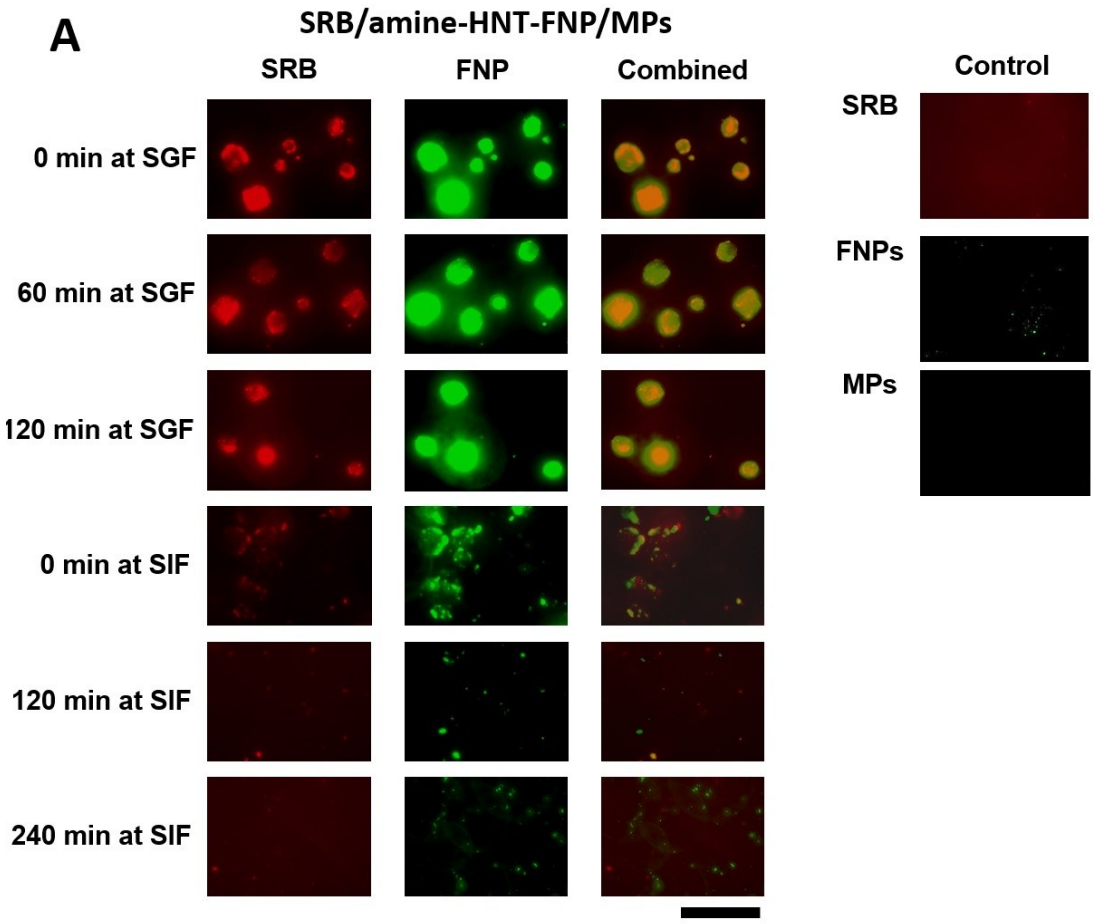

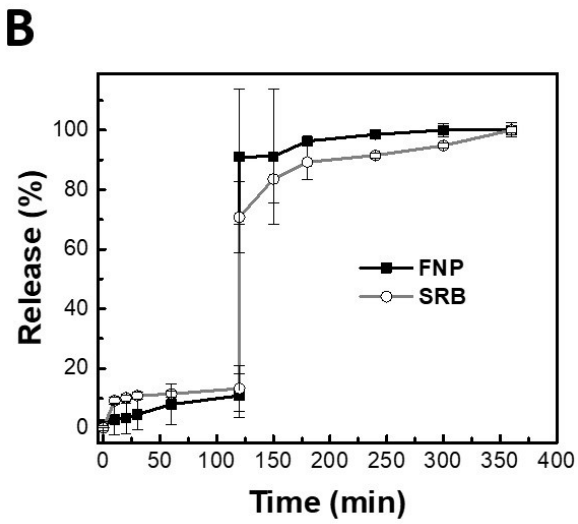

Figure 16. Encapsulation/release of the model drugs from amine-HNT-S100 MPs. **a**) Fluorescence microscopy images of the SRB/amine-HNT-FNP/S100 MPs samples at various stages of the simulated digestion process and **b**) release profile of the model drugs. (Scale bar: 100 μm)

Upon exposure to SIF, an instant release of the loaded ingredients was observed as evidenced by the fluorescence microscope images monitored during incubation in the SIF. The release of SRB from amine-HNTs and FNPs from MPs can be explained by the dissolution and/or opening of pH-responsive pores made of anionic copolymers (S100, L100) in SIF. This result is in agreement with the typical release behavior of the systems made of Eudragit copolymers reported in other publications [59,60]. This instant release of both drugs at the absorption site is really promising, since multiple drugs with different activities can be formulated simultaneously to exhibit a maximum level of therapeutic activity in a coherent manner. That is, co-delivery of mucolytic enzyme and oral drug based on amine-HNT-S100 MPs can resolve two major challenges (improved drug stability in harsh GI tract environment, enhanced mucopenetration and drug absorption) faced by scientists in developing oral drugs with high bioavailability.

Quantitative analysis on the release behavior of the SRB/amine-HNTs-FNP/S100 MPs was performed by measuring fluorescence intensity changes over the course of the gastrointestinal

digestive process. As shown in Fig. 16b, 2-hr incubation in SGF induced about 10% of leakage of SRB and FNPs, which was attributed to the non-closed surface pores of the MPs [16,17,46]. Upon the exposure to SIF, the main significant release of the ingredients was instantly observed, which is consistent with fluorescence microscopy analysis in Fig. 16a. As predicted from observation by fluorescence microscopy, the drug release was rapid and almost complete at the initial stage of the 4-hr incubation in SIF.

Encapsulation/release of the real drugs

For a proof-of-concept demonstration of efficient oral drug delivery system with enhanced stability in GI tract and mucopenetration, it is important to test the encapsulation and preservation of multi-drugs (i.e. mucolytic enzyme and therapeutics). To this end, amine-HNT-S100 MPs with pH-responsive macropores were proposed as an efficient strategy for the co-delivery of bromelain and lactase to represent mucolytic enzyme and drug, respectively. To verify the efficacy of the proposed system, bromelain was loaded into amine-HNTs, and bromelain/amine-HNTs were incorporated into S100 MPs (i.e. bromelain/amine-HNT-S100 MPs). Also, amine-HNT-S100 MPs were separately prepared and encapsulated with lactase (i.e. amine-HNT-lactase/S100 MPs). Indeed, in order to prevent potential concurrent/counter effects of the enzymes in concentration and activity measurements, two separate batches of amine-HNT-S100 MPs were prepared: one only loaded with bromelain (i.e. bromelain/amine-HNT-S100 MPs) and the other one only loaded with lactase (i.e. amine-HNT-lactase/S100 MPs). The encapsulated samples were incubated for 2 hours in SGF and subsequently transferred to SIF for another 4-hour incubation.

Fig. 17a shows the loading efficiency of amine-HNT-S100 MPs calculated based on the final concentrations of the released enzymes. As shown in the plot, 5.5 ± 0.6 μg/mg and 70.1 ± 6.3

μg/mg of encapsulation efficiency were measured from bromelain/amine-HNT-S100 MPs and amine-HNT-lactase/S100 MPs, respectively. This difference in the amounts of the encapsulated drugs can be explained by the difference in the volumes of the interior hollow of HNTs and MPs. That is, the interior volume of the amine-HNTs into which bromelain is loaded is significantly less compared to that of the hollow MPs with macropores. Accordingly, larger amounts of drugs can be encapsulated inside the MPs than those loaded into amine-HNTs. However, it should be noted that the dose of the enzyme delivered through amine-HNTs can be regulated by adjusting the amount of the amine-HNTs incorporated into the MPs.

The remaining activity/stability of the released enzymes was also measured to evaluate the preservation capacity of the co-delivery system based on amine-HNT-S100 MPs with pH-responsive macropores. For this purpose, remaining activity of bromelain and lactase released from the amine-HNT-S100 MP formulation was compared with that of negative controls (i.e. unprotected bromelain and lactase without being loaded into amine-HNT-S100 MPs). As shown in Fig. 17b, unprotected lactase showed a significant loss of its activity due to exposure to acidic condition of SFG (remaining activity: 5.7 ± 1.1%), indicating that acid-induced conformational change of the enzyme in SGF did not recover after it was transferred to near neutral pH environment (SIF) [16,46]. In contrast to lactase, unprotected bromelain was less vulnerable to the digestive conditions, and thus maintained 76.3 ± 1.3% of its remaining activity under the simulated GI tract. The pH-induced destabilization of the bromelain depends on the concentration: i.e. the higher concentration, the more stability [61]. As such, concentrated encapsulation of bromelain inside a small tubular hollow of HNTs might have resulted in higher level of its activity under GI tract conditions, which represents another significant advantage of using HNTs. Unlike unprotected drugs, it is interesting to note that enzyme formulations based on amine-HNT-S100

MPs exhibited a significant improvement in their stability under digestive conditions of GI tract. As a result, 94.5 ± 3.3% (bromelain) and 70 ± 14.1% (lactase) of functional activity was observed from bromelain/amine-HNT-S100 MPs and amine-HNT-lactase/S100 MPs, respectively. The improvement in functional activity/stability of the released enzymes can be explained by the protection of the enzymes against acidic pH due to the pore-closure of both HNTs and MPs in the SGF, and their complete release due to pore opening in response to neutral/basic pH of the SIF [61].

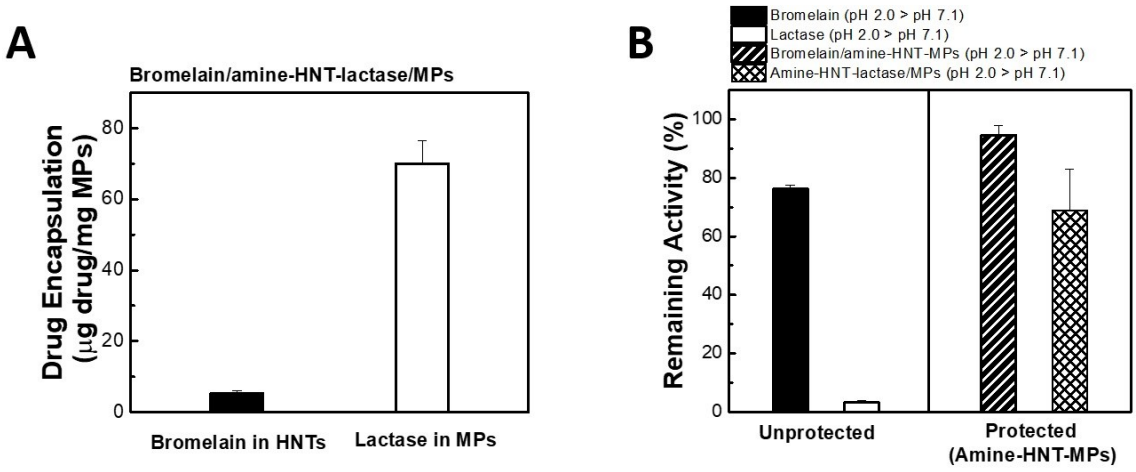

Figure 17. Encapsulation/release of the real drugs from amine-HNT- MPs. a) Encapsulation efficiency of the large MP system for real therapeutics (i.e. bromelain and lactase) and b) remaining activity of the released drugs from the protected formulation (i.e. amine-HNT-MPs) compared to the unprotected formulation. (n = 12)

3.3.5. *Ex vivo* mucopenetration of amine-HNT-S100 MPs in the pig intestine

To investigate mucopenetration behavior through co-delivering mucolytic enzyme (bromelain) and drug (biopharmaceuticals or vaccines), diffusion of FNPs released from amine-HNT-S100 MPs loaded with bromelain and 100 nm FNPs (i.e. bromelain/amine-HNT-FNPs/S100 MPs) through native mucus of pig intestine tissue has been characterized by microscopic examination of histologically stained tissue sections. For the comparison of mucopenetration efficiency, different types of samples (i.e. FNPs/S100 MPs, bromelain/HNT-FNPs/S100 MPs) were exposed to simulated digestive conditions (i.e. 2-hr incubation in SGF, followed by 4-hr incubation in SIF), and the released media were applied for 30 minutes to the surface of porcine intestinal tissues (i.e. 1 ml of MP suspension (50 mg/ml) in SIF applied to ~ 1.14 cm^2 tissue surface).

As shown in Fig. 18a, in the control samples (FNPs/S100 MPs) a thick mucus layer was found to maintain its intact structure (Fig. 18a (i) and (ii)). Thus FNPs released from MPs in the absence of bromelain could not diffuse across the mucus layer, and mostly remained on the surface of the outer mucus as shown in Fig. 18a (iii) and (iv) (see Fig. 19 for low magnification images, and fig 20 for outer mucus removal using lower concentrations of bromelain). To achieve systemic circulation, it is critical for the drugs to penetrate thick mucus layer prior to absorption. For this purpose, the concept of co-delivering mucolytic enzyme and drug to enhance diffusion through mucus has been tested *ex vivo* using bromelain/amine-HNT-FNPs/S100 MPs formulation (i.e. bromelain: mucolytic enzyme, FNPs: model drug). The MPs were incubated in simulated digestion process, and the final concentrations of the mucolytic enzyme were regulated to be 20 μg/ml and 200 μg/ml through dilution of the released samples in release media background (containing the same concentrations of polymer, HNTs and FNPs) to study the minimum concentration of the mucolytic enzyme needed for mucus-penetration properties. When exposed to 20 μg/ml of released bromelain in FNP suspension, mucus was partially disrupted as shown in Fig. 18b, which

resulted in increased penetration of FNPs in the mucus compared to bromelain-free formulation (compare Fig. 18b with Fig. 18a). In the case of 200 µg/ml of released bromelain in FNP suspension, FNPs were significantly more diffusive through the disrupted mucus (Fig. 18c), which supports the facilitated penetration of drugs due to mucolytic enzyme. It was also noted that even the mucus layer was too fragile after exposure to bromelain to keep the mucus intact during histology sample preparation. This supports that co-delivered mucolytic enzyme facilitated the penetration of the model drugs through intestinal mucus, and further implies on significant improvements in the absorption efficiency of the oral drugs in real conditions. Despite the structural differences in intestinal mucus between humans and pigs, it is well-known that mucus impedes the absorption of the drug [37,38]. Therefore, the superior encapsulation and preservation capability of amine-HNT-S100 MPs formulation can enable the development of highly effective oral therapeutics and oral vaccines.

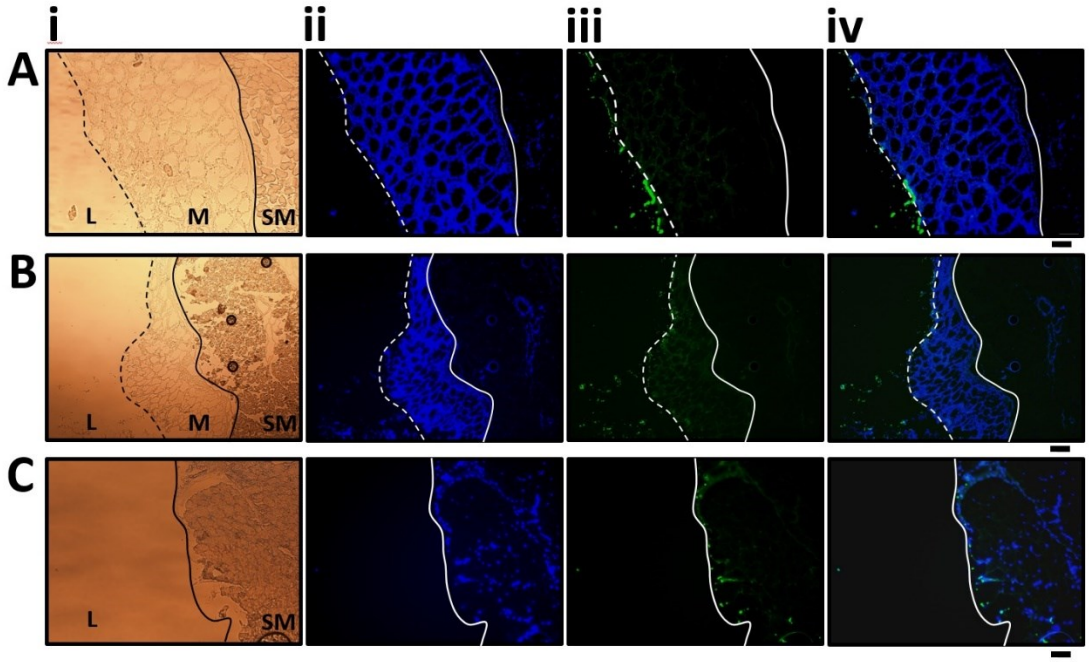

Figure 18. Histological analysis using an *ex vivo* porcine intestine tissue to evaluate the mucus permeation efficiency of the oral drug formulation based on MPs. **a**) Tissue

exposed to FNPs released from FNPs/S100 MPs with an intact mucus layer (see Fig. 19 for its low magnification image), **b**) tissue exposed to FNPs released from bromelain/amine-HNT-FNPs/S100 MPs (released bromelain: 20 µg/ml) with a partially disrupted mucus layer, and **c**) tissue exposed to FNPs released from bromelain/amine-HNT-FNPs/S100 MPs (released bromelain: 200 µg/ml). **i**) BF image, **ii**) DAPI image, **iii**) FITC image, and iv) Merged (DAPI+FITC) image. (L: lumen, M: mucosa, SM: submucosa; scale bar: 200 µm)

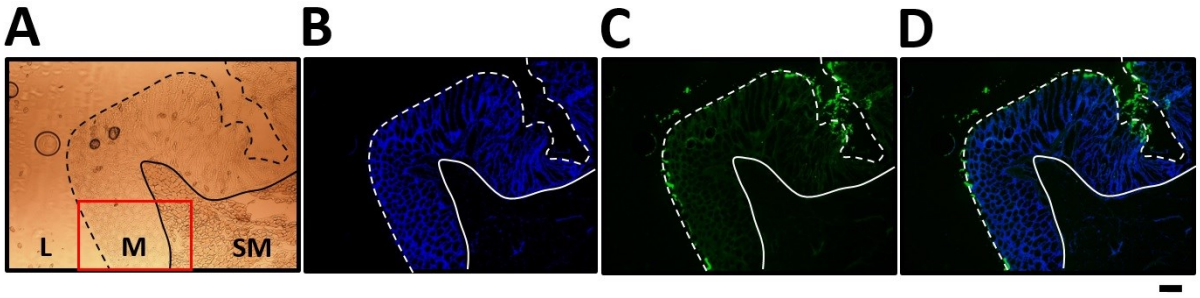

Figure 19. Histological analysis using an *ex vivo* porcine intestine tissue to evaluate the mucus permeation efficiency of the oral drug formulation based on MPs. FNPs released from large S100 MPs (i.e. FNPs/S100 MPs) exposed to the intestinal folds (i.e. plicae circulares): **a**) BF image, **b**) DAPI image, **c**) FITC image, and **d**) Merged (DAPI+FITC) image. A magnified view of a rectangular box is shown in **Fig. 18(a)**. (L: lumen, M: mucosa, SM: submucosa; scale bar: 400 µm)

3.4. Discussion

Oral delivery is known as the most promising administration route. Microencapsulation systems have been significantly successful in addressing a number of challenges associated with oral administration: preservation against gastric acid, digestive enzymes and bacterial exposure, to name but a few [5,62,63]. These systems, however, are still facing major issues impeding their commercialization and universal application. The major technological challenges against the commercialization of oral MPs are insufficient throughput of the system, drug

instability/denaturation during the microencapsulation process, and difficulty of meeting the demand for high dosage application [14,16,64]. Microfluidics with parallel multi-channel designs resolved the issues with polydispersity of the MPs and considerably increased the fabrication throughput; however, the systems still need further improvements [13,14,64,65]. Previously in this group, MPs with pH-responsive surface pores were developed to specifically address the drug denaturation during the microencapsulation process and instability of vulnerable biopharmaceuticals against harsh gastric conditions. In that microencapsulation scheme, the drug is completely excluded from the fabrication process of the MPs. After the fabrication is complete, drugs are loaded into the MPs through the pH-sensitive surface pores in favorable environmental conditions for the drugs. The surface pores are subsequently closed to isolate the drugs from unfavorable surroundings, and they will open again in the target, where the environmental pH is above the pKa of the MPs. These MPs, however, do not show enough loading capacity for applications that require high-dose therapy. Apart from technical issues, mucus barrier and tight junctions of the intestinal tissue are the main biological barriers to deal with for successful oral delivery. These problems along with gastric fluid could dramatically reduce the efficacy of the system [30,32,35,62]. Therefore, an ideal oral formulation should meet all proposed requirements by resolving the whole set of problems.

The present work was aimed at designing a new architecture of microencapsulation systems addressing a number of the challenges in developing oral drug formulation. To this end, the pored MP fabrication method developed in the present work looks very promising in terms of throughput and ease of fabrication. The throughput of the microencapsulation systems is usually reported as the volume of the final formulation versus time [64,66–68]. The present system exhibited about 36.75 ± 4.45 % MPs production yield; also, the fabrication protocol developed in this study is a

continuous and facile process to be simply scaled up even to significantly higher production scales. The main problem concerned with emulsion solvent evaporation protocols is the wide polydispersity of the final product. However, the MPs fabricated in this work showed superior size controllability (PDI: 1.21 for large S100 MPs, and 1.15 for amine-HNT-S100 MPs). A high loading capacity as well as narrow polydispersity make the present system very promising for further investigations. Also, regarding the loading efficiency as the other technical problem of the pored microencapsulation system, the results clearly demonstrated drastic increases in the amounts of various drugs loaded into the large MPs in comparison with those into the small ones: ~ 20-fold increase for 100 nm FNPs, ~ 40-fold increase for 1 μm FNPs, and ~ 50-fold increase for lactase.

The incorporation of the amine-HNTs provided the system with new capabilities for co-delivery of multiple drugs. A novel co-delivery scheme with totally isolated loading channels, resolving any concerns associated with potential interactions between different drugs. Mucolytic enzymes loaded HNTs embedded on the surface of the MPs played considerably promising roles in solving the issues with mucus layer, which will in turn dramatically improves the drug absorption efficiency of the MP-based oral drug delivery system. The dose of the model drugs (or real drugs) delivered per mg of the MPs is dependent on the initial concentration of the drug stock solution used for the encapsulation and the amount of the amine-HNTs incorporated into the body of the MPs. Therefore, the dose of the enzyme loaded into and released from the system can be easily controlled based on the final concentration needed at the absorption site. The new system showed significant improvements in a number of the technical and biological barriers against the oral administration routes, reflecting its significance for further assessments, especially in future *in vivo* studies. As the next step of the project, this new system is being loaded in edible gelatin capsules for delivery and packed in blister sheets, as shown in Fig. 20. The stability of different

vulnerable drugs in this new microencapsulation formulation under various environmental conditions will be examined. The conditions will include different environmental humidity levels and temperatures to make sure of the universal applicability of the formulation and the system. We believe that amine-HNT-S100 MPs can play an important role as a universally applicable microencapsulation platform for oral drug delivery applications.

Figure 20. Gelatin capsules (a) containing bromelain/amine-HNT-lactase/S100 MPs formulation packaged in a blister pack (b).

3.5.Conclusion

Amine-functionalized halloysite-embedded MPs with pH-responsive macropores (amine-HNT-MPs) have been proposed as a potential candidate for oral delivery of multi-drugs. The size of the pored MPs can be successfully increased up to ~ 40 µm without any negative change in the morphology and pore closing/opening behavior of the particles. The increase in the size of the MPs exhibited about 50-times higher enzyme-loading efficiency, compared to that of small MPs (i.e.

102 ± 1.8 μg of lactase per mg of MPs). Noteworthy, the large MPs showed even better preservation efficiency of the vulnerable biopharmaceuticals against the gastric harsh conditions compared to small MPs. Loaded ingredients showed ≥ 60% remaining activity after release in the simulated absorption site environment. The incorporation of the amine-functionalized HNTs into the MPs matrix provided a new capability for the system—that is—co-delivery applications. Loading the amine-HNTs with mucolytic enzymes (bromelain) led to much more efficient permeation through the mucosal layer at the absorption site. According to *ex vivo* results, the drugs released from bromelain-loaded MPs were proven to exhibit a facilitated diffusion through mucus layer in small intestine. Thus, we believe that amine-HNT-MPs with pH-responsive macropores would provide benefits to resolve long lasting challenges for the development of efficient oral drug formulations with high bioavailability.

4. Chapter 4

Macropored Microparticles with a Core-Shell Architecture for Oral Delivery of Biopharmaceuticals

4.1. Preface

Microparticles (MPs) have been extensively researched as a potential drug delivery vehicle. Here, we investigated the fabrication of MPs with pH-responsive macropores and evaluated their potential applicability in developing solid oral drug formulations. Our previous chapters showed that macropored MPs, made of Eudragit® L100-55, could encapsulate 100 nm, 1 μm, and 4 μm sized fluorescent beads – model drugs that are mimicking vaccines, bacteria, and cells. In the present study, closed-pored MPs after freeze-drying were coated with a gastric soluble Eudragit® EPO layer to protect MPs in the simulated pregastric environment. Subsequently, drug encapsulated MPs maintained their intact closed-pored structure in the simulated gastric environment and exhibited a rapid release in the simulated intestine environment (Fig. 21). Our MP system was found to provide a significantly higher level of protection to the encapsulated lactase enzyme compared to the control sample (i.e. without using MPs). Real-time fluorescence microscopy analysis showed that macropored MPs released encapsulated drugs in a burst-release pattern and in a size-independent manner. This work shows that our proposed EPO-coated MPs with pH-responsive macropores can meet the challenges posed by the multiple physiological environments of the digestive tract and be used in developing highly effective solid oral drug/vaccine formulations.

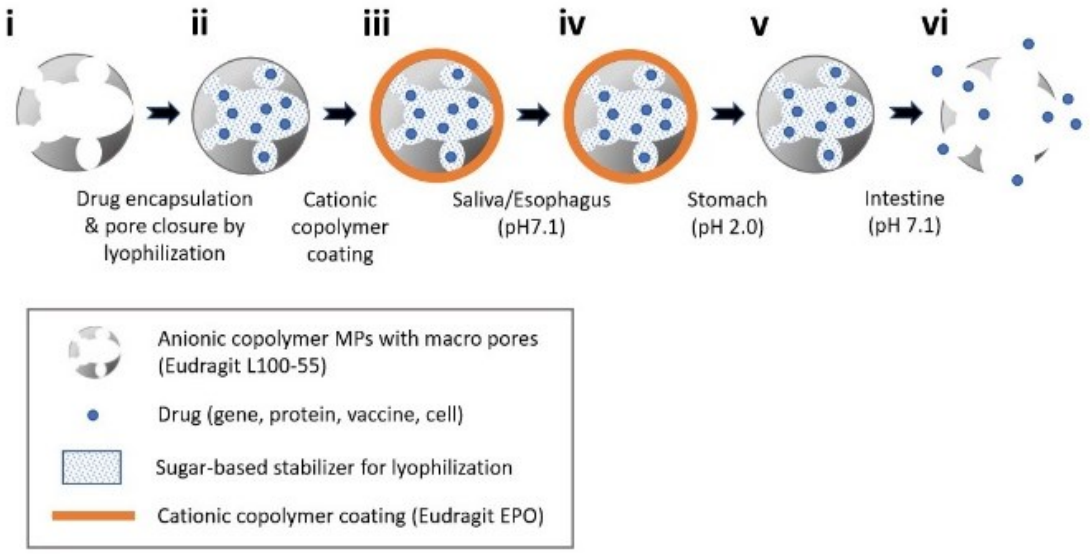

Figure 21. Schematic representation of smart microparticles (MPs) with pH-responsive macropores for targeted oral drug delivery to the intestine. (i) Pored MPs made of L100, (ii) encapsulation of drug and pore closure by freeze-drying, (iii) formation of protective coating, using EPO, on close pored-MPs, (iv) exposure to pregastric environment (saliva/esophagus), (v) exposure to simulated acidic environment of the stomach, and (vi) release of encapsulated drugs under simulated intestinal environment.

4.2. Materials and methods

4.2.1. Materials

Eudragit® L100-55 and Eudragit® EPO were received from Evonik Canada Inc. (Burlington, Ontario, Canada). Carboxylate-modified polystyrene beads with different sizes (100 nm, 1 µm, and 4 µm) were purchased from Life Technologies (Carlsbad, CA, USA). Lactase from Aspergillus Oryzae, 2-Nitrophenyl β-D-galactopyranoside and halloysite nanoclay were

purchased from Sigma-Aldrich (St Louis, Missouri, USA). Micro BCA protein assay kit was also obtained from Thermo Fisher Scientific (Waltham, IL, USA).

4.2.2. Fabrication of pored MPs, pore closure process, and formation of EPO coating layer

Anionic MPs were fabricated according to the protocol recently published in our previous work [149]. Concisely, L100 powder suspension in DCM (0.05 g/ml) was transferred to a sealed container and incubated at 39 °C (stirring at 50-60 rpm) for 120 min in a water bath. After 120 min incubation, aliquots of 10 mL were taken from the suspension and dried in glass petri-dish in an oven (initially the temperature was set at 65 °C for 30 min and subsequently decreased to 37 °C for overnight incubation) (Isotemp Incubator, Fisher Scientific). To close the surface pores, 500 mg of as-prepared MPs was suspended in 15 ml DI water, followed by freezing in liquid nitrogen and freeze-drying using the protocol, as previously reported [145].

For the coating step, the freeze-dried anionic MPs were suspended in EPO in DCM solution followed by an evaporation stage. Different concentrations of EPO in DCM (0.05, 0.1, 0.2, and 0.5 g/ml) and various time ranges for stirring the freeze-dried L100 MPs in EPO solution (2, 5, 15, and 30 min) were investigated. The challenge was reaching a cationic layer thick enough to protect the anionic MPs in saliva/esophagus simulated fluid for 10 min and at the same time thin enough to prevent the attachment of the MPs. As the best condition meeting both the requirements, EPO in DCM solution (0.1 g/ml) was prepared for the formation of the coating layer on the surface of L100 MPs. 2 g of freeze-dried L100 MPs was added to 20 mL of EPO solution, followed by the addition of Tween 20 (500 µl) to the suspension. The final mixture was stirred at RT in a glass beaker for 5 minutes (120-130 rpm). The suspension was subsequently filtered through Whatman

filter papers (Sigma-Aldrich; No. 4, pore size: 20-25 μm). The coated MPs were collected from the top of the filter papers after drying (initial drying at room temperature (RT) for 4 hrs, followed by overnight vacuum drying).

4.2.3. Characterization of the coated MPs

The morphology of the MPs before and after coating as well as the thickness of the coating were characterized utilizing field emission scanning electron microscopy (FESEM; S4800 Electron Microscope; Hitachi, Japan). Ground MPs (using an agate mortar) were also analyzed to study the cross-section of the coating. In order to verify the formation of the EPO coating layer, halloysite nanoclay was also added to the EPO coating solution (100 mg in 10 ml of EPO solution). MPs samples were placed on a double-sided carbon tape and subsequently coated with a 20 nm Au/Pd for SEM analysis (10 kV, 20 μA). To test pH response of the coated MPs, 100 μl of the incubated samples were collected at each step of the simulated ingestion/digestion process for SEM analysis. Average sizes of the MPs and polydispersity indexes before and after coating were directly measured from SEM images (300 measurements from each condition). In order to measure the zeta potential of the samples, coated and non-coated MPs were separately suspended in 1 mM KCl solution (20 mg/ml), and potentials were measured using zeta sizer (Nano ZS, Malvern, UK). Encapsulation and release behavior of the MPs were also investigated using an inverted microscope (Olympus IX81, Germany), equipped with a DP 80 digital camera. Transmission electron microscope (TEM; JEOL JEM 2100; JEOL, Peabody, MA) and fourier transform infrared (FTIR) spectroscopy (Thermo Nicolet NEXUS 870 FTIR ESP, Thermo Fisher Scientific) were employed to investigate the morphology of EPO-coated MPs/pH responsiveness and the presence

of EPO coating, respectively. TEM samples were prepared following the previously reported protocol [145].

4.2.4. Encapsulation, preservation, and release behavior of the macropored MPs with a protection layer

Fluorescent beads (100 nm, 1 μm, and 4 μm) solutions were 10-fold diluted in DI water prior to encapsulation experiments. 500 mg of L100 MPs was added to 10 mL of the fluorescent bead solution, followed by the application of vacuum on/off cycle for the encapsulation of the beads into pored MPs [145]. After 3-4 hrs of incubation in the dark, the precipitated MPs were collected from the bottom of the tubes and resuspended in 15 ml DI water. Samples were freeze-dried following rapid freezing in liquid nitrogen.

Freeze-dried MPs were coated with EPO according to the protocol discussed in **Fabrication of pored MPs, pore closure process, and formation of EPO coating layer**. 50 mg of encapsulated MPs with an EPO coating layer was incubated in a solution composed of KCl (0.05 M), HCl (0.05 M), and Na_2HPO_4 (1 wt%, pH 7.1) at 37 °C for 10 min to test the stability of MPs in the simulated pregastric conditions. The MP samples were subsequently incubated in simulated gastric fluid (abbreviated as SGF; 0.05M KCl and 0.05 M HCl, pH 2.0) for 2 hrs and finally in simulated intestinal fluid (abbreviated as SIF) for 4 hrs, respectively. During all the incubation steps, the time-dependent preservation/release behavior of the coated MPs was monitored through direct observation under a fluorescence microscope. Also, the fluorescence emission was measured from the samples every 10 minutes (excitation wavelength: 490 nm, emission wavelength: 500-530 nm). MP samples incubated in the simulated digestive process were taken out at different time intervals for fluorescence microscopy analysis (FITC filter).

4.2.5. Lactase encapsulation, preservation and release efficiency of the coated MPs

1 g of as-prepared MPs was added to 10 mL of lactase solution in DI water (20 mg/ml lactase enzyme, 15 wt% trehalose, 0.5 wt% carboxymethyl cellulose). Similar to the encapsulation process used for fluorescent beads, lactase enzyme was encapsulated into the MPs through the surface pores by the application of vacuum on/off cycles. Lactase-encapsulated MPs were freeze-dried to close the surface pores, followed by a subsequent EPO coating as described in **Fabrication of pored MPs, pore closure process, and formation of EPO coating layer**.

Lactase-encapsulated MPs with an EPO protection layer were incubated in simulated oral/gastric/intestinal fluids. The concentration and the activity of the released enzyme were measured using micro BCA assay and 2-nitrophenyl β-D-galactopyranoside (o-NPG) assays, respectively. The assays and the control samples were implemented according to previously described protocols [145]. The same concentration of the enzyme in pH 2.0 solution and pH 7.1 buffer were used as a negative and a positive control, respectively.

4.3. Results

4.3.1. Fabrication of macropored MPs with a protection layer

As was explained in detail in the previous chapters, to simplify the process by eliminating all variables associated with emulsification process, unprocessed L100 powder was used as a starting material for the production of MPs with macropores [149]. In a typical procedure, L100 powder suspension in DCM (Tb: 39.6 °C) was incubated at 39 °C for 120 min, followed by solvent removal after overnight incubation at 65 °C (30 min)/37 °C (overnight). This was based on the hypothesis

that evaporation of the solvent from a swollen polymer plays a critical role in creating pores in polymeric MPs [118]. As shown in Fig. 22 a, solvent evaporation successfully formed macroscopic pores in L100 MPs. The size of MP pores was measured to be in the range of between 300 nm and 6 μm (mean diameter ~ 3 μm) [149]. To seal these pores, as-prepared samples were freeze-dried by using a recipe reported in our previous work. As shown in the SEM image (Fig. 22 b), it is evident that freeze-drying induced pore closure of MPs, which is consistent with our previous findings. Considering the end application is the oral administration of these MPs, pore closing by freeze-drying is a critical factor in protecting encapsulated drugs from gastrointestinal fluids, and thus in developing formulations with a higher level of therapeutic efficacy.

Since pored MPs are made of anionic copolymers (L100), as-synthesized MPs may dissolve in pregastric conditions before entering the stomach. To prevent the oral disintegration of MPs, a protection layer made of the cationic copolymer (EPO) was coated on freeze-dried MPs (see Fig. 22 c and 26 d for low- and high-magnification images of EPO-coated MPs, respectively). To verify the formation of the protection layer, electron microscopy and FTIR analyses were performed to observe the morphological change and obtain structural information of EPO-coated MPs, respectively. As can be seen in cross-sectional view of MPs in Fig. 23 a, a thin shell was observed to cover the outer surface of MP wall. The structural feature of the EPO-coated MPs was further characterized using FTIR by comparing three samples (i.e. EPO-only, MPs-only, and EPO-coated MPs).

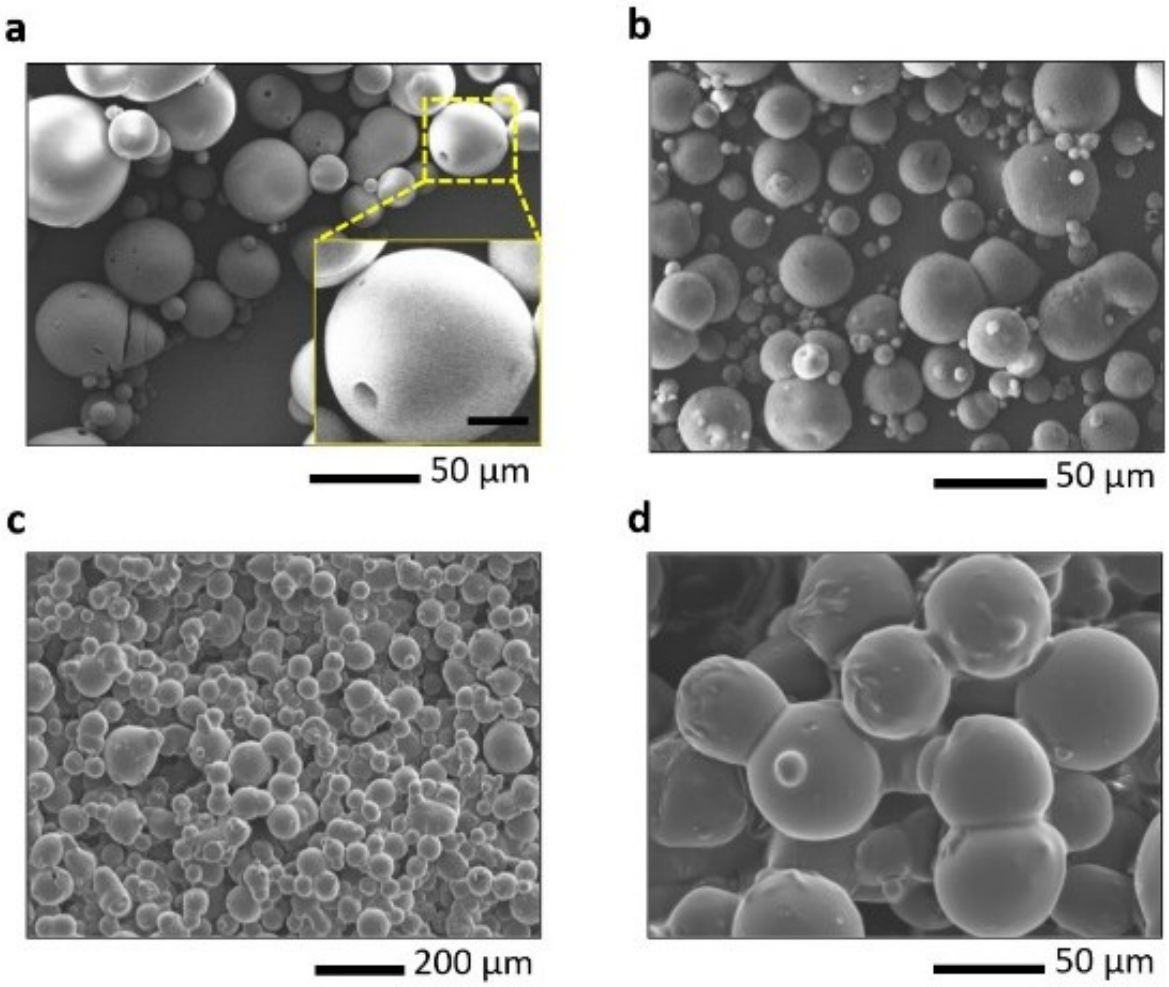

Figure 22. Fabrication of pored MPs and their pore closure by the freeze-drying process. SEM images of (a) pored MPs (inset scale bar: 10 µm) and (b) freeze-dried MPs. Formation of EPO-coated MPs with closed macropores. (c) Low-magnification and (d) high- magnification SEM images of L100 MPs

As shown in FTIR spectra in Fig. 23 b, EPO-coated MPs showed bands corresponding to dimethyl amino groups of EPO (2770 cm-1 and 2820 cm-1), matching those of EPO-only

[178,179]. This clearly validates that the protection layer (shell) formed on the surface of MPs is the EPO coating.

It should be noted that in many cross-sectional views of the fractured samples, it was difficult to identify the difference in morphology between EPO-coated MPs and MPs-only. Thus, to clarify the formation of the shell, halloysite-suspended EPO formulation was used to create the protection layer. Halloysite nanotubes (Al2Si2O5(OH)4·2H2O) are aluminosilicate clay, which can be easily identified by their tubular morphology in the coated layer [162,163,180]. Thus, halloysites were used as a marker to indicate the EPO coating. It is interesting to note that the interface between halloysite-added EPO coating and MP wall was more clearly visible compared to EPO-only, as shown in Fig. 23 c (i). The same sample was further characterized using TEM to confirm the formation of the protection layer on MPs. As shown in TEM image of Fig. 23 c (ii), it was found that about 450 nm thick halloysite-embedded EPO coating layer was created on the surface of MPs. Halloysite nanotubes displayed their typical tubular architecture in the EPO matrix. Due to the presence of heavy elements (Al, Si, and O) in halloysites, they exhibited a darker contrast compared to EPO polymer matrix, which is composed of light elements (C, O, and N). Furthermore, TEM analysis is consistent with SEM data in Fig. 23 (a) and 24 c (i).

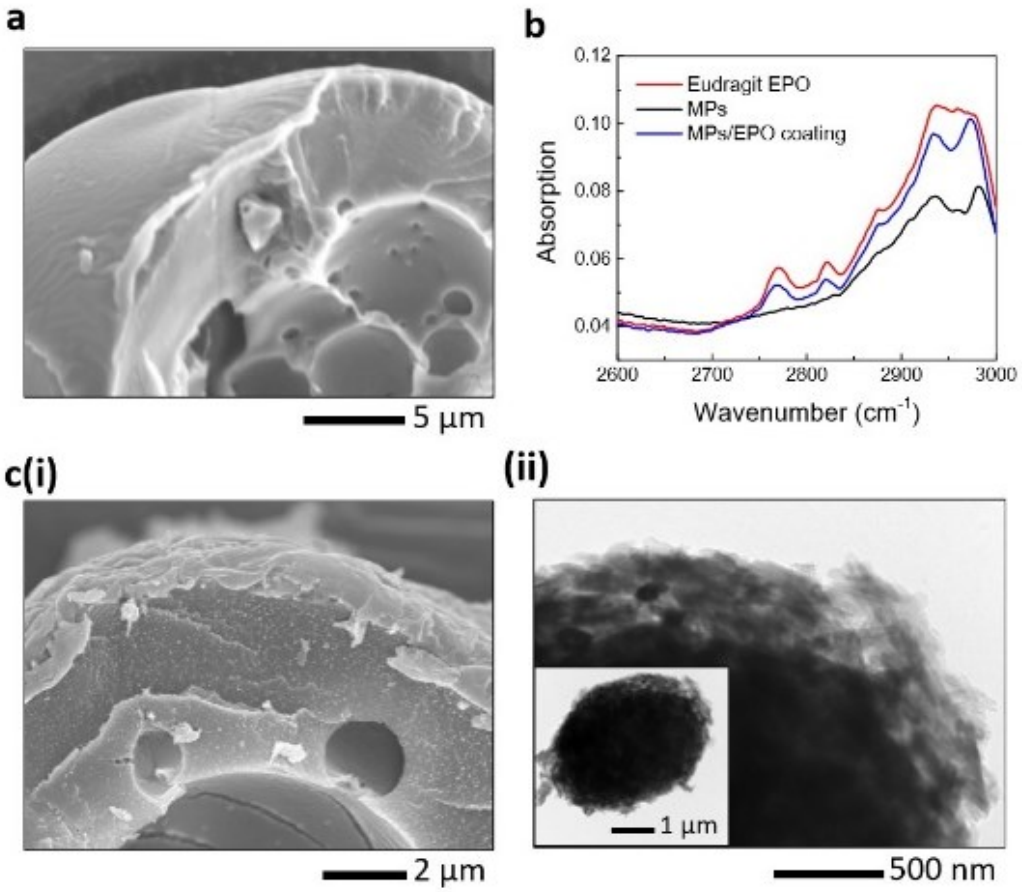

Figure 23. Verification of the EPO protective coating using electron microscopy and FTIR analyses. (a) SEM image of the cross-sectional view of EPO-coated MPs, (b) FTIR spectra of EPO-only, MPs-only, and MPs with EPO protective layer, and (c) (i) SEM and (ii) TEM images of MPs with halloysite-incorporated EPO coating

Table 3. The properties of the MPs before and after coating with EPO

Sample	Surface Charge (mv)	Average size (µm)	Poly-dispersity index	Pore size (µm)
L100 MPs	-60.17±7.3	27.5±15	1.31	3.13± 2.8
Coated MPs	-32.27±2.8	47±14	1.21	NA

The average size of the MPs, their polydispersity indexes as well as their surface charges before and after coating are summarized in Table 3. The average size, pore size and the preservation efficiency of the non-coated MPs have already been reported in our previous paper [149]. As shown in the table, the EPO coating on the surface of the anionic L100 MPs induces positive charge due to its cationic nature. In addition, as could be expected, due to the filtration step done on the MPs during the coating process, coated MPs show a larger average diameter, narrower size range, and lower polydispersity index.

After successful fabrication of protective layer-coated MPs, the pH-dependent structural stability of MPs was investigated by electron microscopy and FTIR analyses. Upon exposure to simulated gastric fluid (SGF), the outer EPO shell was completely dissolved, and the remaining MPs were observed to be highly rough, as can be seen in Fig. 24 a (i). Alternatively, when halloysite-containing EPO-coated MPs were exposed to SIF, only enteric-soluble MPs remained due to the dissolution of the EPO coating. This observation is further supported by FTIR analysis.

As shown in Fig. 24 b, EPO-coated MPs exhibited dimethyl amino bands when exposed to SIF. This can be explained by the maintenance of EPO coating's intact structure of EPO coating in near neutral pH condition (mimicking the pH of both saliva/esophagus and intestine). However, when exposed to SGF, EPO coating was dissolved, as evidenced by the disappearance of dimethyl amino band in the FTIR spectra. This supports our observation of electron microscopy analyses in Fig. 24 a. Due to their exposure to SGF, MPs without a protection layer were found to have completely dissolved in simulated pregastric conditions (see TEM image in Fig. 24 c). This can be justified by the enteric-soluble properties of anionic copolymer-based MPs; L100 anionic copolymer is supposed to dissolve at pH ≥5.5 due do the ionization of carboxylic acid. For this reason, L100 MPs with an EPO coating layer can have unique characteristics to i) protect L100 MPs in the near neutral pH of pregastric conditions, ii) selectively dissolve only EPO layer in acidic pH of the stomach, and iii) dissolve MPs in neutral pH of the intestine (see SEM image in Fig. 24 d). This means that drug-loaded MPs will be protected from mouth to stomach by the presence of EPO coating layer, and encapsulated drugs will be released in the intestine by both pore opening and dissolution of MPs.

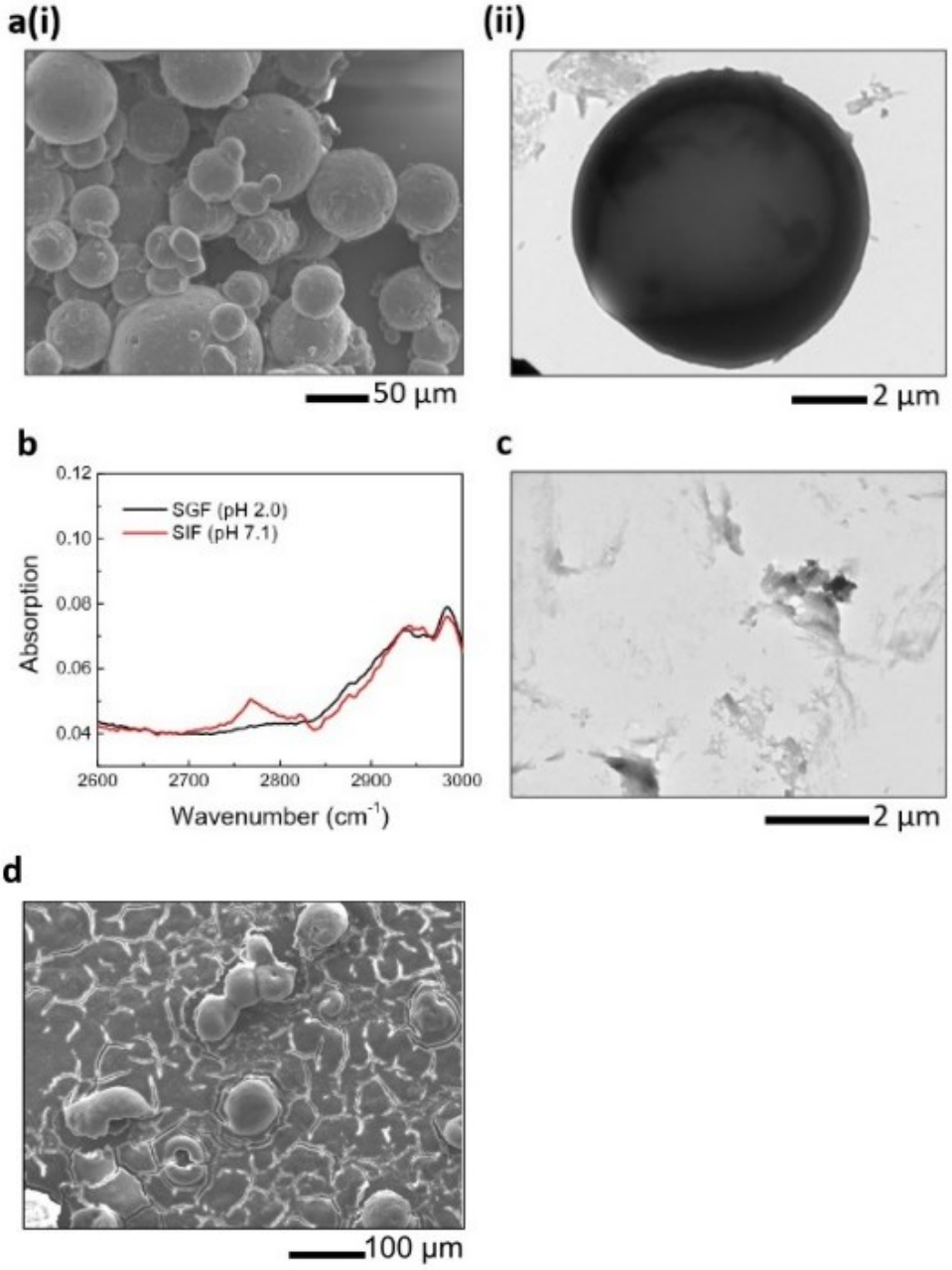

Figure 24. Morphological evolution of MPs with EPO coating after exposure to pH 2.0. (a) (i) SEM image of MPs, (ii) TEM image of MPs with a halloysite-incorporated EPO coating, (b) FTIR spectra of MPs with EPO coating after exposure to SGF and SIF, (c) TEM image of MPs without EPO coating after exposure to simulated pregastric conditions, and (d) SEM image of MPs with EPO coating after exposure to pregastric conditions, SGF, followed by SIF.

s

4.3.2. Encapsulation and release of pored MPs using model drugs in simulated digestive conditions

Our experiments so far implement the idea of pH-responsive MPs with macropores. Since our goal is to develop universal oral drug delivery system, our next step was to investigate the encapsulation and release behavior of MPs in simulated digestive conditions. Encapsulation and release studies were carried out using fluorescent beads with a diameter of 100 nm, 1 μm, and 4 μm as to mimic the inactivated virus vaccine, bacteria, and cells, respectively. Fluorescent beads were loaded into MPs through their pores by repeatedly turning the vacuum on and off, followed by pore sealing via lyophilization [145]. Closed-pored MPs were further coated with EPO protection layer to evaluate their time-dependent release behavior at different pH conditions of digestive tracts.

Fig. 25 shows fluorescent microscope images collected over the course of incubation of fluorescent beads-loaded MPs in simulated digestive conditions (see Fig. 25 a: 100 nm, Fig. 25 b: 1 μm, and Fig. 25 c: 4 μm). It should be noted that as-prepared MPs were successful in encapsulating all three different sizes of fluorescent beads [149]. MPs upheld their intact spherical morphology during the initial 10 min of incubation in simulated pregastric conditions without any significant leakage of fluorescent beads. This can be rationalized by the maintenance of the intact structure of EPO coating layer in near neutral pH condition, providing protection to beads-loaded MPs. Interestingly, exposure to SGF did not cause any noticeable level of leakage or morphological evolution during the course of 2-hr incubation. This result is particularly important because of the data evidence that dissolution of EPO in SGF did not exert a deteriorative effect on the stability of closed-pored MPs. That is, in acidic pH, gastric-soluble EPO is selectively removed without opening pores of MPs. This can be further supported by the microscopic images shown in

Fig. 26 a. After 2-hr incubation in SGF, fluorescent beads-loaded MPs were further subjected to SIF. As can be seen in fluorescent microscope images, fluorescent beads showed a rapid release upon exposure to pH 7.1, irrespective of their size. This is different from our previous observation of size-dependent release behavior for S100 MPs, indicating that a release of encapsulated beads occurs via a different mechanism.

Real-time fluorescence microscopy analysis was performed for precise monitoring of release mechanism from the initial period of release. Representative still video images are shown in Fig. 26 a and b after exposing 100 nm fluorescent bead-encapsulated MPs to pH 2.0 and pH 7.1, respectively. As can be seen in Fig. 24 a, no significant morphological change was observed for MPs at pH 2.0. However, MPs began to exhibit a burst-release pattern within 1 min after being subjected to pH 7.1. Based on the observation of both release pattern and morphological change of MPs during incubation at pH 7.1, it is reasonable to assume that a rapid release of fluorescent beads from L100 MPs can be accounted for by the dissolution of the polymer as well as rapid pore opening. This explains why release pattern was seemingly independent of ingredient size in the case of L100 MPs.

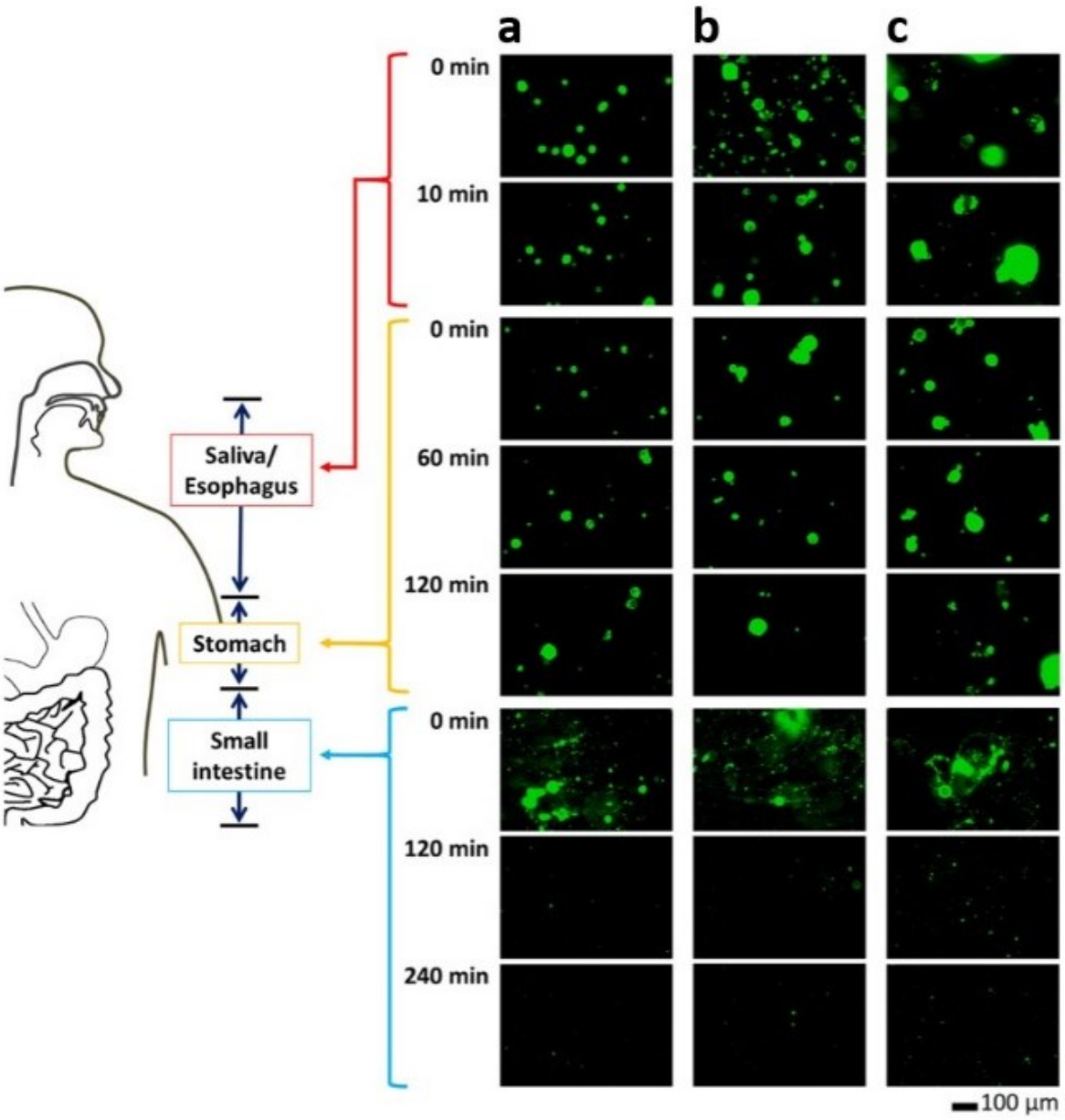

Figure 25. Fluorescence microscopy of fluorescent beads-encapsulated MPs with EPO coating. Representative fluorescence micrographs of (a) 100 nm fluorescent nanobead-, (b) 1 µm microbead-, and (c) 4 µm microbead-encapsulated MPs subjected to simulated GI tract environment (simulated pregastric environment: 10-min incubation at pH 7.1 and 37 °C; SGF: 2-hr incubation at pH 2.0 and 37 °C; SIF: 4-hr incubation at pH 7.1 and 37 °C)

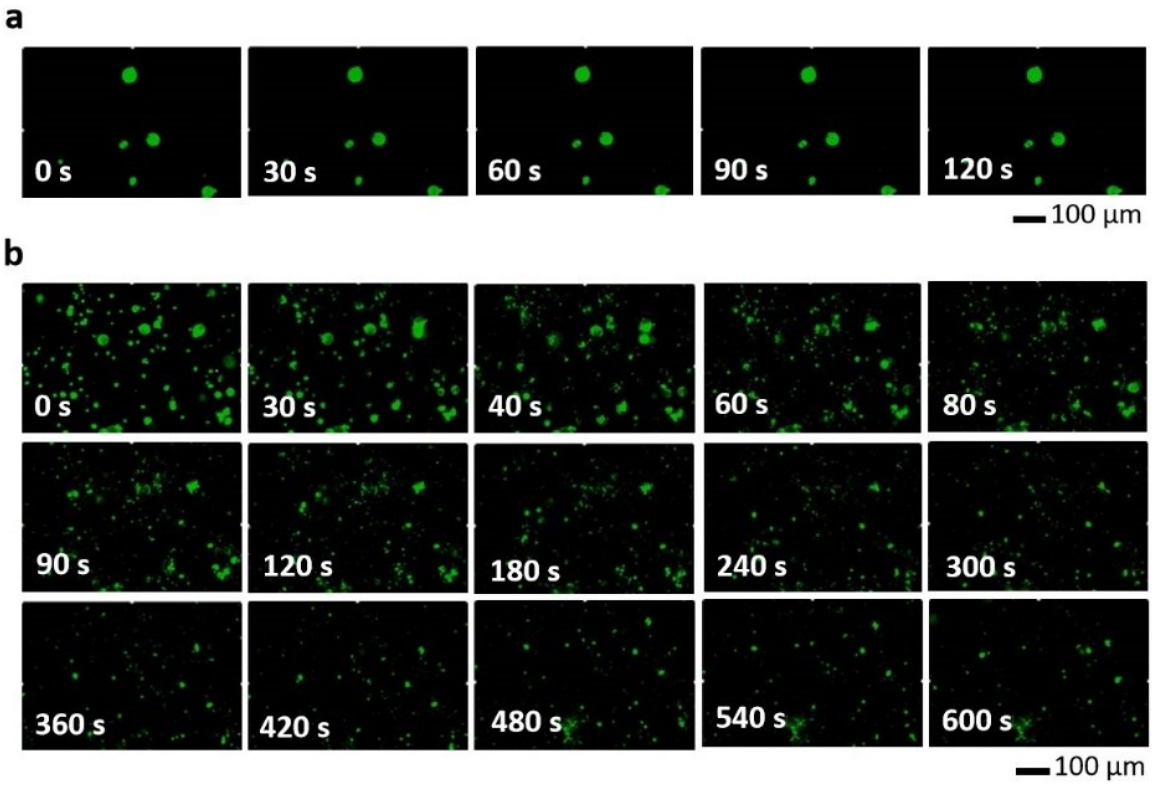

Figure 26. Still video images from real-time fluorescence microscopy analysis of 100 nm fluorescent bead-encapsulated MPs in simulated GI tract environment. MPs in (a) SGF for initial 2 min and (b) SIF for initial 10 min.

Quantitative analysis of release behavior was characterized by measuring time-dependent fluorescent intensity change in digestive conditions (see Fig. 27). Consistent with our observation from fluorescence microscopy (Fig. 26) and SEM (Fig. 24 a) analyses, 10 min incubation in simulated pregastric conditions did not show any difference in fluorescence intensity, indicating no leakage or destabilization of MPs. When EPO-coated MPs were subjected to SGF, a small number of fluorescent beads was released gradually within initial 20-30 min of incubation. Based on the fluorescent intensity, this was around 20% of the total encapsulated beads that was released in the acidic medium. We presume that this release is associated with fluorescent beads bound to the outer surface of MPs and/or those from partially sealed-MPs. In our previous study, a similar

level of initial leakage at pH 2.0 was observed from 100 nm fluorescent bead-encapsulated S100 MPs.

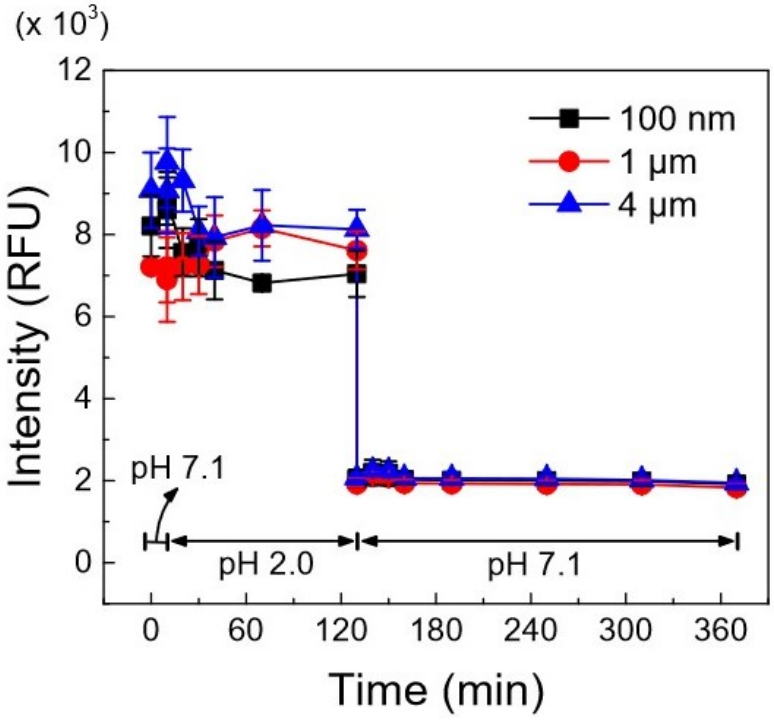

Figure 27. The release of fluorescent beads from MPs in simulated GI conditions. Time-dependent release profile of encapsulated (a) 100 nm, (b) 1 μm, and (c) 4 μm fluorescent beads from MPs (simulated salivary and esophageal environment: 10-min incubation at pH 7.1 and 37 °C; SGF: 2-hr incubation at pH 2.0 and 37 °C; SIF: 4-hr incubation at pH 7.1 and 37 °C). (n = 5, mean ± SD)

Post 2-hr incubation in SGF, exposure to SIF resulted in a rapid decrease in fluorescent intensity. This fast release is consistent with our observation from Fig. 26 and further supports the burst-release mechanism due to the rapid dissolution of enteric-soluble L100 polymer and pore opening. Overall, these results support the fabrication and feasibility of our proof-of-concept

macropored MPs with cationic shell coating, which can encapsulate and protect biopharmaceuticals from diverse physiological conditions of digestive tracts, such as the simulated mouth, stomach, and intestine environments.

4.3.3. Protection and targeted delivery of lactase to the intestine

Following our demonstration of concept using model drugs, practicality of the macropored MP delivery system has been tested using β- galactosidase, a lactase enzyme. For this purpose, the structural and functional stability of lactase was evaluated in simulated digestive conditions by comparing their enzymatic activities. The selection of lactase is based on its vulnerability to acidic pH. Also, destabilized lactase at low pH does not recover to their original conformation when they are exposed to the neutral pH. Hence, the monitoring of enzyme activity at different physiological conditions provides a valuable information about the protective efficacy of the proposed MP formulation in this work. In comparison with our previous study on the non-coated MPs, this part of the experiments can show the effect of the coating step on drug activity loss.

Fig. 28 represents a histogram showing remaining activities of lactase at different physiological conditions compared to that of the intact lactase. It appears that lactase enzyme without MP formulation lost most of their activity upon exposure to acidic pH (pH 2.0) followed by pH 7.1 medium (Lactase (pH 2.0>7.1) (remaining activity: 1.4 ± 0.5%, Lactase (pH 2.0>7.1) in Fig. 28).

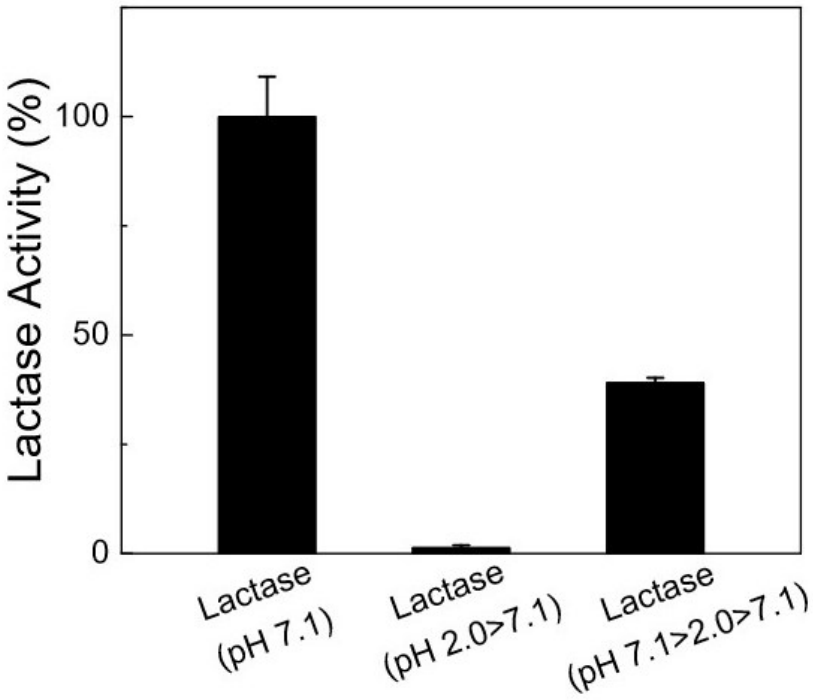

Figure 28. Remaining activities of lactase enzyme. Lactase after 4-hr incubation at pH 7.1 (Lactase (pH 7.1)), lactase after 2-hr incubation at pH 2.0 followed by 4-hr incubation at pH 7.1 (Lactase (pH 2.0)), and lactase after incubation in simulated digestive conditions (i.e. 10-min incubation in pregastric condition, followed by 2-hr incubation in SGF and 4-hr incubation in SIF; Lactase (pH 7.1>2.0>7.1)). (n = 3, mean ± SD).

In contrast, lactase encapsulated in MPs maintained about 40% of the activity of the positive control sample in simulated digestive conditions (Lactase (pH 7.1>2.0>7.1) in Fig. 28), demonstrating the strong protective efficacy of MPs. This higher level of protection (28 times higher protective efficacy) can be attributed to the individual and combined effects of the programmed response in the digestive tract. In other words, each functional component of lactase-encapsulated MP formulation includes 1) formation of macropored MPs using anionic copolymer

(L100), 2) lactase encapsulation into pored MPs without activity loss, 3) stabilizing lactase formulation against lyophilization process, 4) pore-closure by freeze-drying, 5) formation of protection layer using cationic copolymer (EPO) on MPs, 6) protection of lactase-encapsulated MPs in pregastric (saliva, esophagus) pH condition by EPO, 7) selective dissolution of EPO layer in gastric pH condition and protection of lactase encapsulated in closed-pored MPs, and 8) efficient release of lactase through dissolution/pore opening of MPs in intestinal pH condition. In spite of the need of the further process optimization research, the noticeable increase in protection efficacy proves the potential applicability of our MPs with pH-responsive macropores in developing diverse oral drug and vaccine formulations.

4.4. Discussion

We investigated the cationic copolymer (shell)-coated and anionic copolymer (core)-consisted MPs with pH-responsive macropores as a prospective oral drug delivery system. This shell/core structure is proposed to overcome the physiological constraints imposed by different pH conditions of digestive tracts. To create protection layer on MPs, an important parameter to consider is the solvent compatibility of the materials used for fabrication of the shell and core consisting MPs. As addressed in the method section, L100 powder was suspended in DCM, followed by solvent removal to create macropored MPs. This was possible because DCM is a poor solvent to L100 polymer. On the other hand, the fact that DCM is a good solvent for EPO allowed for the formation of a continuous protection layer on the outer surface of macropored MPs made of L100 without dissolving or destabilizing them. Considering that drug-encapsulated MPs with closed pores are mixed with EPO in DCM solution to produce EPO-coated MPs, dissolution of MPs by DCM

would have opened macropores and exposed drugs to destabilizing solvent environment. Therefore, the main advantage of using DCM is to create EPO shell around the closed-pored MPs without denaturing biopharmaceuticals. This is supported by well-defined coating in Fig. 25 and no significant leakage during the EPO coating process as confirmed by Figs. 24 and 25.

When exposed to SGF, it is important that the closed-pored MPs remain intact upon removal of the shell. To this end, first, pKa of the polymer used to fabricate MP backbone should be close to the pH of the site of interest, thus maintaining the structural integrity of the closed-pored MPs in acidic pH of the stomach, and sensing and responding only to the pH of the site of interest. In addition, the protection layer (i.e. shell) should not be chemically linked to the core of the MPs. That way, gastric-soluble shell layer can be selectively removed in the stomach to prevent the negative destabilization impact on drug-loaded MPs. Therefore, L100 with pKa ~ 5.5 could maintain intact structure in SGF without a protection layer (see Fig. 26), as supported by no significant leakage from fluorescence measurements (Figs. 24, 25, and 27). When exposed to SIF, the intestinal pH triggered deprotonation of carboxyl groups, which resulted in a rapid dissolution and pore opening of MPs. Unlike MPs made of S100 (pKa ~ 6.8), L100 MPs exhibited a rapid release of drugs in a size-independent manner. In the case of S100, drug release through pore opening is believed to be a dominant mechanism, compared to the release through the dissolution of the MP backbone, and thus the release rate is limited by the size of pores and drugs (i.e. faster release for smaller drugs). However, due to the use of easily ionizable moieties with a lower pKa value in L100 MPs, drug release by polymer dissolution is more dominant than by pore opening in response to the intestinal pH, leading to a faster release of drugs when comparing to S100. This is supported by our real-time fluorescence microscopy analysis in Fig. 26 and time-dependent release behavior in Figs. 26 and 27.

Another important aspect of pored MPs is that they provide biopharmaceuticals a solid drug formulation platform such as solid oral vaccines. Although effective, the current liquid form of the vaccine has several significant disadvantages, including relative instability and need for proper infrastructure (i.e. electrical cold chain systems for transport, shipping, and storage) [130]. These issues raise the vaccine price and represent hurdles when stockpiling them. To this end, pored MPs exhibit promising characteristics for the implementation of solid vaccine formulation to protect vaccine against harsh GI tract environments. Vaccines encapsulated into MPs would be protected from proteolysis in the acidic stomach and would be released in the intestine due to the dissolution of the polymer. To fabricate solid vaccine, stabilizing excipients should be added to the liquid-based biopharmaceutical formulation to prevent denaturation during the dehydration process. For this purpose, disaccharides (trehalose and sucrose) and viscosity enhancer (carboxymethyl cellulose) have been used as excipients in microneedle formulation to stabilize vaccines during drying [97,181]. According to previous reports, the addition of disaccharides is known to suppress the gel-to-fluid phase transition temperature of the lipid membrane and preserve the original structure of biomolecules under dehydration conditions [182,183]. Furthermore, biomolecules can better maintain their conformation in a glassy sugar matrix. Viscosity enhancer functions to increase the viscosity of the formulation, hence reducing the effective osmotic pressure applied to the vaccine and also suppressing the phase transformation by slowing the diffusivity of sugar molecules [2,6,180]. Phase transformations, such as crystallization and phase separation of the sugar matrix, have been reported to be a major vaccine destabilizing factor during the initial drying and long-term storage stages. In this work, 15% trehalose/0.5% carboxymethyl cellulose was used as a stabilizing formulation for the lactase enzyme. Although not investigated in this work, in our future research, we will perform long-term stability tests under diverse storage conditions and at

different stabilizing formulations. Especially, in the case of pored MPs, it will be interesting to determine the effects of physical confinement of drug/vaccine in the pores of MPs on their long-term stability, specifically their phase transformation. Our next challenge also includes optimization of MP fabrication process (control over the pore and particle size), increase pore-closure efficiency (optimize freeze-drying process), stability test (optimize formulation to increase shelf-life), release rate (modify formulation or release mechanism), *in vitro-in vivo* correlations, and mucoadhesion/cellular uptake. Also, it will be of high significance to further modify the loading capacity and the preservation efficiency of the system to prepare it for *ex vivo*/*in vivo* studies.

This work showed that shell-core composite MP structure with macropores provides programmed behaviors in response to different physiological pH conditions of the digestive tract. Also, this behavior can be utilized for providing protection to MPs in the pregastric and gastric environment, and releasing encapsulated drugs in the intestinal environment. The unique benefits observed from the performance evaluation of macropored MPs cannot be met by conventional delivery vehicles that have been reported to date. Despite the need for further research, our macropored MPs are expected to make a significant contribution towards the development of solid, cold chain-free, oral drug/vaccine formulations, having a long-term stability and extended shelf life.

5. Chapter 5

The application of the system for other administration routes

5.1. Preface

As was already mentioned in chapter 1, one of the principal advantages of oral delivery systems is their capability for solid formulations. Solid formulations do not need refrigeration and can be easily transferred worldwide. Solid edible formulations enjoy patients' compliance; so can they be easily administered without need for well-trained health care personnel. In comparison with liquid injectable formulations, oral solid formulations do not leave biohazardous wastes, nor do they induce extra health risks in the case of pathogen spread, such as needle reuse in the case of IM/IN/IV administration techniques. Considering all these advantages, long term stability of the oral formulations developed in this study in various environmental conditions would be critical. Specially, as these products are not supposed to be refrigerated, they should exhibit considerable levels of stability against environmental humidity and higher temperature, like the average temperature in tropical regions. To this aim, samples were prepared and tested under various conditions.

Also, microencapsulation systems are specifically designed and fabricated to protected the drugs against harsh surroundings and safely deliver them to the absorption sites or the targets. Therefore, the application of these systems never limit to oral administration. In this chapter of this thesis, it has been tried to demonstrate the application of the system developed in chapter 3 of this thesis for intranasal administration. In the first step, the details of intranasal delivery will be discussed hereunder, which has been directly adopted from the review paper previously published by this group [1].

Intranasal drug delivery entails the infusion of the drug into the highly vascularized mucosal layer of the nose to subsequently reach systemic circulation [184]. IN drug delivery is crucially significant for neurological diseases, where drugs are required to reach the central nervous system

(CNS) by bypassing the blood-brain barrier (BBB). In general, the IN route is preferred for local diseases due to its limited systemic effects compared to the other methods. The IN route also has its own specific physiological and physicochemical barriers. The physiological barriers include capillary barriers, nasal mucus, mucus clearance and nasal metabolism. Other factors such as pH, possible drug-mucus interactions and the viscosity of the mucus may also influence drug diffusion and absorption in IN administration. Mucoadhesive microencapsulation systems have been developed to deal with the mucus-associated barriers of IN delivery and improve the bioavailability of nasally-administered drugs. For example, Nanaki et al. coated nasal microcapsules with thiolated chitosan to aid the mucoadhesion of the system, both physically (electrostatic attractions) and chemically (disulfide bonds) [185]. However, it should be noted that mucociliary clearance and discharge considerably limits the drug residence time, even if the carriers develop a strong bonding/binding with the mucus [186]. Physicochemical barriers concern the molecular weight of the drug, and its lipophilicity and degree of ionization, which also define the absorption mechanisms [187]. Despite multiple challenges, IN is an advantageous route for the delivery of a variety of the drugs. It avoids first-pass metabolism and GI complications. Due to its considerable absorption rate, IN is an applicable method for emergency cases and rapid drug action. Neurological drugs especially can be transported directly to the CNS through the IN route.

The nasal-associated lymphoid tissue (NALT) is the principal target for inducing mucosal immunity in nasal vaccination. The innate immunity is achieved by macrophages and dendritic cells, and the adaptive immunity at the mucosal layer is induced by IgA [188]. Hence, IN vaccination can induce both mucosal and systemic immunity. However, physiological barriers, especially mucociliary clearance, need to be adequately addressed for the effective delivery of antigens to the target site. Furthermore, due to the limitations of the nasal cavity, as well as the

narrow passages beneath the thick mucus, nasal vaccination is only permitted for small dosage and low molecular weight compounds. In order to pass biosafety requirements, IN delivery devices need to be suitable for narrow nasal entrances and the complex geometry of the nasal passage. On top of that, lung exposure should be properly addressed in these systems. Among the various physical states of drugs (gels, droplets, powders, or aerosol sprays), aerosol sprays are usually preferred for IN administration. New technologies are constantly under development to improve the dispersion of the drugs and modify the deposition and clearance behavior through combining solid and liquid phases. However, human anatomy as well as the physiology of the nasal cavity and passage still limit clinical applications and delivery efficiency. Low bioavailability (<5%) causes another major challenge for IN administration systems [189].

As was discussed before in chapter 3, the HNT-S100 MPs developed in this study can be used for co-delivery of any combination of drugs. As a well-known biological barrier against the absorption of the drugs through intranasal route, biofilms can significantly impede the transportation of the drug molecules through the bacterial layer and drastically reduce the nasal bioavailability of the drug. HNT-S100 MPs would be great candidates for the co-delivery of antibiotics to the absorption site of the drug, so that the system can effectively remove the biofilm and significantly improve the drug absorption. In that scheme, antibiotics can be loaded into HNTs, while the main drug is loaded into the interior space of the MPs. The first steps of the project for developing this system were designed and followed as explained below.

5.2. Methods

5.2.1. Materials and chemicals

Poly(methacrylic acid-co-methyl methacrylate) in 2:1 ratio, known as Eudragit® S100 was received from Evonik Canada Inc. (Burlington, Ontario, Canada). Halloysite nanoclay, 2Nitrophenyl β-D-galactopyranoside; poly (vinyl alcohol) (PVA) Mw: 9,000–10,000; D-(+)-Trehalose dehydrate (Tre); Carboxymethylcellulose (CMC) sodium salt (low viscosity); and β-galactosidase from Aspergillus oryzae were purchased from Sigma Aldrich (St Louis, Missouri, USA).

5.2.2. MPs preparation

Due to their highest loading capacity as well as their highest preservation efficiency, large S100 MPs discussed in chapter 3 of this thesis were used for this part of the project. Briefly, 10 ml of organic phase (5 wt% S100 dissolved in the cosolvent system (dichloromethane:ethanol:isopropanol = 2:1:1)) was emulsified in 200 ml of the aqueous phase (0.5 wt% PVA and 5% Tween 20). The emulsion was stabilized through stirring at 325 rpm and sonication at 15 W for 5 min using a GE-130 ultrasonic processor (Sonics & Materials, Inc.; Newtown, CT). The emulsion was further stirred at 125 rpm under fume hood for about 1 hour to the let the solvents evaporate and MPs form. The emulsion was finally filtered using a sieve (45 μm mesh size), the filtered particles were washed in DI 4 times at 10,000 g for 10 min (Eppendorf Model 5810; Hamburg, Germany), the final suspension was centrifuged at 100g for 1 min, and the MPs suspended in the supernatant were collected as the large S100 MPs. The MPs were transferred into 2 ml Eppendorf tubes, in aliquots of 1 ml, frozen in liquid nitrogen and lyophilized (AdVantage Pro Freeze Dryer, SP Scientific; Warminster, PA) according to the cycle already discussed before.

5.2.3. MPs encapsulation

For this part of the test, lactase was centrifuge-washed 5 times using 100 K molecular weight cutoff filter tubes, before the encapsulation to remove all the formulation sugars. 1 ml of the lactase (20 mg/ml washed lactase from Aspergillus oryzae in 15 wt% Trehalose and 0.5 wt% CMC aqueous solution) stock solution was added to each tube. The MPs were encapsulated under vacuum on/off cycles. Loaded S100 MPs were resuspended in lactase-free sugar formulation (15 wt% Trehalose and 0.5 wt% CMC aqueous solution), frozen in liquid nitrogen and finally freeze dried under the same protocol.

5.2.4. The formation of biofilm

K. penumoniae cells were cultured in MH broth medium at 37°C in shaking incubator at 200 rpm and aeration to an optical density of 0.3 at 600 nm. Biofilms were incubated at 37 ºC for 24 hours in 12 well plates (medium replacement was done every 12 hours).

5.2.5. The effects of antibiotics

Different concentrations of gentamicin ranging from 0 to 125 µg/ml were added to the wells, and the plate was incubated at 37 ºC for 6 hours. All the wells were washed 3 at least 3 times with PBS to make sure of the removal of all planktonic cells. Biofilms were detached from the plate, diluted to various concentrations and replaced into MH agar plates. The densities were measured from the plate after overnight incubation at 37 ºC.

Gentamicin released form MPs in PBS as well as Gentamicin in DI water (control) were used for this part of the experiments. The encapsulation efficiency of gentamycin in MPs was measured and subsequently diluted to 125 μg/ml. The released medium was then added to the wells, and Cfu/ml values were counted for the plates following the same procedure.

5.3. Results

5.3.1. Intranasal delivery

Figure 29 shows the effect of different concentrations of gentamycin aqueous solution on bacteria densities in the well. As shown, increasing the concentration of gentamycin administered leads to higher bacterial detachment from the biofilms and lowers the cfu/ml of the wells. Aqueous solutions of gentamycin with ≥ 125 μg/ml should be suitable for diluting the biofilms and removing the biological barrier against the drug uptake.

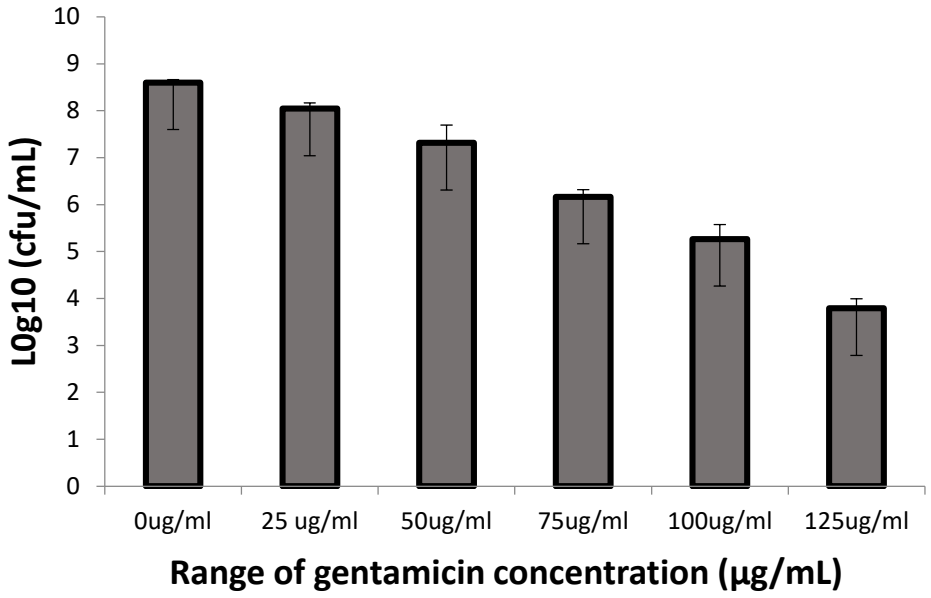

Figure 29. The effect of different concentrations of gentamycin on bacterial density in biofilms (data has been produced by Jashan Baidwan and Surjith Kumaran).

Figure 30 also demonstrates the effect of the gentamycin released from the MPs on diluting the biofilm. As shown, both the drug released from the MPs and the drug dissolved in DI, as the control sample, are showing the same levels of activity in killing bacteria and diluting the biofilms. In other words, there is no negative effects on the activity of the drug (gentamycin) due to microencapsulation or freeze drying.

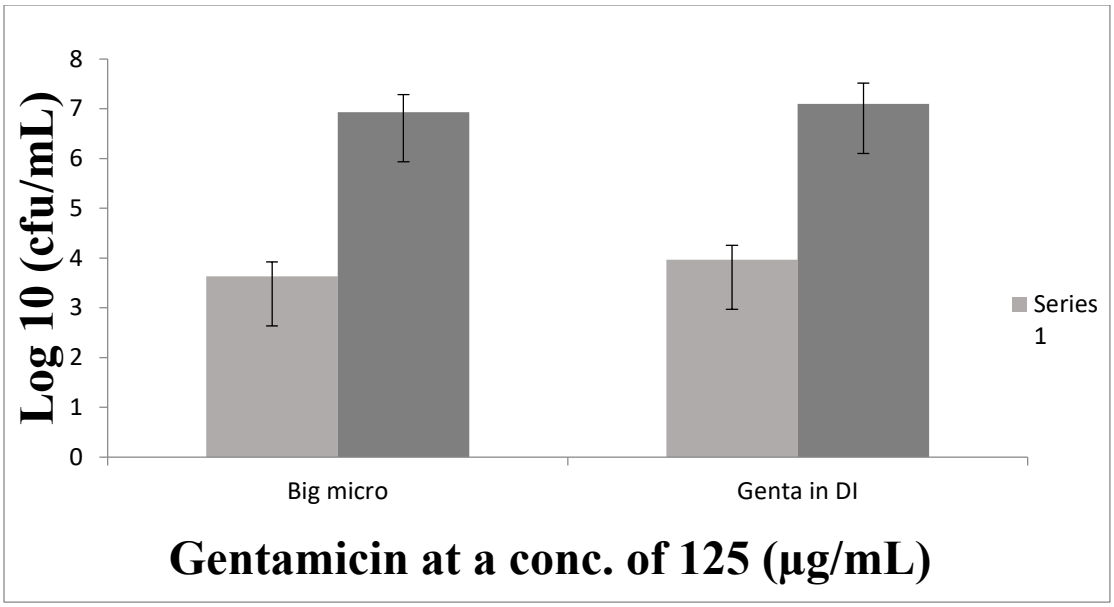

Figure 30. The effect of gentamycin (encapsulated and control) on bacterial dilution in biofilms (data has been produced by Jashan Baidwan and Surjith Kumaran).

5.4. Discussion

According to the results obtained so far, antibiotics can also be successfully co-delivered to the target through the new microencapsulation scheme developed in this project. This strategy will definitely help the absorption of the drug at the target through removing the biological barriers imposed by biofilms covering the surface of the tissue. Clearly, significantly more experiments and investigations will be needed in the future to confirm the applicability of the system in this newly developed route. The results so far reflect the promising potentials of the system for further analyses.

Stable solid formulations play crucial roles in pharmaceutical industry. Such formulations can easily be transferred worldwide with varied environments. They can be especially delivered even to the places with restricted storage conditions. Oral formulations developed in this project have

demonstrated great potentials in vitro, long-term stability would be a new advantage for them. Gelatin capsules start to partially dissolve/degrade in aqueous media shortly after incubation. As a consequence, gelatin capsules cannot be used for further protection of the loaded drugs, but merely for protection in saliva and esophagus (about 10 min). With this in mind, MPs would play crucial role in gastric preservation of the drug, which cannot be afforded by other containers.

Regarding long-term stability, drug molecules embedded in the formulation developed in this work showed better stability in remaining activity, in comparison with unprotected bare enzyme. If the same experiment is repeated with more sensitive biopharmaceuticals, there would probably be more significant drops in the remaining activity of the drug with longer incubation. There will be further analyses and investigations needed to point out the main reasons why drug molecules denature by the passage of time. Above that, it would be clarified how this formulation can preserve the drug over the incubation time frame.

5.5. Conclusion

MPs play crucial role in preserving the drugs against gastric environment. Gelatin capsules cannot protect the drug molecules in gastric environment, as they start to partially/locally degrade in aqueous environment shortly after incubation. Also, sugar formulation can effectively protect the drug in long-term incubation in different environmental conditions, including highly humid conditions.

6. Chapter 6

On-going work, Conclusion and Future Works

6.1. Ongoing work work

In addition to the application of the system for intranasal delivery, the system developed in this project is under investigation for long-term stability and prolonged shelf-life without the need for refrigeration. This step of the project has been recently started and will be under progress in the future.

6.1.1. Stability studies

Oral formulations reserve a unique significance compared to other designs—that is—stability in uncontrolled environmental conditions and extended shelf life even without refrigeration. The samples for stability tests were considered as tabulated in tables 2 and 3. The solid powders after encapsulation and freeze-drying were transferred to gelatin capsules, placed in blister packs and sealed. The photos demonstrating the samples after loading into gelatin capsules and after blister packing are provided below.

The samples listed in table 4 were tested under in acidic conditions and neutral environmental conditions, while those tabulated in table 5 were only tested under neutral environmental conditions. In summary, acidic conditions mean simulated digestive test: 2 hours of incubation in simulated gastric fluid (SGF) followed by 4 hours of incubation is simulated intestinal fluid (SIF), and neutral environmental conditions means direct exposure to SIF. The reasons for this decision were:

1) Since the large anionic S100 MPs were not coated with cationic hydrogels, they would be vulnerable to near neutral conditions, especially in saliva and esophagus. The gelatin

capsules need to be investigated under simulated digestive conditions to see whether they can properly preserve anionic MPs in saliva and esophagus.

2) As was discussed before, not all the anionic MPs can be completely sealed through freeze drying, which in turn lead to partial denaturation of the loaded drug. Gelatin capsules can provide extra protection over the anionic MPs in gastric surroundings and improve the preservation efficiency of the system and consequently yield higher remaining activity of the released drug.
3) The system discussed in this thesis has been precisely controlled release of the loaded ingredients to make sure that the drug is delivered exactly to the proper absorption site. The incorporation of a new component to the system (gelatin capsules) necessitates further investigations to confirm there is no potential negative effect on the protection/release pattern of the system.

Table 4. Sample conditions for stability tests without incubation

Number	Drug	Encapsulation Formulation	Microencapsulation
1	Lactase from Aspergillus oryzae	DI water only	No MPs or capsules
2	Lactase from Aspergillus oryzae	15wt% Tre, 0.5wt% CMC	No MPs or capsules
3	Lactase from Aspergillus oryzae	DI water only	Only gelatin capsules
4	Lactase from Aspergillus oryzae	15wt% Tre, 0.5wt% CMC	Only gelatin capsules
5	Lactase from Aspergillus oryzae	DI water only	First encapsulated in S100 MPs and then gelatin capsules
6	Lactase from Aspergillus oryzae	15wt% Tre, 0.5wt% CMC	First encapsulated in S100 MPs and then gelatin capsules

Table 5. Sample conditions for stability tests after long-term incubation periods (0 min, 1, 3, 7 and 30 days)

Number	Sample	Incubation Conditions
1	Lactase in DI in gelatin capsules	37 °C Humidity 80%
2	Lactase in DI in gelatin capsules	Room Temperature Shelf Storage

3	Lactase in DI in gelatin capsules, packed in blister sheets	37 °C Humidity 80%
4	Lactase in DI in gelatin capsules, packed in blister sheets	Room Temperature Shelf Storage
5	Lactase in 15wt% Tre, 0.5wt% CMC, in gelatin capsules	37 °C Humidity 80%
6	Lactase in 15wt% Tre, 0.5wt% CMC, in gelatin capsules	Room Temperature Shelf storage
7	Lactase in 15wt% Tre, 0.5wt% CMC, in gelatin capsules, packed in blister sheets	37 °C Humidity 80%
8	Lactase in 15wt% Tre, 0.5wt% CMC, in gelatin capsules, packed in blister sheets	Room Temperature Shelf Storage
9	Lactase in 15wt% Tre, 0.5wt% CMC, encapsulated in S100 MPs, packed in gelatin capsules	37 °C Humidity 80%
10	Lactase in 15wt% Tre, 0.5wt% CMC, encapsulated in S100 MPs, packed in gelatin capsules	Room Temperature Shelf Storage

The concentration of the released enzymes as well as the remaining activities were measured through micro BCA and ONPG assays, respectively. The assays were executed according to the procedures already explained in previous chapters of this thesis.

6.2. Conclusion

Although it is always regarded as the most promising administration route, oral delivery is facing principal technical problems and biological complications. MPs with pH-responsive surface macropores can address a number of these problems, especially the concerns with drug denaturation during the encapsulation process and drug instability in harsh gastric conditions. However, the pored MPs previously available were not showing satisfactory levels of preservation efficiency, loading capacity and enough fabrication throughput. Furthermore, they did not represent satisfactory properties dealing with biological barriers at the absorption site of the drug. This work represented two new protocols for the fabrication of MPs with considerable levels of preservation efficiency of the drug against gastric conditions ($\geq$ 60 %), significant throughput and reasonable potentials for scale-up. From these two protocols, emulsion-solvent evaporation exhibited significantly better control over the interior morphology of the MPs. As a consequence, the MPs fabricated through emulsion-solvent evaporation yielded considerably higher loading capacity due to their larger interior void spaces and wider surface pores.

The incorporation of halloysite nanotubes into the matrix of the MPs provided the capability for the co-delivery applications. As a result, the nanotubes could successfully be loaded with mucolytic enzymes, such as bromelain, to locally remove the mucus barrier at the absorption site and increase the uptake efficiency of the drug. This new system could also be employed for the codelivery of any given couple of drugs, as the drugs will be loaded into two completely separated channels to eliminate any undesirable interactions between the drugs. Both the drug loaded into the system, whether into the HNTs or into the MPs, could be properly protected against undesirable surroundings and safely released at the target on time. In the case of bromelain, the ex-vivo results

clearly demonstrated that the mucus could be considerably diluted at the absorption site, which can in turn drastically improve the uptake efficiency and subsequently the oral drug bioavailability.

At the final stage, the MPs were coated with cationic copolymers (Eudragit EPO) with pKa values well below the oral pH value. The results confirmed that EPO coating can effectively protect the anionic MPs against saliva and esophagus simulated environment and prevent any unpunctual release of the ingredients from the MPs. Coating process causes some decreases in the final remaining activity of the released drug, which is probably due to the possible contact between the loaded drug and the harsh organic solvent used in EPO coating process—that is—Dichloromethane. The EPO coating is properly dissolved and removed from the MPs inside the simulated gastric fluid, and the anionic MPs will release the loaded drugs on time at the target. Also, the leakage from the MPs during the coating process was not considerable.

In summary, the present thesis represents a new microencapsulation system with novel features addressing a number of most common issues with oral delivery systems and especially the previous MPs with pH-responsive surface pores:

1) The newly modified MPs showed significantly higher loading capacity and considerable improvements in preservation efficiency of the loaded vulnerable biomolecules.
2) The new pored MPs are capable for the encapsulation of biopharmaceuticals of various size ranges, from small protein therapeutics to viruses (~100 nm), bacteria (~1 μm) and cells (~4 μm).
3) Swelling-solvent evaporation protocol for fabricating pored MPs offers a much higher payload in the expense of limited control over the morphology, polydispersity and loading efficiency of the final product.

4) The new emulsion-solvent evaporation protocol, on the other hand, offers great control over the interior as well as exterior morphology of the MPs and also promising potentials for scale-up and elevated throughput.
5) The new features included in the system (halloysite nanoclay, which was incorporated into the MPs for codelivery applications) can successfully load mucolytic enzymes to address the biological barrier associated with mucus at the absorption target.
6) Cationic EPO coating can effectively protect the anionic pored MPs in saliva and esophagus and prevent any unpunctual release of the loaded ingredients without any negative effects over the pH-responsiveness of the anionic MPs.
7) The microencapsulation formulation developed in this thesis can successfully preserve the drug in solid conditions for at least 30 days in various harsh environmental conditions.

6.3. Future works

The new microencapsulation system developed in this study showed considerable potential for solvent free microencapsulation of biopharmaceuticals. This new scheme can be used for the development of oral solid vaccines, such as influenza vaccine. In the next step of the project, it would be highly recommended to encapsulate some vaccines into the system and evaluate the preservation efficiency of the system over whole inactivated influenza vaccines *in vitro*. Subsequently, after adjusting the parameters of the system *in vitro*, vaccine encapsulated samples can be studied *in vivo* through animal studies on mice. These two steps will be principal milestones for developing oral vaccines.

In the next step, HNT-S100 MPs can be employed for co-delivery of mucolytic enzymes and vaccines to the ileum of animals *in vivo* to investigate potential improvements in the absorption

efficiency of the system. Co-delivery of mucolytic enzymes has already proved their efficacy *in vitro* and *ex vivo*, as was discussed in the 3rd chapter of this thesis.

The other aspect of the project to focus on can be increasing the fabrication throughput of the MPs. As was discussed in chapters 2 and 3, the new protocols developed in this thesis already showed considerable improvements in the fabrication yield of the MPs. The application of microfluidic systems for the emulsification process, and developing multi-channel new geometries with higher infusion rate can be a good starting point for this step of the project.

7. References

1. Homayun, B.; Lin, X.; Choi, H. Challenges and Recent Progress in Oral Drug Delivery Systems for Biopharmaceuticals. *Pharmaceutics* **2019**, *11*, 129–158.

2. Choi, H. J.; Kim, M. C.; Kang, S. M.; Montemagno, C. D. The osmotic stress response of split influenza vaccine particles in an acidic environment. *Arch. Pahrmacal Res.* **2014**, *37*, 1607–1616.

3. Banerjee, A.; Qi, J.; Gogoi, R.; Wong, J.; Mitragotri, S. Role of nanoparticle size, shape and surface chemistry in oral drug delivery. *J. Control. Release* **2016**, *238*, 176–185.

4. Araújo, F.; Pedro, J.; Granja, P. L.; Santos, H. A.; Sarmento, B. Functionalized materials for multistage platforms in the oral delivery of biopharmaceuticals. *Prog. Mater. Sceince* **2017**, *89*, 306–344.

5. Hu, Q.; Luo, Y. Recent advances of polysaccharide-based nanoparticles for oral insulin delivery. *Int. J. Biol. Macromol.* **2018**, *120*, 775–782.

6. Choi, H.-J.; Ebersbacher, C. F.; Kim, M. C.; Kang, S. M.; Montemagno, C. D. A mechanistic study on the destabilization of whole inactivated influenza virus vaccine in gastric environment. *PLoS One* **2013**, *8*, 1–14.

7. Schenk, M.; Mueller, C. The mucosal immune system at the gastrointestinal barrier. *Best Pract. Res.* **2008**, *22*, 391–409.

8. Ensign, L. M.; Cone, R.; Hanes, J. Oral drug delivery with polymeric nanoparticles: The gastrointestinal mucus barriers. *Adv. Drug Deliv. Rev.* **2012**, *64*, 557–570.

9. Leal, J.; Smyth, H. D. C.; Ghosh, D. Physicochemical properties of mucus and their impact on transmucosal drug delivery. *Int. J. Pharm.* **2017**, *532*, 555–572.

10. Fievez, V.; Garinot, M.; Schneider, Y.; Préat, V. Nanoparticles as potential oral delivery systems of proteins and vaccines: A mechanistic approach. *J. Control. Release* **2006**, *116*, 1–27.

11. Brayden, D. J.; Jepson, M. A.; Baird, A. W. Intestinal Peyer's patch M cells and oral vaccine targeting. *Drug Discov. Today* **2005**, *10*, 1145–1157.

12. Kwon, K.; Daniell, H. Oral delivery of protein drugs bioencapsulated in plant cells. *Mol. Ther.* **2016**, *24*, 1342–1350.

13. Ma, S.; Wang, L.; Huang, X.; Wang, X.; Chen, S.; Shi, W.; Qiao, X.; Jiang, Y. Oral recombinant Lactobacillus vaccine targeting the intestinal microfold cells and dendritic cells for delivering the core neutralizing epitope of porcine epidemic diarrhea virus. *Microb. Cell Fact.* **2018**, *17*, 1–12.

14. Maharjan, S.; Singh, B.; Jiang, T.; Yoon, S.; Li, H.; Kim, G.; Jeong, M.; Ji, S.; Park, O.; Hyun, S.; et al. Systemic administration of RANKL overcomes the bottleneck of oral vaccine delivery through microfold cells in ileum. *Biomaterials* **2016**, *84*, 286–300.

15. Azizi, A.; Kumar, A.; Diaz-mitoma, F.; Mestecky, J. Enhancing oral vaccine potency by targeting intestinal M cells. *PLoS Pathog.* **2010**, *6*, 1001147–1001154.

16. Mudie, D. M.; Amidon, G. L.; Amidon, G. E. Physiological parameters for oral delivery and in vitro testing. *Mol. Pharm.* **2010**, *7*, 1388–1405.

17. Vllasaliu, D.; Thanou, M.; Stolnik, S.; Fowler, R. Recent advances in oral delivery of biologics : nanomedicine and physical modes of delivery. *Expert Opin. Drug Deliv.* **2018**, *15*, 759–770.

18. Tao, S. L.; Desai, T. A. Micromachined devices: The impact of controlled geometry from cell-targeting to bioavailability. *J. Control. Release* **2005**, *109*, 127–138.

19. Rzhevskiy, A. S.; Raghu, T.; Singh, R.; Donnelly, R. F.; Anissimov, Y. G. Microneedles as the technique of drug delivery enhancement in diverse organs and tissues. *J. Control. Release* **2018**, *270*, 184–202.

20. Dimmitt, R. A.; Sellers, Z. M.; Sibley, E. XIV-Gastrointestinal system-70 Gastrointestinal tract development. In *Avery's Diseases of the Newborn*; Elsevier Inc., 2012; pp. 1032–1038.

21. Treuting, P. M.; Dintzis, S. M.; Montine, K. Upper gastrointestinal tract. In *Comparative Anatomy and Histology (Second Edition), A Mouse, Rat, and Human Atlas*; Academic Press, Elsevier: London, 2018; pp. 190–211.

22. Cheng, H. Origin, differentiation and renewal of the four main epithelial cell types in the mouse small intestine. *Am. J. Anat.* **1974**, *141*, 481–502.

23. Lennernas, H. Human intestinal permeability. *Int. J. Pharm. Sci.* **1998**, *87*, 403–410.

24. Rubin, D. C.; Langer, J. C. Anatomy and development-small intestine: anatomy and structural anomalies. In *Yamada's Atlas of Gastroenterology*; Podolsky, D. K.; Camilleri, M.; Shanahan, F.; Fitz, J. G.; Wang, T. C.; Kalloo, A. N., Eds.; Wiley Blackwell: Oxford, UK, 2016; pp. 19–24.

25. Dressman, J. B.; Berardi, R. R.; Dermentzoglou, L. C.; Russell, T. L.; Schmaltz, S. P.; Barett, J. L.; Jarvenpaa, K. M. Upper gastrointestinal (GI) pH in young, healthy men and women. *Pharm. Res.* **1990**, *7*, 756–761.

26. Rouge, N.; Buri, P.; Doelker, E. Drug absorption sites in the gastrointestinal tract and dosage forms for site-specific delivery. *Int. J. Pharm.* **1996**, *136*, 117–139.

27. Moroz, E.; Matoori, S.; Leroux, J. Oral delivery of macromolecular drugs: Where we are after almost 100 years of attempts. *Adv. Drug Deliv. Rev.* **2016**, *101*, 108–121.

28. Bar-zeev, M.; Assaraf, Y. G.; Livney, Y. D. β-casein nanovehicles for oral delivery of chemotherapeutic drug combinations overcoming P-glycoprotein-mediated multidrug resistance in human gastric cancer cells. *Oncotarget* **2016**, *7*, 23322–23335.

29. Huang, J.; Shu, Q.; Wang, L.; Wu, H.; Wang, A. Y.; Mao, H. Layer-by-layer assembled milk protein coated magnetic nanoparticle enabled oral drug delivery with high stability in stomach and enzyme-responsive release in small intestine. *Biomaterials* **2015**, *39*, 105–113.

30. Ruiz, G. A.; Opazo-Navarrete, M.; Meurs, M.; Minor, M.; Sala, G.; Boekel, M. Van; Stieger, M.; Janssen, A. E. M. Denaturation and in vitro gastric digestion of heat-treated quinoa protein isolates obtained at various extraction pH. *Food Biophys.* **2016**, *11*, 184–197.

31. Yamagata, T.; Morishita, M.; Kavimandan, N. J.; Nakamura, K. Characterization of insulin protection properties of complexation hydrogels in gastric and intestinal enzyme fluids. *J. Control. Release* **2006**, *112*, 343–349.

32. Cerchiara, T.; Abruzzo, A.; Parolin, C.; Vitali, B.; Bigucci, F.; Gallucci, M. C.; Nicoletta, F. P.; Luppi, B. Microparticles based on chitosan/carboxymethylcellulose polyelectrolyte complexes for colon delivery of vancomycin. *Carbohydr. Polym.* **2016**, *143*, 124–130.

33. O'Neill, M. J.; Bourre, L.; Melgar, S.; O'Driscoll, C. M. Intestinal delivery of non-viral gene therapeutics: Physiological barriers and preclinical models. *Drug Discov. Today* **2011**, *16*, 203–218.

34. Rawlings, N. D.; Barrett, A. J. Families of serine peptidases. In *Methods in Enzymology*; Academic Press, Elsevier, Inc., 1994; Vol. 244, pp. 19–61.

35. Davies, M.; Pieber, T. R.; Hartoft-Nielsen, M. L.; Hansen, O. K. H.; Jabbour, S.; Rosenstock, J. Effect of oral semaglutide compared with placebo and subcutaneous semaglutide on glycemic control in patients with type 2 diabetes a randomized clinical trial. *J. Am. Med. Assoc.* **2017**, *318*, 1460–1470.

36. Layer, P.; Go, V. L. W.; Dimagno, E. P. Fate of pancreatic enzymes aboral transit in humans during small intestinal aboral transit in humans. *Am. J. Physiol.* **1986**, *251*, 475–80.

37. Fallingborg, J.; Christensen, L. A.; Ingeman-Nielsen, M.; Jacobsen, B. A.; Abildgaard, K.; Rasmussen, H. H. pH-profile and regional transit fimes of the normal gut measured by a radiotelemetry device. *Aliment. Pharmacol. Ther.* **1989**, *3*, 605–613.

38. Lozoya-agullo, I.; Araújo, F.; González-álvarez, I.; Merino-sanjuán, M.; González-álvarez, M.; Bermejo, M.; Sarmento, B. PLGA nanoparticles are effective to control the colonic release and absorption on ibuprofen. *Eur. J. Pharm. Sci.* **2018**, *115*, 119–125.

39. Varum, F. J. O.; Mcconnell, E. L.; Sousa, J. J. S.; Veiga, F.; Basit, A. W.

Mucoadhesion and the gastrointestinal tract. *Crit. Rev. Ther. Drug Carrier Syst.* **2008**, *25*, 207–258.

40. Dawson, M.; Krauland, E.; Wirtz, D.; Hanes, J. Transport of polymeric nanoparticle gene carriers in gastric mucus. *Biotechnol. Prog.* **2004**, *20*, 851–857.

41. Hounnou, G.; Destrieux, C.; Desme, J.; Bertrand, P.; Velut, S. Anatomical study of the length of the human intestine. *Surg. Radiol. Anat.* **2002**, *24*, 290–294.

42. Helander, H. F.; Fändriks, L. Surface area of the digestive tract – revisited. *Scand. J. Gastroenterol.* **2014**, *49*, 681–689.

43. Valon, L.; Levayer, R. Dying under pressure: cellular characterisation and in vivo functions of cell death induced by compaction. *Biol. Cell* **2019**, *111*, 1–16.

44. France, K. J. De; Chan, K. J. W.; Cranston, E. D.; Hoare, T. Enhanced mechanical properties in cellulose nanocrystal−poly(oligoethylene glycol methacrylate) injectable nanocomposite hydrogels through control of physical and chemical cross-linking. *Biomacromolecules* **2016**, *17*, 649–660.

45. Yang, J.; Zhao, J.; Xu, F.; Sun, R. Revealing strong nanocomposite hydrogels reinforced by cellulose nanocrystals: insight into morphologies and interactions. *Appl. Mater. Interfaces* **2013**, *5*, 12960–12967.

46. Mert, O.; Lai, S. K.; Ensign, L.; Yang, M.; Wang, Y.; Wood, J.; Hanes, J. A poly(ethylene glycol)-based surfactant for formulation of drug-loaded mucus penetrating particles. *J. Control. Release* **2012**, *157*, 455–460.

47. Liu, Y.; Yang, T.; Wei, S.; Zhou, C.; Lan, Y.; Cao, A. Mucus adhesion- and penetration-enhanced liposomes for paclitaxel oral delivery. *Int. J. Pharm.* **2018**, *537*, 245–256.

48. Shan, W.; Zhu, X.; Liu, M.; Li, L.; Zhong, J.; Sun, W.; Zhang, Z.; Huang, Y. Overcoming the diffusion barrier of mucus and absorption barrier of epithelium by self-assembled nanoparticles for oral delivery of insulin. *ACS Nano* **2015**, *9*, 2345–2356.

49. Liu, M.; Zhang, J.; Zhu, X.; Shan, W.; Li, L.; Zhong, J.; Zhang, Z.; Huang, Y. Efficient mucus permeation and tight junction opening by dissociable "mucus-inert" agent coated trimethyl chitosan nanoparticles for oral insulin delivery. *J. Control. Release* **2016**, *222*, 67–77.

50. Leal, J.; Dong, T.; Taylor, A.; Siegrist, E.; Gao, F.; Smyth, H. D. C. Mucus-penetrating phage-displayed peptides for improved transport across a mucus-like model. *Int. J. Pharm.* **2018**, *553*, 57–64.

51. Zhang, X.; Cheng, H.; Dong, W.; Zhang, M.; Liu, Q.; Wang, X.; Guan, J. Design and intestinal mucus penetration mechanism of core-shell nanocomplex. *J. Control. Release* **2018**, *272*, 29–38.

52. Navarro, L. A.; French, D. L.; Zauscher, S. Advances in mucin mimic synthesis and applications in surface science. *Curr. Opin. Colloid Interface Sci.* **2018**, *38*, 122–134.

53. Kufe, D. W. Mucins in cancer: function, prognosis and therapy Donald. *Nat. Rev. Cancer* **2009**, *9*, 874–885.

54. Atuma, C.; Strugala, V.; Allen, A.; Holm, L. The adherent gastrointestinal mucus gel layer: thickness and physical state in vivo. *Am. J. Physiol. Liver Physiol.* **2001**, *280*, 922–929.

55. Chassaing, B.; Gewirtz, A. T. Identification of inner mucus-associated bacteria by laser capture microdissection. *Cell. Mol. Gastroenterol. Hepatol.* **2019**, *7*, 157–160.

56. Bansil, R.; Turner, B. S. The biology of mucus: Composition, synthesis and organization. *Adv. Drug Deliv. Rev.* **2018**, *124*, 3–15.

57. Boegh, M.; García-díaz, M.; Müllertz, A.; Nielsen, H. M. Steric and interactive barrier properties of intestinal mucus elucidated by particle diffusion and peptide permeation. *Eur. J. Pharm. Biopharm.* **2015**, *95*, 136–143.

58. Hansson, G. C.; Johansson, M. E. V The inner of the two Muc2 mucin-dependent mucus layers in colon is devoid of bacteria. *Gut Microbes* **2010**, *1*, 51–54.

59. Johansson, M. E. V; Larsson, J. M. H.; Hansson, G. C. The two mucus layers of colon are organized by the MUC2 mucin, whereas the outer layer is a legislator of host–microbial interactions. *PNAS* **2011**, *108*, 4659–4665.

60. Bajka, B. H.; Rigby, N. M.; Cross, K. L.; Macierzanka, A.; Mackie, A. R. The influence of small intestinal mucus structure on particle transport ex vivo. *Colloids Surfaces B Biointerfaces* **2015**, *135*, 73–80.

61. Li, X.; Chen, D.; Le, C.; Zhu, C.; Gan, Y.; Hovgaard, L.; Yang, M. Novel mucus-penetrating liposomes as a potential oral drug delivery system: preparation, in vitro characterization, and enhanced cellular uptake. *Int. J. Nanomedicine* **2011**, *6*, 3151–3162.

62. Cu, Y.; Saltzmanr, W. M. Controlled surface modification with poly(ethylene)glycol enhances diffusion of PLGA nanoparticles in human cervical mucus. *Mol. Pharm.* **2009**, *6*, 173–181.

63. Muller, C.; Leithner, K.; Hauptstein, S.; Hintzen, F.; Salvenmoser, W.; Bernkop-Schnurch, A. Preparation and characterization of mucus-penetrating papain/poly(acrylic acid) nanoparticles for oral drug delivery applications. *J. Nanopart. Res.* **2013**, *15*, 1353–1366.

64. DeSousa, I. P.; Cattoz, B.; Wilcox, M. D.; Griffiths, P. C.; Dalgliesh, R.; Rogers, S.; Bernkop-schnürch, A. Nanoparticles decorated with proteolytic enzymes, a promising strategy to overcome the mucus barrier. *Eur. J. Pharm. Biopharm.* **2015**, *97*, 257–264.

65. Moreno, J. A. S.; Mendes, A. C.; Stephansen, K.; Engwer, C. Development of electrosprayed mucoadhesive chitosan microparticles. *Carbohydr. Polym.* **2018**, *190*, 240–247.

66. Park, C. G.; Huh, B. K.; Kim, S.; Lee, S. H.; Hong, H. R.; Choy, Y. B. Nanostructured mucoadhesive microparticles to enhance oral drug bioavailability. *J. Ind. Eng. Chem.* **2017**, *54*, 262–269.

67. Krauland, A. H.; Guggi, D.; Bernkop-schnurch, A. Thiolated chitosan microparticles: A vehicle for nasal peptide drug delivery. *Int. J. Pharm.* **2006**, *307*, 270–277.

68. Romero, G. B.; Keck, C. M.; Müller, R. H.; Bou-chacra, N. A. Development of cationic nanocrystals for ocular delivery. *Eur. J. Pharm. Biopharm.* **2016**, *107*, 215–222.

69. DeLima, J. A. De; Paines, T. C.; Motta, M. H.; Weber, W. B.; Santos, S. S.; Cruz, L.; Silva, C. D. B. Novel Pemulen/Pullulan blended hydrogel containing clotrimazole-loaded cationic nanocapsules: Evaluation of mucoadhesion and vaginal permeation. *Mater. Sci. Eng. C* **2017**, *79*, 886–893.

70. Kim, K.; Kim, K.; Hyun, J.; Lee, H. Chitosan-catechol: A polymer with long-lasting mucoadhesive properties. *Biomaterials* **2015**, *52*, 161–170.

71. Ertl, B.; Heigl, F.; Wirth, M.; Gabor, F. Lectin-mediated bioadhesion: Preparation, stability and Caco-2 binding of wheat germ agglutinin-functionalized poly(D,L-lactic-co-glycolic acid)-microspheres. *J. Drug Target.* **2000**, *8*, 173–184.

72. Anirudhan, T. S.; Parvathy, J. Novel thiolated chitosan-polyethyleneglycol blend/Montmorillonite composite formulations for the oral delivery of insulin. *Bioact. Carbohydrates Diet. Fibre* **2018**, *16*, 22–29.

73. Bernkop-schnurch, A.; Hornof, M.; Guggi, D. Thiolated chitosans. *Eur. J. Pharm. Biopharm.* **2004**, *57*, 9–17.

74. Deutel, B.; Laf, F.; Palmberger, T.; Saxer, A.; Thaler, M.; Bernkop-schnürch, A. In vitro characterization of insulin containing thiomeric microparticles as nasal drug delivery system. *Eur. J. Pharm. Sci.* **2016**, *81*, 157–161.

75. Sajeesh, S.; Vauthier, C.; Gueutin, C.; Ponchel, G.; Sharma, C. P. Thiol functionalized polymethacrylic acid-based hydrogel microparticles for oral insulin delivery. *Acta Biomater.* **2010**, *6*, 3072–3080.

76. Farris, E.; Heck, K.; Lampe, A. T.; Brown, D. M.; Ramer-tait, A. E.; Pannier, A. K. Oral non-viral gene delivery for applications in DNA vaccination and gene therapy. *Curr. Opin. Biomed. Eng.* **2018**, *7*, 51–57.

77. Batista, P.; Castro, P. M.; Raquel, A.; Sarmento, B. Recent insights in the use of nanocarriers for the oral delivery of bioactive proteins and peptides. *Peptides* **2018**, *101*, 112–123.

78. Zhang, Y.; Wu, X.; Meng, L.; Zhang, Y.; Ai, R.; Qi, N.; He, H.; Xu, H.; Tang, X. Thiolated Eudragit nanoparticles for oral insulin delivery: Preparation, characterization and in vivo evaluation. *Int. J. Pharm.* **2012**, *436*, 341–350.

79. Cone, R. A. Barrier properties of mucus. *Adv. Drug Deliv. Rev.* **2009**, *61*, 75–85.

80. Huckaby, J. T.; Lai, S. K. PEGylation for enhancing nanoparticle diffusion in mucus. *Adv. Drug Deliv. Rev.* **2018**, *124*, 125–139.

81. Jung, T.; Kamm, W.; Breitenbach, A.; Kaiserling, E.; Xiao, J. X.; Kissel, T. Biodegradable nanoparticles for oral delivery of peptides: is there a role for polymers to affect mucosal uptake? *Eur. J. Pharm. Biopharm.* **2000**, *50*, 147–160.

82. Lai, S. K.; Wang, Y. Y.; Hanes, J. Mucus-penetrating nanoparticles for drug and gene delivery to mucosal tissues. *Adv. Drug Deliv. Rev.* **2009**, *61*, 158–171.

83. S. Zhaeentana; Amjadib, F. S.; Zandieb, Z.; Joghataei, M. T.; Bakhtiyari, M.; Aflatoonian, R. The effects of hydrocortisone on tight junction genes in an in vitro model of the human fallopian epithelial cells. *Eur. J. Obstet. Gynecol. Reprod. Biol.* **2018**, *229*, 127–131.

84. Bein, A.; Eventov-friedman, S.; Arbell, D.; Schwartz, B. Intestinal tight junctions are severely altered in NEC preterm neonates. *Pediatr. Neonatol.* **2018**, *59*, 464–473.

85. Gamboa, J. M.; Leong, K. W. In vitro and in vivo models for the study of oral delivery of nanoparticles. *Adv. Drug Deliv. Rev.* **2013**, *65*, 800–810.

86. Linnankoski, J.; Makela, J.; Palmgren, J.; Mauriala, T.; Vedin, C.; Ungell, A.-L.; Artursson, P.; Urtti, A.; Yliperttula, M. Paracellular porosity and pore size of the human intestinal epithelium in tissue and cell culture models. *J. Pharm. Sci.* **2010**, *99*, 2166–2175.

87. Salama, N. N.; Eddington, N. D.; Fasano, A. Tight junction modulation and its relationship to drug delivery. *Adv. Drug Deliv. Rev.* **2006**, *58*, 15–28.

88. Kim, J.; Yoon, I.; Cho, H.; Kim, D.; Choi, Y.; Kim, D. Emulsion-based colloidal nanosystems for oral delivery of doxorubicin: Improved intestinal paracellular absorption and alleviated cardiotoxicity. *Int. J. Pharm.* **2014**, *464*, 117–126.

89. Taverner, A.; Dondi, R.; Almansour, K.; Laurent, F.; Owens, S.; Eggleston, I. M.; Fotaki, N.; Mrsny, R. J. Enhanced paracellular transport of insulin can be achieved via transient induction of myosin light chain phosphorylation. *J. Control. Release* **2015**, *210*, 189–197.

90. Almansour, K.; Taverner, A.; Eggleston, I. M.; Mrsny, R. J. Mechanistic studies of a cell-permeant peptide designed to enhance myosin light chain phosphorylation in polarized intestinal epithelia. *J. Control. Release* **2018**, *279*, 208–219.

91. Banerjee, A.; Mitragotri, S. Intestinal patch systems for oral drug delivery. *Curr. Opin. Pharmacol.* **2017**, *36*, 58–65.

92. Banerjee, A.; Lee, J.; Mitragotri, S. Intestinal mucoadhesive devices for oral delivery of insulin. *Bioeng. Traslational Med.* **2016**, *1*, 338–346.

93. Shen, Z.; Mitragotri, S. Intestinal patches for oral drug delivery. *Pharm. Res.* **2002**, *19*, 391–395.

94. Toorisaka, E.; Hashida, M.; Kamiya, N.; Ono, H. An enteric-coated dry emulsion formulation for oral insulin delivery. *J. Control. Release* **2005**, *107*, 91–96.

95. Toorisaka, E.; Watanabe, K.; Ono, H.; Hirata, M.; Kamiya, N. Intestinal patches with an immobilized solid-in-oil formulation for oral protein delivery. *Acta Biomater.* **2012**, *8*, 653–658.

96. Lee, J. W.; Prausnitz, M. R. Drug delivery using microneedle patches: not just for skin. *Expert Opin. Drug Deliv.* **2018**, *15*, 541–543.

97. Ma, Y.; Tao, W.; Krebs, S. J.; Sutton, W. F.; Haigwood, N. L.; Gill, H. S. Vaccine delivery to the oral cavity using coated microneedles induces systemic and mucosal immunity. *Pharm. Res.* **2014**, *31*, 2393–2403.

98. Traverso, G.; Schoellhammer, C. M.; Schroeder, A.; Maa, R.; Lauwers, G. Y.; Polat, B. E.; Anderson, D. G.; Blankschtein, D.; Langer, R. Microneedles for Drug Delivery via the Gastrointestinal Tract. *J. Pharm. Sci.* **2015**, *104*, 362–367.

99. Dabholkar, R. D.; Sawant, R. M.; Mongayt, D. A.; Devarajan, P. V; Torchilin, V. P. Polyethylene glycol–phosphatidylethanolamine conjugate (PEG–PE)-based mixed micelles: Some properties, loading with paclitaxel, and modulation of P-glycoprotein-mediated efflux. *Int. J. Pharm.* **2006**, *315*, 148–157.

100. Yu, H.; Cui, Z.; Yu, P.; Guo, C.; Feng, B.; Jiang, T. pH- and NIR light-responsive micelles with hyperthermia-triggered tumor penetration and cytoplasm drug release to reverse doxorubicin resistance in breast cancer. *Adv. Funct. Mater.* **2015**, *25*, 2489–2500.

101. Suzuki, H.; Bae, Y. H. Evaluation of drug penetration with cationic micelles and their penetration mechanism using an in vitro tumor model. *Biomaterials* **2016**, *98*, 120–130.

102. Sosnik, A.; Raskin, M. M. Polymeric micelles in mucosal drug delivery: Challenges towards clinical translation. *Biotechnol. Adv.* **2015**, *33*, 1380–1392.

103. Torchilin, V. P. Fluorescence microscopy to follow the targeting of liposomes and micelles to cells and their intracellular fate. *Adv. Drug Deliv. Rev.* **2005**, *57*, 95–109.

104. Byrne, R. S.; Deasy, P. B. Use of commercial porous ceramic particles for sustained drug delivery. *Int. J. Pharm.* **2002**, *246*, 61–73.

105. Hoffman, A. S. Hydrogels for biomedical applications. *Adv. Drug Deliv. Rev.* **2012**, *64*, 18–23.

106. Li, J.; Mooney, D. J. Designing hydrogels for controlled drug delivery. *Nat. Rev. Mater.* **2016**, *1*, 1–17.

107. Chai, Q.; Jiao, Y.; Yu, X. Hydrogels for biomedical applications: Their characteristics and the mechanisms behind them. *Gels* **2017**, *3*, 1–15.

108. Caló, E.; Khutoryanskiy, V. Biomedical applications of hydrogels: A review of patents and commercial products. *Eur. Polym. J.* **2015**, *65*, 252–267.

109. Klouda, L. Thermoresponsive hydrogels in biomedical applications A seven-year update. *Eur. J. Pharm. Biopharm.* **2015**, *97*, 338–349.

110. Torres-lugo, M.; Peppas, N. A. Molecular design and in vitro studies of novel pH-sensitive hydrogels for the oral delivery of calcitonin. *Macromolecules* **1999**, *32*, 6646–6651.

111. Simpson, M. J.; Corbett, B.; Arezina, A.; Hoare, T. Narrowly dispersed, degradable, and scalable poly(oligoethylene glycol methacrylate)-based nanogels via thermal self-assembly. *Ind. Eng. Chem. Res.* **2018**, *57*, 7495–7506.

112. Choi, J.; Moquin, A.; Bomal, E.; Na, L.; Maysinger, D.; Kakkar, A. Telodendrimers for physical encapsulation and covalent linking of individual or combined therapeutics. *Mol. Pharm.* **2017**, *14*, 2607–2615.

113. DeFrance, K. J.; Xu, F.; Hoare, T. Structured macroporous hydrogels: progress, challenges, and opportunities. *Adv. Healthc. Mater.* **2018**, *7*, 1–17.

114. Annabi, N.; Nichol, J. W.; Zhong, X.; Ji, C. Controlling the porosity and microarchitecture of hydrogels for tissue engineering. *Tissue Engneering Part B* **2010**, *16*, 371–385.

115. Kim, U.; Park, J.; Li, C.; Jin, H.; Valluzzi, R.; Kaplan, D. L. Structure and properties of silk hydrogels. *Biomacromolecules* **2004**, *5*, 786–792.

116. Yokoyama, E.; Masada, I.; Shimamura, K.; Ikawa, T.; Monobe, K. Morphology and structure of highly elastic poly(vinyl alcohol) hydrogel prepared by repeated freezing-and-melting. *Colloid Polym. Sci.* **1986**, *601*, 595–601.

117. Hermansson, A. M.; Buchheim, W. Characterization of protein gels by scanning and transmission electron microscopy. *J. Colloid Interface Sci.* **1981**, *81*, 510–530.

118. Hyuk Im, S.; Jeong, U.; Xia, Y. Polymer hollow particles with controllable holes in their surfaces. *Nat. Mater.* **2005**, *4*, 671–675.

119. Staruch, R. M. T.; Glass, G. E.; Rickard, R.; Hettiaratchy, S.; Butler, P. E. M.

Injectable pore-forming hydrogel scaffolds for complex wound tissue engineering: designing and controlling their porosity and mechanical properties. *Tissue Engneering Part B* **2017**, *23*, 183–198.

120. Loh, Q. L.; Choong, C. Three-dimensional scaffolds for tissue engineering applications: role of porosity and pore size. *Tissue Engneering Part B* **2013**, *19*, 485–502.

121. Li, Y.; Huang, G.; Zhang, X.; Wang, L.; Du, Y.; Jian, T.; Xu, F. Engineering cell alignment in vitro. *Biotechnol. Adv.* **2014**, *32*, 347–365.

122. Vlierberghe, S.; Cnudde, V.; Dubruel, P.; Masschaele, B.; Cosijns, A.; DePaepe, I. De; Jacobs, P. J. S.; Hoorebeke, L.; Remon, J. P.; Schacht, E. Porous gelatin hydrogels: 1. Cryogenic formation and structure analysis. *Biomacromolecules* **2007**, *8*, 331–337.

123. Lai, J.; Li, Y. Functional assessment of cross-linked porous gelatin hydrogels for bioengineered cell sheet carriers. *Biomacromolecules* **2010**, *11*, 1387–1397.

124. Lewus, R. K.; Carta, G. Protein transport in constrained anionic hydrogels: diffusion and boundary-layer mass transfer. *Ind. Eng. Chem. Res.* **2001**, *40*, 1548–1558.

125. Soudry-kochavi, L.; Naraykin, N.; DiPaola, R.; Gugliandolo, E.; Peritore, A.; Cuzzocrea, S.; Ziv, E.; Nassar, T.; Benita, S. Pharmacodynamical effects of orally administered exenatide nanoparticles embedded in gastro-resistant microparticles. *Eur. J. Pharm. Biopharm.* **2018**, *133*, 214–223.

126. Agüero, L.; Zaldivar-silva, D.; Pena, L.; Dias, M. L. Alginate microparticles as oral colon drug delivery device: A review. *Carbohydr. Polym.* **2017**, *168*, 32–43.

127. Chen, Q.; Gou, S.; Huang, Y.; Zhou, X.; Li, Q. Facile fabrication of bowl-shaped microparticles for oral curcumin delivery to ulcerative colitis tissue. *Colloids Surfaces B Biointerfaces* **2018**, *169*, 92–98.

128. Nadal, J. M.; Gomes, M. L. S.; Borsato, D. M.; Almeida, M. A.; Barboza, F. M.; Zawadzki, S. F.; Kanunfre, C. C.; Farago, P. V.; Zanin, S. M. W. Spray-dried Eudragit® L100 microparticles containing ferulic acid: Formulation, in vitro cytoprotection and in vivo anti-platelet effect. *Mater. Sci. Eng. C* **2016**, *64*, 318–328.

129. Ratzinger, G.; Agrawal, P.; Korner, W.; Lonkai, J.; Sanders, H. M. H. F.; Terreno, E.; Wirth, M.; Strijkers, G. J.; Nicolay, K.; Gabor, F. Surface modification of PLGA nanospheres with Gd-DTPA and Gd-DOTA for high-relaxivity MRI contrast agents. *Biomaterials* **2010**, *31*, 8716–8723.

130. Koch, B.; Rubino, I.; Quan, F.-S.; Yoo, B.; Choi, H.-J. Microfabrication for drug delivery. *Materials (Basel).* **2016**, *9*, 646–682.

131. Noguchi, H.; Takasu, M. Fusion pathways of vesicles: A Brownian dynamics simulation. *J. Chem. Phys.* **2001**, *115*, 9547–9551.

132. Pekarek, K. J.; Jacob, J. S.; Mathiowitz, E. Double-walled polymer microspheres for controlled drug release. *Nature* **1994**, *367*, 258–60.

133. Zolnik, B. S.; Burgess, D. J. Effect of acidic pH on PLGA microsphere degradation and release. *J. Control. Release* **2007**, *122*, 338–344.

134. Wong, M. S.; Cha, J. N.; Choi, K. S.; Deming, T. J.; Stucky, G. D. Assembly of nanoparticles into hollow spheres using block copolypeptides. *Nano Lett.* **2002**, *2*, 583–587.

135. Du, J.; O'Reilly, R. K. Advances and challenges in smart and functional polymer vesicles. *Soft Matter* **2009**, *5*, 3544–3561.

136. Yokoyama, M.; Inoue, S.; Kataoka, K.; Yui, N.; Okano, T.; Sakurai, Y. Molecular design for missile drug: Synthesis of adriamycin conjugated with immunoglobulin G using poly(ethylene glycol)-block-poly(aspartic acid) as intermediate carrier. *Die Makromol. Chemie* **1989**, *190*, 2041–2054.

137. Batycky, R. P.; Hanes, J.; Langer, R.; Edwards, D. A. A theoretical model of erosion and macromolecular drug release from biodegrading microspheres. *J. Pharm. Sci.* **1997**, *86*, 1464–1477.

138. Steijn, V.; Korczyk, P. M.; Derzsi, L.; Abate, A. R.; Weitz, D. A.; Garstecki, P. Block-and-break generation of microdroplets with fixed volume. *Biomicrofluidics* **2013**, *7*, 1–8.

139. Abbaspourrad, A.; Carroll, N. J.; Kim, S.; Weitz, D. A. Polymer microcapsules with programmable active release. *J. Am. Chem. Soc.* **2013**, *135*, 7744–7750.

140. Ostafe, R.; Prodanovic, R.; Ung, W. L.; Weitz, D. A.; Fischer, R. A high-throughput cellulase screening system based on droplet microfluidics. *Biomicrofluidics* **2014**, *8*, 1–5.

141. Bitar, C.; Markwick, K. E.; Hoesli, C. A. Encapsulation of pancreatic islet cells for type 1 diabetes treatment. In *XXV International Conference on Bioencapsulation, La Chapelle sur Erdre, France, July 3-6, 2017*; Bioencapsulation Innovations, La Chapelle sur Erdre, France, July 3-6, 2017: La Chapelle sur Erdre, France, 2017; Vol. November 2, pp. 10–11.

142. Deng, N.-N.; Wang, W.; Ju, X.-J.; Xie, R.; Weitz, D. A.; Chu, L.-Y. Reply to the 'Comment on "Wetting-induced formation of controllable monodisperse multiple emulsions in microfluidics"' by J. Guzowski and P. Garstecki, Lab Chip, 2014, 14, DOI: 10.1039/ C3LC51229K. *Lab Chip* **2014**, *14*, 1479–1480.

143. Massenburg, S. S.; Amstad, E.; Weitz, D. A. Clogging in parallelized tapered microfluidic channels. *Microfluid. Nanofluidics* **2016**, *20*, 1–5.

144. Wyss, H. M.; Blair, D. L.; Morris, J. F.; Stone, H. A.; Weitz, D. A. Mechanism for

clogging of microchannels. *Phys. Rev. E* **2006**, *74*, 1–4.

145. Kumar, A.; Montemagno, C.; Choi, H. -j. Smart microparticles with a pH-responsive macropore for targeted oral drug delivery. *Sci. Rep.* **2017**, *7*, 1–15.

146. Caruso, F. Nanoengineering of particle surfaces. *Adv. Mater.* **2001**, *13*, 11–22.

147. Cai, Y.; Chen, Y.; Hong, X.; Liu, Z.; Yuan, W. Porous microsphere and its applications. *Int. J. Nanomedicine* **2013**, *8*, 1111–1120.

148. Kim, K. K.; Pack, D. W. Volume I: Biological and biomedical nanotechnology-Microspheres for drug delivery. In *BioMEMS and biomedical nanotechnology*; Ferrari, M.; Lee, A.; Lee, J., Eds.; Springer: Boston, MA, 2006; pp. 19–50.

149. Homayun, B.; Sun, C.; Kumar, A.; Montemagno, C.; Choi, H.-J. Facile fabrication of microparticles with pH-responsive macropores for small intestine targeted drug formulation. *Eur. J. Pharm. Biopharm.* **2018**, *128*, 316–326.

150. Homayun, B.; Kumar, A.; Nascimento, P. T. H.; Choi, H.-J. Macropored microparticles with a core–shell architecture for oral delivery of biopharmaceuticals. *Arch. Pharm. Res.* **2018**, *41*, 848–860.

151. Tzeng, S. Y.; Guarecuco, R.; Mchugh, K. J.; Rose, S.; Rosenberg, E. M.; Zeng, Y.; Langer, R.; Jaklenec, A. Thermostabilization of inactivated polio vaccine in PLGA-based microspheres for pulsatile release. *J. Control. Release* **2016**, *233*, 101–113.

152. Khan, M. Z. I.; Prebeg, Z.; Kurjakovic, N. A pH-dependent colon targeted oral drug delivery system using methacrylic acid copolymers I . Manipulation of drug release using Eudragit ® L100-55 and Eudragit ® S100 combinations. *J. Control. Release* **1999**, *58*, 215–222.

153. Han, M. I. N.; Fang, Q.; Zhan, H.; Luo, T. A. O.; Liang, W.; Gao, J. In Vitro and In Vivo Evaluation of a Novel Capsule for Colon-Specific Drug Delivery. *J. Pharm. Sci.* **2009**, *98*, 2626–2635.

154. Saint-Cricq, P.; Deshayes, S.; Zink, J. I.; Kasko, A. M. Magnetic field activated drug delivery using thermodegradable azo-functionalised PEG-coated core-shell mesoporous silica nanoparticles. *Nanoscale* **2015**, *7*, 13168–72.

155. Kim, J.; Rubino, I.; Lee, J.; Choi, H. Application of halloysite nanotubes for carbon dioxide capture. *Mater. Res. Express Pap.* **2016**, *3*, 045019.

156. Ari, N.; Matuszczak, B.; Shahzadi, I.; Dizdarevic, A.; Bernkop-schnürch, A. Trypsin decorated self-emulsifying drug delivery systems (SEDDS): Key to enhanced mucus permeation. *J. Colloid Interface Sci.* **2018**, *531*, 253–260.

157. Fredenberg, S.; Wahlgren, M.; Reslow, M.; Axelsson, A. Pore formation and pore closure in poly(D,L-lactide-co-glycolide) films. *J. Control. Release* **2011**, *150*, 142–149.

158. Gurgel, M.; Vieira, A.; Altenhofen, M.; Oliveira, L.; Beppu, M. M. Natural-based plasticizers and biopolymer films : A review. *Eur. Polym. J.* **2011**, *47*, 254–263.

159. Kang, J.; Schwendeman, S. P. Pore closing and opening in biodegradable polymers and their effect on the controlled release of proteins. *Mol. Pharm.* **2007**, *4*, 104–118.

160. Lvov, Y. M.; Shchukin, D. G.; Mohwald, H.; Price, R. R. Halloysite clay nanotubes for controlled release of protective agents. *ACS Nano* **2008**, *2*, 814–820.

161. Ghebaur, A.; Garea, S. A.; Iovu, H. New polymer – halloysite hybrid materials — potential controlled drug release system. *Int. J. Pharm.* **2012**, *436*, 568–573.

162. Santos, A. C.; Ferreira, C.; Veiga, F.; Ribeiro, A. J.; Panchal, A.; Lvov, Y.; Agarwal, A. Halloysite clay nanotubes for life sciences applications: From drug encapsulation to bioscaffold. *Adv. Colloid Interface Sci.* **2018**, *257*, 58–70.

163. Lvov, Y.; Wang, W.; Zhang, L.; Fakhrullin, R. Halloysite clay nanotubes for loading and sustained release of functional compounds. *Adv. Mater.* **2016**, *28*, 1227–1250.

164. Ma, J.; Rubin, B. K.; Voynow, J. A. Mucins , Mucus , and Goblet Cells. *Chest* **2017**, *154*, 169–176.

165. Lock, J. Y.; Carlson, T. L.; Carrier, R. L. Mucus models to evaluate the diffusion of drugs and particles ☆. *Adv. Drug Deliv. Rev.* **2018**, *124*, 34–49.

166. Yildiz H. M., Carlson T. L., Goldstein A. M., C. R. L. Mucus Barriers to Microparticles and Microbes are Altered in Hirschprung's Disease Dr. *Macromol Biosci.* **2015**, *15*, 712–718.

167. Dhaliwal, S.; Jain, S.; Singh, H. P.; Tiwary, A. K. Mucoadhesive Microspheres for Gastroretentive Delivery of Acyclovir : In Vitro and In Vivo Evaluation. *AAPS Journal,* **2008**, *10*, 322–330.

168. Cetin, M.; Atila, A.; Kadioglu, Y. Formulation and in vitro characterization of Eudragit® L100 and Eudragit® L100-PLGA nanoparticles containing diclofenac sodium. *AAPS PharmSciTech* **2010**, *11*, 1250–1256.

169. Jain, D.; Panda, A. K.; Majumdar, D. K. Eudragit S100 Entrapped Insulin Microspheres for Oral Delivery. *AAPS PharmSciTech* **2005**, *6*, 100–107.

170. Hale, L. P.; Greer, P. K.; Trinh, C. T.; James, C. L. Proteinase activity and stability of natural bromelain preparations. *Int. Immunopharmacol.* **2005**, *5*, 783–793.

171. V., J. M. E.; H., S.; Hansson G. C. The gastrointestinal mucus system in health and disease. *Nat Rev Gastroenterol Hepatol.* **2013**, *10*, 352–361.

172. Conchouso, D.; Castro, D.; Khan, S. A.; Foulds, I. G. Three-dimensional parallelization of microfluidic droplet generators for a litre per hour volume production

of single emulsions. *Lab Chip* **2014**, *14*, 3011–3020.

173. Nisisako, T.; Ando, T.; Hatsuzawa, T. High-volume production of single and compound emulsions in a microfluidic parallelization arrangement coupled with coaxial annular world-to-chip interfaces. *Lab Chip* **2012**, *12*, 3426–3435.

174. Stolovicki, E.; Ziblat, R.; Weitz, D. A. Throuput enhancement of parallel step emulsifier devices by shear-free and efficient nozzle clearance. *Lab Chip* **2018**, *18*, 132–138.

175. Tendulkar, S.; Mirmalek-Sani, S.-H.; Childers, C.; Saul, J.; Opara, E. C.; Ramasubramanian, M. K. A three-dimensional microfluidic approach to scaling up microencapsulation of cells. *Biomed Microdevices* **2012**, *14*, 9623–9626.

176. Holtze, C. Large-scale droplet production in microfluidic devices—an industrial perspective. *J. Phys. D. Appl. Phys.* **2013**, *46*, 1–10.

177. Xu, Q.; Hashimoto, M.; Dang, T. T.; Hoare, T.; Kohane, D. S.; Whitesides, G. M.; Langer, R.; Anderson, D. G.; David, H. Preparation of monodisperse biodegradable polymer microparticles using a microfluidic flow-focusing device for controlled drug delivery. *Small* **2009**, *5*, 1575–1581.

178. Moustafine, R. I.; Zaharov, I. M.; Kemenova, V. A. Physicochemical characterization and drug release properties of Eudragit w E PO / Eudragit w L 100-55 interpolyelectrolyte complexes. *Eur. J. Pharm. Biopharm.* **2006**, *63*, 26–36.

179. Mousta, R. I.; Bukhovets, A. V; Sitenkov, A. Y.; Kemenova, V. A.; Rombaut, P.; Mooter, G. Van Den Eudragit E PO as a Complementary Material for Designing Oral Drug Delivery Systems with Controlled Release Properties : Comparative Evaluation of New Interpolyelectrolyte Complexes with Countercharged Eudragit L100 Copolymers. *Mol. Pharm.* **2013**, *10*, 2630–2641.

180. Choi, H. J.; Bondy, B. J.; Yoo, D. G.; Compans, R. W.; Kang, S. M.; Prausnitz, M. R. Stability of whole inactivated influenza virus vaccine during coating onto metal microneedles. *J. Control. Release* **2013**, *166*, 159–171.

181. Gill, H. S.; Prausnitz, M. R. Coated microneedles for transdermal delivery. *J. Control. Release* **2007**, *117*, 227–237.

182. Crowe, J. H.; Crowe, L. M.; Carpenter, J. F.; Wistrom, C. A. Stabilization of dry phospholipid bilayers and proteins by sugars. *Biochem. J.* **1987**, *242*, 1–10.

183. Crowe JH, Crowe LM, C. D. Preservation of Membranes in Anhydrobiotic Organisms : The Role of Trehalose. *Science (80-.).* **1984**, *223*, 701–704.

184. Harshad, P.; Anand, B.; Dushyant, S. Recent techniques in nasal drug delivery: A review. *Int. J. Drug Dev. Res.* **2010**, *2*, 565–572.

185. Nanaki, S.; Tseklima, M.; Christodoulou, E.; Triantafyllidis, K.; Kostoglou, M.; Bikiaris, D. N. Thiolated chitosan masked polymeric microspheres with incorporated mesocellular silica foam (MCF) for intranasal delivery of paliperidone. *Polymers (Basel).* **2017**, *9*, 617–638.

186. Grassin-delyle, S.; Buenestado, A.; Naline, E.; Faisy, C.; Blouquit-laye, S.; Couderc, L.; Le, M.; Fischler, M.; Devillier, P. Intranasal drug delivery: An efficient and non-invasive route for systemic administration Focus on opioids. *Pharmacol. Ther.* **2012**, *134*, 366–379.

187. Bhise, S. B.; Yadav, A. V.; Avachat, A. M.; Malayandi, R. Bioavailability of intranasal drug delivery system. *Asian J. Pharm.* **2008**, *2*, 201–215.

188. Ramvikas, M.; Arumugam, M.; Chakrabarti, S. R.; Jaganathan, K. S. Nasal vaccine delivery (Chapter fifteen). In *Micro- and Nanotechnology in Vaccine Development*; Elsevier Inc., 2017; pp. 279–301.

189. Bakri, W.; Donovan, M. D.; Cueto, M.; Wu, Y.; Orekie, C.; Yang, Z. Overview of intranasally delivered peptides: key considerations for pharmaceutical development. *Expert Opin. Drug Deliv.* **2018**, *15*, 991–1005.